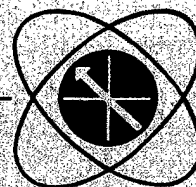


MSNW



DESIGN INVESTIGATION OF SOLAR POWERED LASERS FOR SPACE APPLICATIONS

FINAL REPORT

**PREPARED FOR THE NASA-LEWIS RESEARCH CENTER
LASER DIVISION
2000 BROOK PARK ROAD
CLEVELAND, OHIO**

MAY 1979

DTIC QUALITY INSPECTED 5



MATHEMATICAL SCIENCES NORTHWEST, Inc.

BND 0
19980123 002

Report Number: MSNW 79-1087/1090-1

Accession Number: 4104

Title: Design Investigation of Solar
Powered Lasers for Space

Applications

Personal Author: Taussig, R.; Bruzzone, C.; Quimby,
D.; Nelson, L.; et al.

Contract Number: NAS3-21134

Report Number Assigned by Contract Monitor: SLL 79-080

Corporate Author or Publisher: Mathematical Sciences Northwest
Inc., PO Box 1887, Bellevue, WA
98009

Report Prepared For: National Aeronautics and Space
Administration, Washington, DC

Publication Date: May 01, 1979

Pages: 175

Comments on Document: Archive, RRI, DEW

Descriptors, Keywords: Design Investigation Solar Power

Laser Space Application Pump Heat

Exchanger Cavity Absorber Collector

Concentrator Transmission Rocket

Propulsion Satellite GDL EDL

Electric Discharge Gas Dynamic

Efficiency

DESIGN INVESTIGATION OF SOLAR POWERED LASERS
FOR SPACE APPLICATIONS

FINAL REPORT

Prepared for the NASA-Lewis Research Center
Laser Division
2000 Brook Park Road
Cleveland, Ohio

Contract No. NAS3-21134

By

R. Taussig	W. Christiansen
C. Bruzzzone	S. Neice
D. Quimby	P. Cassady
L. Nelson	A. Pindroh

MATHEMATICAL SCIENCES NORTHWEST, INC.
P.O. Box 1887
Bellevue, Washington 98009

May, 1979

1. Report No. CR-159554		2. Government Accession No.		3. Recipient's Catalog No.	
4. Title and Subtitle DESIGN INVESTIGATION OF SOLAR POWERED LASERS FOR SPACE APPLICATIONS				5. Report Date May, 1979	
				6. Performing Organization Code	
7. Author(s) R. Taussig, C. Bruzzone, D. Quimby, L. Nelson, W. Christiansen, S. Neice, P. Cassady, A. Pindroh				8. Performing Organization Report No. MSNW 1087/1090	
9. Performing Organization Name and Address MATHEMATICAL SCIENCES NORTHWEST, INC.				10. Work Unit No. V7892	
				11. Contract or Grant No. NAS3-21134	
12. Sponsoring Agency Name and Address NASA Washington, DC				13. Type of Report and Period Covered Contractor Report	
				14. Sponsoring Agency Code 4360	
15. Supplementary Notes Project Manager, Richard B. Lancashire, Power Generation & Storage Division NASA Lewis Research Center, Cleveland, Ohio 44135					
16. Abstract The purpose of this study is to investigate the feasibility of solar powered lasers for continuous operation in space power transmission. Existing lasers are already able to deliver high power over long distances making the solar laser power satellite, laser rocket propulsion and other space applications attractive and competitive concepts. Laser power transmission in space over distances of 10 to 100 thousand kilometers appears possible. Further, there appears to be no fundamental principle limiting the power of solar powered lasers. A variety of lasers was considered, including solar-powered GDLs and EDLs, and solar-pumped lasers. A new indirect solar-pumped laser was investigated which uses a solar-heated black body cavity to pump the lasant. Efficiencies in the range of 10 to 20 percent (i.e., laser energy out ÷ solar energy in) are projected for these indirect optically pumped lasers (IOPLs). The weights and efficiencies for each class of laser system can be related to the different pumping mechanisms. GDLs require thermal pumping and will be inefficient and heavy because all of the gas must be heated and cooled. EDLs use electron beam pumping which is more selective than thermal pumping. Therefore EDLs will be more efficient and lighter than GDLs. OPLs use the most selective of all the pumping mechanisms and are not subject to electricity conversion losses; these are the lightest and most efficient systems. These intuitive arguments are substantiated in detail by the analysis carried out.					
17. Key Words (Suggested by Author(s)) Solar powered laser Solar pumped laser Heat Exchanger Cavity Absorbers Collector-Concentrators				18. Distribution Statement Unlimited	
19. Security Classif. (of this report) Unclassified		20. Security Classif. (of this page) Unclassified		21. No. of Pages 175	
				22. Price*	

* For sale by the National Technical Information Service, Springfield, Virginia 22161

16. Abstract Continued

Each laser concept studied consists of a complete laser system including laser loop and laser excitation components, gas supply and circulation system, solar power supply, waste heat radiator and any other elements required for its operation in space. A 1 megawatt laser output power was chosen as a common basis for comparing the different concepts. Each laser system was weighed on a common, self-consistent basis. Technologies were required to be available in the 1990 time frame. The critical technologies, system reliability and weight determined the feasibility and cost-effectiveness of each concept. A comparative analysis using these figures of merit showed that the indirect solar pumped laser was the most desirable laser system.

As a result, three conceptual designs were developed for indirect solar pumped lasers: A static CO_2 system (10.6μ), a flowing CO system ($5.2\text{--}5.4\mu$) and a mixing CO/CO_2 flow system. The best performance is anticipated for the static CO_2 laser; it weighs approximately 8000 kg and has a 17 percent efficiency at the 1 megawatt output power level. For this reason, it was selected for optimization and for a minimum risk development program. A minimum risk program to obtain low earth orbit tests for a 1 MW laser was projected to cost approximately \$77 M (1978 dollars) and to be completed by 1995. A crash program was also formulated which could shorten the development period to about 1988 at a total cost of \$121 M. The latter program utilizes the more conventional technology of a flowing CO system with the possible disadvantages of greater system weight and decreased reliability in orbit.

An immediate next step would be to build prototype IOPL laser cavities to verify performance and test the most critical technologies: laser tube materials and design, and the heat pipe/radiator system. Component technology development over a period of 12 years was estimated to cost in the range of \$8M to \$12M dollars. Laser tests included in the program plans were projected for the 25 kW, 250 kW and 1 MW levels.

TABLE OF CONTENTS

<u>Section</u>	<u>Page</u>
1 INTRODUCTION	1
2 SOLAR PUMPED LASERS	7
2.1 Survey of Possible Solar Pumped Lasants	8
2.2 Direct Solar Pumped Lasers	17
2.3 Indirect Solar Pumped Lasers	22
3 COMPARISON TO OTHER LASERS	49
3.1 Collector-Concentrators	49
3.2 Cavity Absorbers	56
3.3 Brayton Cycle Power Units	64
3.4 Heat Exchanger	75
3.5 Waste Heat Radiator	79
3.6 Solar Powered Gas Dynamic Laser	82
3.7 Solar Powered Electric Discharge Laser	89
3.8 Direct Solar Pumped Laser	95
3.9 Indirect Solar Pumped Laser	95
3.10 Comparative Analysis	96
4 PRELIMINARY CONCEPTUAL DESIGNS OF THE INDIRECT SOLAR PUMPED LASER	101
4.1 Mixing Gas Laser System	101
4.2 Static CO Laser System	116
4.3 Non-Mixing Flowing CO Laser	127
4.4 Comparative Analysis of Indirect Solar Pumped Lasers	133
4.5 Optimum Design Parameters for the Solar Pumped Laser	137
5 DEVELOPMENT PROGRAM	140
5.1 Minimum Risk Development Program	140
5.2 Crash Development Program	151
5.3 Program Costs	156
6. SUMMARY AND CONCLUSIONS	163
REFERENCES	165
APPENDIX A: Material Properties for Laser Tubes	170
NOMENCLATURE LIST	171
DISTRIBUTION LIST	

LIST OF TABLES

<u>Table</u>		<u>Page</u>
1	Summary of Visible Pumped Laser Systems	12
2	Potential VIS - IR Lasants	14
3	Potential Infrared Pumped - Infrared Lasants	16
4	Optimum Coupling Efficiency vs. Body Temperature	30
5	Fractional Absorption Losses Associated with Transparent Materials Versus Black Body Temperature	32
6	Absorption of Black Body Radiation by Lasants	38
7	Collector-Concentrator Materials and Properties	55
8	Materials and Temperatures for Cavity Absorber Examples	60
9	Selected Brayton Cycle Space Power Units	65
10	Supersonic CO ₂ GDL (1 MW)	85
11	Specific Weights for Comparative Evaluation of Solar Lasers	88
12	Subsonic CO ₂ EDL (1 MW)	90
13	Supersonic CO EDL (1 MW)	93
14	Solar Laser Weight Comparison (1 MW Laser Output)	97
15	Summary of Solar Laser Comparison	100
16	Absorption and Temperatures (Mixing Gas Laser) $f_{ABS}, \Delta T_G^{**}, T_o, T_w (T_G=360K)$	112
17	Mixing Gas Laser System Parameters	113
18	Static CO ₂ Laser Properties ($r = 1.5$ cm, $\lambda = 0.5$ cm)	120
19	Radiator Area and Mass (Static CO ₂ Laser)	123
20	Tube Mass (Static CO ₂ Laser) ($\delta' = .2$ mm, $\ell = 2.3$ m) (M_T in Kg)	125
21	Total Input Power and Mirror Mass (Static CO ₂ Laser) (P_m in MW, M_m in Kg)	126
22	Total Mass and Efficiency (Static CO ₂ Laser)	128
23	Temperatures (Flowing CO Laser) (All Temperatures in Kelvin)	129
24	System Parameters (Flowing CO Laser)	132
25	Summary of Radiator and Total System Masses (T^4 Scaling of Specific Radiator Mass)	136

<u>Table</u>		<u>Page</u>
26	Pointing Accuracy Requirements	143
27	Minimum Risk Development Program for the Static CO ₂ Solar-Pumped Laser	145
28	Laser Tube Development Schedule [Component Sub-tasks of Tasks 2 and 3 of Program No. 1]	149
29	Crash Development Program for the Static CO ₂ Solar-Pumped Laser	155
30	Space Transportation Costs Through 1990, Three Options	158
31	Program Cost Summary: 1 MW Solar-Pumped Laser	162

LIST OF FIGURES

<u>Figure</u>		<u>Page</u>
1	The Three Level Laser	9
2	Different Types of Optical Pumping	18
3	Level Scheme of Photochemical Iodine Laser	20
4	Conceptual View of a Direct Solar-Pumped Laser	21
5	Solar Collection/Concentrator Schemes for Direct Optical Pumping	23
6	Indirect Pumping Via an Intermediate Body	24
7	Blackbody Spectral Distribution at Selected Temperatures	26
8	Transmission of Various Optical Materials	32
9	Efficiency vs P_T/P_M	36
10	Solar Pumped Mixing Laser	41
11	Recuperated Refrigeration Scheme for CO_2 , H_2O Removal	43
12	Cascaded Molecular Sieves for H_2O , CO_2 Removal	44
13	Electrochemical Cell for H_2O , CO_2 Removal	46
14	Static Solar-Pumped Laser System	47
15	Geometry of Solar Radiation Collector and Optics	50
16	Energy Distribution Versus Radius in Focal Plane	51
17	Geometry of Mirror Imperfections of Order α for Rim Angle, θ_m , and Mirror Diameter, D	52
18	Gaussian Intensity Distribution as a Function of Radius, r , and Gaussian Parameter, a	54
19	Gaussian Cutoff Efficiency, η_{Diff} ; Re-radiation Efficiency, η_R and the Product Collection Efficiency, $\eta_c = \eta_R \eta_{Diff}$ as a function of Cavity Aperture (r/a) for Different Cavity Temperatures, T_B	58
20	Possible Cavity Absorber Designs for the Brayton Cycle Power Units	61
21	Solar Radiation Boiler-Receiver Solar Radiation from the Collectors in Focussed (at left) on the Transparent Window and Absorbed in the Heating Zone by the Driver Gas	62
22	Space Solar Spectrum and Potassium Absorption Spectrum for $p = 1$ atm	63

<u>Figure</u>		<u>Page</u>
23	Solar Brayton Systems	66
24	Schematic of Brayton Cycle Power Unit with Regenerator and Intercooled Compressors	67
25	Temperature-Entropy Diagram for Brayton Power Unit Shown in Figure 24	68
26	Photograph of the Full-Scale Gasdynamic Wave Heater Drum Constructed and Operated at CAL	71
27	Schematic of the Supercharging Application of the Compres Waveheater Currently Being Marketed by Brown-Boveri Company	72
28	Schematic of Intercooled, Regenerated Brayton Cycle Utilizing an Energy Exchanger for High Efficiency Operation	73
29	Energy Exchanger/Turbine Efficiency and Regenerator Peak Temperature (T_5/T_1) as functions of Maximum-to-Minimum Temperature Ratio $\tau \equiv T_4/T_1$ and Compressor Ratio π_{CD} [$\tau = 10^*$ for $\eta_{EE} = 70\%$ instead of 85%; (T_5/T_1)* corresponds to $T_5 = 1170$ °K when $T_3 = 300$ °K]	74
30	Heat Source Exchanger	75
31	Heat Exchanger for Liquid Metal to Gas Heat Transfer	77
32	Variation of Boiling Point with Pressure	78
33	Ratio of Heat Exchanger Tube Area (A_H) to Aberrated Image Area (A_S) at Entrance to Cavity for Lithium Coolant as a Function of Temperature	79
34	Meteoroid Impact Frequency as a Function of Minimum Meteoroid Mass	80
35	Possible Radiator Design	81
36	Average Radiator Thickness vs. Temperature	82
37	Temperature-Entropy Diagram of Non-Regenerated CO_2 GDL	83
38	Recuperated CO_2 GDL (1 MW, $\gamma = 1.4$)	83
39	GDL (CO_2) Based on Pratt & Whitney Design with Solar Power Units Included (enclosed in dashed lines)	86
40	Refrigerator Laser Loop for Space Systems	89
41	1 Mwatt CO_2 Laser-Space	92
42	1 MW CO Laser Space	94
43	Total Solar Laser System Weight as a Function of Specific Solar Collector Weight	98

<u>Figure</u>		<u>Page</u>
44	Total Solar Laser System Weight as a Function of Specific Radiator Weight	99
45	Indirectly Pumped Solar Mixing Gas Laser	102
46	Black Body Excitation Chamber and Laser Cavity	103
47	Heat Transfer in Laser Tube	107
48	Details of Beam Penetration of Black Body Cavity Wall (Static CO Laser)	117
49	Indirect Optically Pumped Solar Laser System Mass vs. Pumping (Black Body) Temperature with Constant Specific Radiator Mass	134
50	Indirect Optically Pumped Laser System Mass vs. Pumping (Black Body) Temperature with T^4 Scaling of Radiator Mass for $T_R > 475$ °K	135
51	Artist's Conception of 1 MW Solar-Pumped Laser	142
52	Examples of Collector Technology for Solar Laser Program	152
53	Close-up Artist's View of Flowing CO Solar-Pumped Laser	153
54	Costs for Shipping to Low Earth Orbit [taken from Ref. 6]	160

SECTION I

INTRODUCTION

The purpose of this study was to investigate the feasibility of using solar powered lasers for continuous operation in space power transmission and to select the best of several competing concepts for a conceptual design. Gas dynamic lasers, electric discharge lasers, and optically pumped lasers were evaluated on the basis of weight, efficiency, size, and technology. The evaluation of optically pumped lasers included a new, indirectly pumped laser in which a solar heated black body cavity provides uniform illumination to pump the lasant. Except for reradiation losses from the cavity and unwanted absorption losses to the laser tubes, all of the sunlight entering the black body cavity can ultimately be used to optically pump the laser gas. The potential efficiency of this approach can therefore be orders of magnitude greater than any direct solar pumping scheme.

The interest in space applications of high energy lasers stems from the ability of existing high power closed cycle lasers to deliver high intensity power over long distances.^{1,2} Remote space vehicles³ and ground stations can receive power from a solar laser power satellite (SLPS).⁴ Similar concepts to the SLPS have already been developed in much greater detail for microwave solar power stations orbiting the earth. The laser version has a distinct advantage because it can function in a low earth orbit using relatively small relay satellites to reach a wide range of receiving stations on the earth. In contrast, the microwave version must operate in geosynchronous orbit in order to keep contact with the ground stations. The overall SLPS system efficiency appears to be as high or higher than the microwave version. Also, the area required on the ground for receiving stations is much less for the laser system because of its narrow beam spread. Consequently, the overall system cost of the SLPS could be much lower than the microwave version.

Laser power transmission has also been studied for rocket propulsion.⁵ Very high specific impulses can be achieved through laser heating, because of the high temperatures achieved in this way. Hence, a laser driven rocket would be much lighter and capable of much higher payloads than a comparable chemically powered rocket.

Transmission distances of tens or even hundreds of thousands of kilometers appear to be within the realm of possibility with space based lasers. These dimensions suggest that the applications listed above can be motivated by a very wide range of missions. The distances also bear a strong influence on the economics achievable via laser power transmission, since no mass transport over such distances is required. The potential for high-powered laser systems has been rapidly expanding for the past decade, in pace with the explosive development of new and larger lasers in this field. Several hundred kilowatts appear possible now on a CW basis: these systems can be scaled up using realistic technology to very large sizes in the multi-megawatt range in the near future (e.g. by 1990). There appears to be no fundamental principle in general which limits the power of lasers.

In a recent survey on the use of lasers for power transmission, the extrapolation of CO EDLs (electric discharge lasers), CO₂ GDLs (gas dynamic lasers), chemical lasers and closed cycle CO₂ EDLs to higher powers was carried out.⁶ It was also noted that the direct or indirect pumping of lasants by solar energy might avoid the inefficiencies of first converting the solar energy to electricity and therefore would possibly yield a more efficient laser. The present study has considered the first two types of laser mentioned above and has included as a distinct item, an investigation of the solar pumped lasers. Pratt and Whitney has carried out a design investigation of the CO₂ GDL in closed cycle for space application.⁷ Their study

emphasized the laser system itself, and did not develop significant new data for the power supply assuming that energy would be supplied from a nuclear reactor. Their laser design has been used as the basis for the current study's investigation of a solar powered closed cycle CO_2 GDL. Similarly, Hughes Aircraft Corporation carried out a design investigation of both CO_2 and CO EDLs for closed cycle space operation, using solar energy as the power source.⁸ The Hughes results were taken over wholly for the purposes of the present study.

Direct solar pumped lasers have been considered by Rather et al.⁹ Their concept uses a selective collector/filter to reflect only those wavelengths which will be absorbed by the lasant. Trifluoromethyl iodide (CF_3I) serves as a donor of optically excited iodine. Rather's scheme has been analyzed along with the indirect solar pumping scheme discussed above.

In addition, free electron lasers may conceivably be driven by solar energy.¹⁰ These lasers utilize an electron storage ring and a slow wave structure (spatially inhomogeneous magnetic field) to pump the free electrons to an excited state. These lasers have not been evaluated here. While high energy free electron lasers may be built at some future date, the technology of electron ring storage suggests that such lasers will be relatively massive and therefore more appropriate for terrestrial use.

Two other reviews of solar powered lasers deserve mention because of their points of view. The first, by Monson,¹¹ has placed all gas flow lasers on a uniform basis by optimizing each according to the flow mach number for supersonic or subsonic nozzle conditions, depending on the type of laser. The second review, by Bain,¹² has surveyed the potential of solar powered lasers for the SLPS concept,

canvassing quite a wide range of current technologies including preliminary results from the present study. Bain has estimated that when the efficiency of the solar powered laser exceeds 10 percent, it becomes an effective competitor to the microwave SPS.

The pumping mechanisms differentiate the likely weights and efficiencies of each of the laser types studied. Gas dynamic lasers, for example, require heating the gas at high pressure and then expanding it rapidly to a low temperature to achieve an inverted state population. Large pressure drops and flow losses are associated with the subsequent diffusion to a slow speed flow. Furthermore, the gas must be cooled after slowing it down so that the gas entering the compressor is not too hot. The heating and cooling aspects of this cycle compete with each other since high temperatures are desirable for high laser efficiency and high output laser power and low input gas temperatures are needed for conventional compressor technology.

In contrast, electric discharge lasers have the advantage of achieving a population inversion without heating the bulk of the gas to a high temperature. Thus, the net cooling and pumping requirements for EDLs is lower than for GDLs. The EDL advantage is partially offset by kinetic deactivation of the excited state. In order to keep this back reaction rate low, the gas density must be lower than for a GDL; therefore, a larger gas volume may be necessary to get the same power output from an EDL.

The solar pumped laser is in many respects like the EDL since selective excitation of lasing states may be obtained without much heating of the bulk of the gas. Moreover, the solar energy input need not be subject to the inefficiency of converting it first to electricity. However, solar pumping is not generally a broad band pumping mechanism so that more energy input compared to an EDL may be required unless the indirect solar pumping approach is used.¹³

These distinctions favor in a general way the solar pumped lasers over the solar-powered EDLs and GDLs. With this fundamental advantage in mind, the study emphasized an investigation of solar pumped lasers. The objectives of this study were to develop optically pumped cw lasers, concepts, to evaluate the feasibility of solar-pumped lasers and solar-powered EDLs and GDLs and to select from these the best laser concept for space power transmission. The laser chosen for detailed study was then carried through to a preliminary conceptual design, for which both a "crash" development program and a minimum risk development program were formulated.

The basic guidelines for this study were to consider a complete system for each of the main laser types, including solar collector, power units, waste heat radiator and laser system. The lasers were conceptualized at the 1 megawatt power output level and scaled to higher powers. Technologies used in these concepts were chosen to be available in the 1990 time frame. The critical technologies, system reliability and weight determined the feasibility and cost-effectiveness of a given solar laser concept.

The results of our analysis show that the basic intuitive advantages discussed above are borne out in detail, with the lightest weight solar laser being the indirect optically pumped laser and the heaviest being the solar powered GDL. However, the solar pumped laser requires the use of relatively new technology in the black-body pumping cavity, whereas the GDL has a well established technology. The solar powered EDL is both intermediate in weight and in technology. The EDL has been built in closed cycle form, but there is still some concern that laser gas purity may be difficult to maintain over long periods of time. Similar problems may also exist for certain versions of the solar-pumped schemes.

Comparing the relative advantages and disadvantages within the study guidelines, the indirect solar-pumped laser concept was chosen for detailed study. Three versions of this concept have been considered: a stationary gas discharge laser, a dynamic gas flow laser, and a mixing gas laser. The gas discharge version employs CO_2 and helium. In this case the lasant and outer tube walls are cooled by gaseous heat conduction to an inner cylinder through which a separate coolant is circulated. The entire laser tube cavity is embedded in the black body cavity. The dynamic gas flow laser uses CO as the basic lasant which flows through transparent tubes in the black body cavity. The mixing gas laser uses CO as the pumping media. Upon emerging from the black body cavity the CO is mixed with CO_2 and some water vapor, and directed to the laser cavity where the CO_2 , energized by the CO^* , lases. In the flowing and mixing lasers, the flowing CO is used to cool the tubes in the black body cavity.

Specific design concepts have been developed for each of the major components of the indirect solar pump laser. Weight and efficiency analysis for each of the components leads to the preliminary conclusion that the 1 megawatt laser system including solar collector/converto, Brayton cycle power unit and waste heat radiator, will weigh approximately 10,000 kg, fully 50 percent lighter than the CO EDL, the closest competitor solar powered laser. The solar pumped laser is easily scalable to larger sizes with an overall efficiency (i.e., laser power out divided by solar power in) of 10 percent or better. Preliminary experimental work exhibiting gain for the black body pumping technique has already been carried out. The next step is to build a prototype of the laser cavity to verify the theoretical predictions for performance and to test the most critical technologies.

SECTION 2

SOLAR PUMPED LASERS

In order to determine the best laser system for use in space, the basic laser types are evaluated according to their system and component design requirements, weight, technological development and cost. This section surveys possible solar pumped laser systems, discusses energy balances and efficiency of the different approaches, and details some specific infrared (IR) laser systems. In engineering these systems an equal level of technology was assumed whenever possible for the collectors, waste heat radiators, and solar powered Brayton cycle units. The evaluations are based on similar waste heat radiator technology and solar power units as those used to evaluate EDLs and GDLs for space usage (summarized in Section 3).

In contrast to solar-powered lasers such as the EDL or GDL, solar-pumped lasers use direct or indirect optical pumping of a lasant. A solar pumped laser concept has been developed by MSNW as a specific task in this study; the basic concepts are discussed in this section. The direct optical pumping schemes focus full or filtered sunlight on the lasant. Indirect optical pumping schemes downshift the solar radiation spectrum in a black-body cavity where the lower temperature radiation pumps the lasant. A survey of lasants was used to select those with the best threshold and gain requirements for solar pumping. The results of that survey are summarized below, followed by a description of both the direct and indirect optically pumped schemes.

The principal result of the solar-pumped laser analysis is that the indirect solar-pumped laser schemes show the greatest promise for space application. They are light weight, simple to build and highly efficient. Three versions of this scheme are discussed; the best appears to be either a static CO_2 system or a flowing CO system, depending on the radiator technology employed.

2.1 Survey of Possible Solar Pumped Lasants

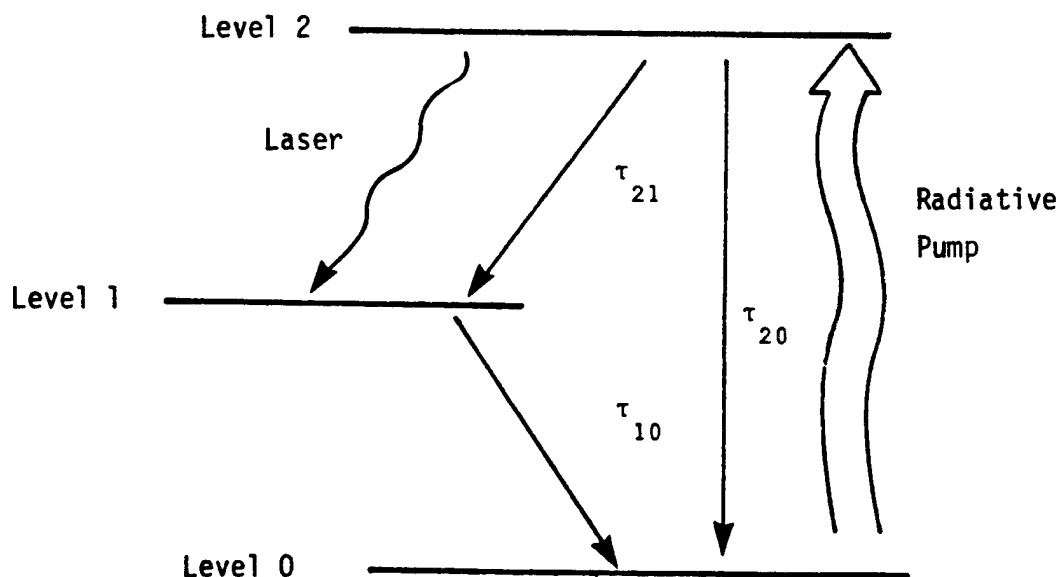
The difficulty in achieving lasing conditions using solar radiation is that sunlight is diffuse and broadband. The maximum practical concentration of sunlight is approximately 1 kilowatt per cm^2 which is below the power threshold for many of the optically pumped lasants and this energy is distributed over a wide band from the ultraviolet (UV) to infrared (IR) wavelengths. Therefore the intensity in any given absorption line width or band width is considerably less than 1 kW/cm^2 . This level of intensity ultimately limits the lasants of interest to those with low threshold requirements.

Laser candidates may be pumped using bound-bound transitions such as atomic or molecular line spectra or bound-free transitions such as photo-dissociation spectra. The possibilities of the first case extend over the whole spectrum whereas the latter case tends toward the visible part of the spectrum because of typical bond strengths. The most direct approach is to find a lasing gas which has a spectral absorption band connecting the upper laser level to the ground state. It is also feasible to use other atomic or molecular gases which can contribute their absorbed energy via collisional transfer. A number of lasant possibilities have been looked at. They are described below along with laser concepts developed for direct and indirect optical pumping.

Lasant candidates have been divided into three categories. The first group is direct or visible pumping with subsequent lasing at visible wavelengths. The second group is visible pumping with IR lasing. The third group receiving the main emphasis of this research, is IR pumped-IR lasers. Each group or candidate was looked at with regard to the net fractional absorption of the optical pump and the implications on system efficiency, the optical depth associated with the optical pump, threshold requirements where known, and gain possibilities for CW operation. The most important feature of the gain criteria is to have the ratio of relaxation time to the radiative lifetime of the absorber be large.

2.1.1 Gain Factor

A simple criteria for gain can be developed on the basis of a three level model of the lasing system (Figure 1). The solid lines represent



78 01886

Figure 1. The Three Level Laser

partition function; τ_2 is the effective collisional lifetime of state 2; $g_{1,2}$ are the statistical weights of the states, A_{21} is the Einstein coefficient for the laser transition. A necessary condition for positive gain in CW operation is

$$\frac{g_2 \tau_{10}}{g_1 \tau_{21}} < 1 \quad (4)$$

High gain is achieved if the laser parameters $\lambda_{21}, A_{21}, g(\nu)$ etc. are large, the flux is large, and if the absorption parameter, α , times lifetime τ_2 is large. Because α is proportional to $N/\tau_{\text{rad}} = p/kT\tau_{\text{rad}}$, a figure of merit is $p\tau_2/\tau_{\text{rad}}$ for $\alpha\tau_2$.

2.1.2 Visible Pumped-Visible Lasing Systems

Table 1 summarizes the status of optically pumped visible dimer and dye laser systems up to late 1977. The lowest thresholds reported are for the Na_2 system using a CW argon ion laser. However, the extremely high monochromaticity of the Ar^+ pump radiation and the relatively tight focussing geometry cannot be realized in a solar pumped situation.

In the case of the alkali metal dimers, the 1 kW/cm² radiation intensity level achievable with solar radiation appears very marginal in terms of the pumping power thresholds required. Also, the absorption is in a series of discrete, non-overlapping bands centered at 4700 Å and at 6596 Å in Na_2 , which makes the percentage of solar radiation usefully absorbed smaller than desired. The sodium dimer does have an attractive feature of lasing in the visible (A to X laser transition) in the range of 6000 Å to 8000 Å. The lithium dimer has an even higher pumping power threshold than sodium (the upper state life-time is on the order of 6 to 12 nanoseconds). The sulfur dimer must be pumped selectively at 3370 Å and therefore seems unsuitable for broad band pumping in general.

collisional transitions with time constants τ , whereas the wavy lines are radiative transitions, the most important ones being the solar pump and laser. The optical pumping of level 1 is neglected.

The absorbed power/volume, P , can be calculated using the equation of radiative transfer and integrating it over all frequencies associated with the absorption and solid angles. That is,

$$P = \int_{\nu} \int_{\Omega} \alpha_{\nu} I_{\nu} d\nu d\Omega = \alpha \Phi \quad (1)$$

where α_{ν} is the absorption coefficient. If the flux density does not vary much with frequency we write the integral as equal to α , the averaged absorption coefficient, times the pump radiation density, Φ , as above. It is known that P is proportional to N the number of absorbers divided by the radiative lifetime of the absorption band.¹⁴ Thus the equations for the three level system with no thermal population are

$$\begin{aligned} \frac{dN_2}{dt} &= \frac{\alpha \Phi}{h\nu_{20}} - \frac{N_2}{\tau_{21}} - \frac{N_2}{\tau_{20}} \\ \frac{dN_1}{dt} &= \frac{N_2}{\tau_{21}} - \frac{N_1}{\tau_{10}} \end{aligned} \quad (2)$$

and

$$N_0 + N_1 + N_2 = N = \text{constant}$$

Solving these for a steady state condition, $\frac{dN_1}{dt} = 0 = \frac{dN_2}{dt}$ and using the results to predict gain $\gamma(\nu)$ on the laser transition gives

$$\gamma(\nu) = \frac{\lambda^2_{21} A_{21}}{8\pi} g(\nu) \frac{\alpha \Phi}{h\nu_{20} g_2} \tau_2 \left[1 - \frac{g_2}{g_1} \frac{\tau_{10}}{\tau_{21}} \right] > 0 \quad (3)$$

where $g(\nu)$ is the line shape of the laser transition and includes the

Table 1
Summary of Visible Pumped Laser Systems

Molecule (Transition)	Pump Laser	Remarks	References
$I_2(B^3\Pi_{0^+u} - X^1\Sigma_g^+)$	doubled Nd, Ar^+	pulsed, CW	15
$Na_2(B^1\Pi_u - X^1\Sigma_g^+)$	doubled Nd, Ar^+	pulsed, CW	16-19
$(A^1\Sigma_u^+ - X^1\Sigma_g^+)$	doubled Nd, dye, Ar^+	pulsed	17-19
$Br_2(B^3\Pi_{0^+u} - X^1\Sigma_g^+)$	doubled Nd	pulsed, CW	20
$S_2(B^3\Sigma_u^- - X^3\Sigma_g^-)$	doubled dye	pulsed	21
$Te_2(AO_u^+ - XO_g^+)$	dye	pulsed	22
$Li_2(B^1\Pi_u - X^1\Sigma_g^+)$	argon ion	cw	19
$HgBr(B^2\Sigma^+ - X^2\Sigma^+)$	ArF	pulsed dissociation of $HgBr_2$	23
Liquid Dyes	flashlamp Ruby argon ion	cw or pulsed (threshold > 50,000 w/cm ²)	24

The absorption bands of all the molecules in Table 1 consist of a fairly complex series of discrete, essentially non-overlapping transitions. Hence, the absorption of solar radiation at typical dimer concentrations (10^{16} cm^{-3}) would not produce a sufficiently high excited state density to reach laser threshold. The S_2 and HgBr systems must be excited at wavelengths shorter than 3600 \AA , which is unsuitable for solar pumping.

On the other hand, the absorption coefficient of the liquid dyes is more or less continuous so that a large fraction of the solar radiation can be absorbed. Unfortunately the population inversion threshold of most dyes is greater than $50,000 \text{ w/cm}^2$ ²⁴ and so these clearly are not a possibility for solar pumping.

As a class of laser possibilities, these lasants probably absorb direct sunlight fairly well, having desirable lasing wavelengths, but have thresholds that are probably too high to be useful.

2.1.3 Visible Pumped-Infrared Lasing Systems

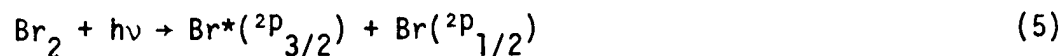
Another class of systems involves visible pumping with IR lasing. Interesting possibilities are shown in Table 2. The first two represent photodissociative lasers in which some of the dissociation products are in an excited state and can be lased.^{25,26} In these cases there is a fairly large, broadband absorption cross section in the visible providing a good pumping source. However, the resulting excited states are rapidly quenched by collisions, making the laser threshold power level relatively high. It also remains to be seen if such systems can be made chemically reversible for long time usage.

The last two cases in Table 2 work on a different principle in which energy of the fragments is transferred to a lasing molecule, in this case CO_2 . In these cases the question of threshold is not a problem.

Table 2
Potential VIS - IR Lasants

Absorber	Laser	Remarks	Reference
NOC1	NO*		Ref. 25
CF ₃ I	I*		Ref. 26
Br ₂	CO ₂	energy transfer from Br* to CO ₂	Ref. 27
I ₂	CO ₂	energy transfer from I* to CO ₂	Ref. 27

The photo dissociative reaction, for example,



yields excited bromine atoms with energy equivalent of 3700 cm⁻¹.

Electronic energy can be resonantly transferred to CO₂ in the reaction



based on the close energy match of Br* and CO₂(101). Laser action at 4.3 μm on the (101)-(100) CO₂ band has been observed by Wittig and co-workers at USC (Ref. 28). Gain at 10.6 μm was also reported by these workers using a CW argon ion laser as a photolysis source (Ref. 29).

The particular advantage of this pair of reactions is that the pump radiation for reaction (5) can be broad band from 3500 Å and 5000 Å near the peak of the solar spectrum. Thus, much of the solar energy can be absorbed and, further, laser tube wall materials can readily be found which are transparent to the primary visible radiation.

For this particular pair of reactions the competing reactions are:



The first reaction is known experimentally²⁷ to be relatively slow, but the rate of the second reaction has not been measured. In the case of chlorine and fluorine, the back reactions equivalent to reaction (7b) listed above are quite fast³⁰ presumably due to the small energy difference between the ground state ($^2p_{1/2}$) and the first excited electronic state ($^2p_{3/2}$) for Cl and F atoms. However, the energy gap for Br atoms is 3700 cm^{-1} and one would therefore expect the reaction (7b) to be relatively slow. Experimental data is required to confirm this assumption.

Iodine may work in much the same way as bromine, but the absorption band of wavelengths does not match the solar spectrum nearly so well since it lies in the less energetic region from 4500 Å and 6500 Å . Similarly, the excited iodine atom, I^* , has an energy equivalent to 8000 cm^{-1} and hence



will probably yield CO_2 (032) which must cascade down in vibrational energy dissipating energy as heat along the way, before it can lase in the $10\text{ }\mu\text{m}$ (001)-(100) band. In this respect the $\text{Br}^* - \text{CO}_2$ system seems more desirable.

The overall quantum efficiency of these systems is also not very high, causing significant heating of the gas mixture. In the case of $\text{Br}^* + \text{CO}_2 \rightarrow \text{CO}_2^* + \text{Br}$, almost 95 percent of the sunlight will end up as heat instead of lasing.²³ This places the system at a disadvantage especially for space laser application in which radiator weight is a significant factor.

2.1.4 Infrared Pumped-Infrared Lasing Systems

Some examples of molecular laser systems with strong IR absorption bands are shown in Table 3 where the criteria for gain and CW laser

Table 3
Potential Infrared Pumped - Infrared Lasants

Laser Molecule	$\frac{g_2 \tau_{10}}{g_1 \tau_{21}}$	$0 \left(\frac{p \tau_2}{\tau_R} \right) \text{ torr}$	References
CO	<1	1000	39
CO ₂	<1	1	31,32
N ₂ O	<1	0.5	33-35
CS ₂	<1	0.2	37-38
OCS	>1	10 ⁻²	36
HF	<1	3(10 ⁻⁴)	40
DF	<1	3(10 ⁻⁴)	
C ₂ H ₂	<1	2(10 ⁻⁵)	41

performance is tabulated. All of these molecules have produced laser emission in the range between 4.5 μ and 10.8 μ . Lasants such as OCS, HF and DF are not good choices because rapid deactivation rates make these systems a relatively high threshold case. On the other hand, CO has very low deactivation rates and is also very efficient. However, CO requires cryogenic temperatures for reaching threshold and for efficient operation. Very low temperature operation may be difficult to achieve in a space system because of heat exchanger and heat radiator requirements. Furthermore, the CO absorption band is not very intense. Acetylene is not a good candidate for direct pumping as this is an example of a molecule in which the upper laser level is not connected to ground via an allowed optical transition. CO₂ and N₂O are quite good candidates, having reasonably low threshold requirements, not too low gas temperature requirement and good chemical stability. N₂O, with modest thermal stability due to low binding energy, is not very susceptible to composition changes due to sun-

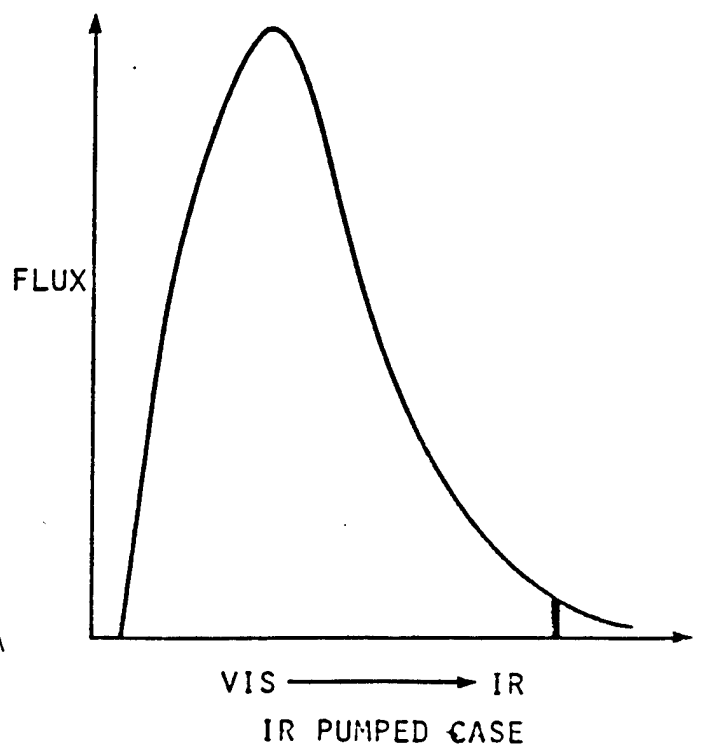
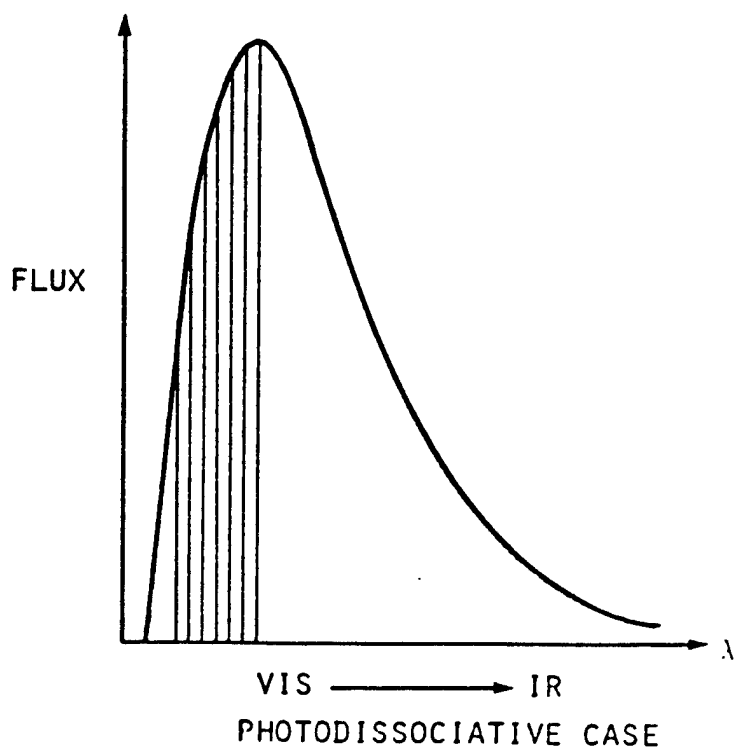
light. It is also possible that mixtures of these gases and their isotopes may be used as laser mediums. These possibilities are not illustrated herein. Table 3 only shows what may be expected on the basis that the lasant is the absorber system.

The above examples are relatively good lasants under special circumstances and can convert a good fraction of pump energy into laser light. Unfortunately these all are bound-bound radiative transitions and therefore do not couple well with sunlight as shown in Figure 2. Thus their overall efficiency will be very low unless the concept of the black body pump can be employed. Various techniques for using indirect solar pumping to power CO and for CO₂ lasers will be discussed in later sections.

2.2 Direct Solar Pumped Lasers

A variety of lasants for direct optical pumping have been noted in the preceding section. Only CF₃I has been studied in any detail for high powered lasers in space. The visible pump-visible laser class of lasants had thresholds too high for solar pumping. The CF₃I belongs to the second class of lasants: visible pump-IR laser. This second class has two possible disadvantages in that either the lasants are chemically unstable and some chemical processing is required to reconstitute the lasant and/or a large portion of the absorbed radiation is dissipated as heat. That is, the quantum efficiency of the lasing transition is low.

Rather et al.,¹⁹ have investigated a preliminary concept for a CF₃I direct solar-pumped laser. Their scheme relies on the use of a selective filter-reflector to focus only that portion of the solar spectrum which can be absorbed for pumping the CF₃I. While this strategy relieves the system of having to dispose of waste heat associated with unwanted absorption of sunlight outside of the lasant absorption band, there is still the need to radiate the waste heat associated with the lasing process. Approximately 80% of the filtered solar energy absorbed by



78 01588

Figure 2. Different Types of Optical Pumping

by the lasant must still be disposed of as waste heat. For a 1 megawatt output laser this means that about 5 megawatts of filtered sunlight must be supplied to the laser absorption cavity and that 4 megawatts is radiated as waste heat.

Also since the absorbing band width is rather narrow, it comprises about 2.5 percent of the full spectrum of the solar energy. Therefore, the filter-reflector must be sized to receive 200 megawatt of solar power so that the correct power level of filtered light is sent on to the lasant. This means that the collector is at least an order of magnitude greater in area relative to other solar laser schemes.

Rather et al.,⁹ have considered some of the details of a solar pumped laser based on CF_3I . They suggest the laser transition as shown in Figure 3 resulting from the release of I^* during the dissociation of CF_3I . The lasing wavelength is $\lambda = 1.315$ microns. Figure 4 reproduced from their report illustrates a possible laser system configuration. Evidently, the balance of plant for such a laser must include a chemical reprocessing plant to retrieve the molecular iodine and reconstitute the CF_3I molecule. Also, waste heat radiators to cool the lasant, windows and laser tubes are required.

Direct optical pumping schemes generally suffer from poor utilization of the solar energy flux. For example, assuming that a transparent vessel contains the pumping medium, the radiation is selectively absorbed wherever there is an absorption band or line. For these transitions, the absorption bandwidth may be only 0.1 percent or less of the average wavelength of the transition. Passage of the unused portion of the light through the medium will produce no additional useful absorption, although the remaining light could perhaps be used for other purposes, such as electricity generation. Typically, a high concentration of the sunlight, corresponding to a small aperture number lens, will yield flux levels of about 25 percent of the black body flux at the sun's surface. Even when a low f number (defined as

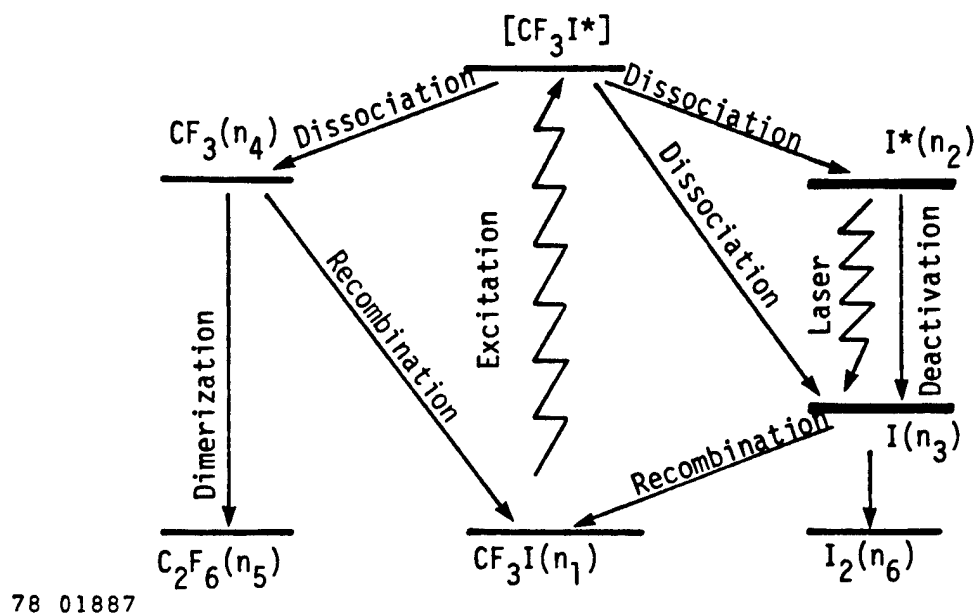
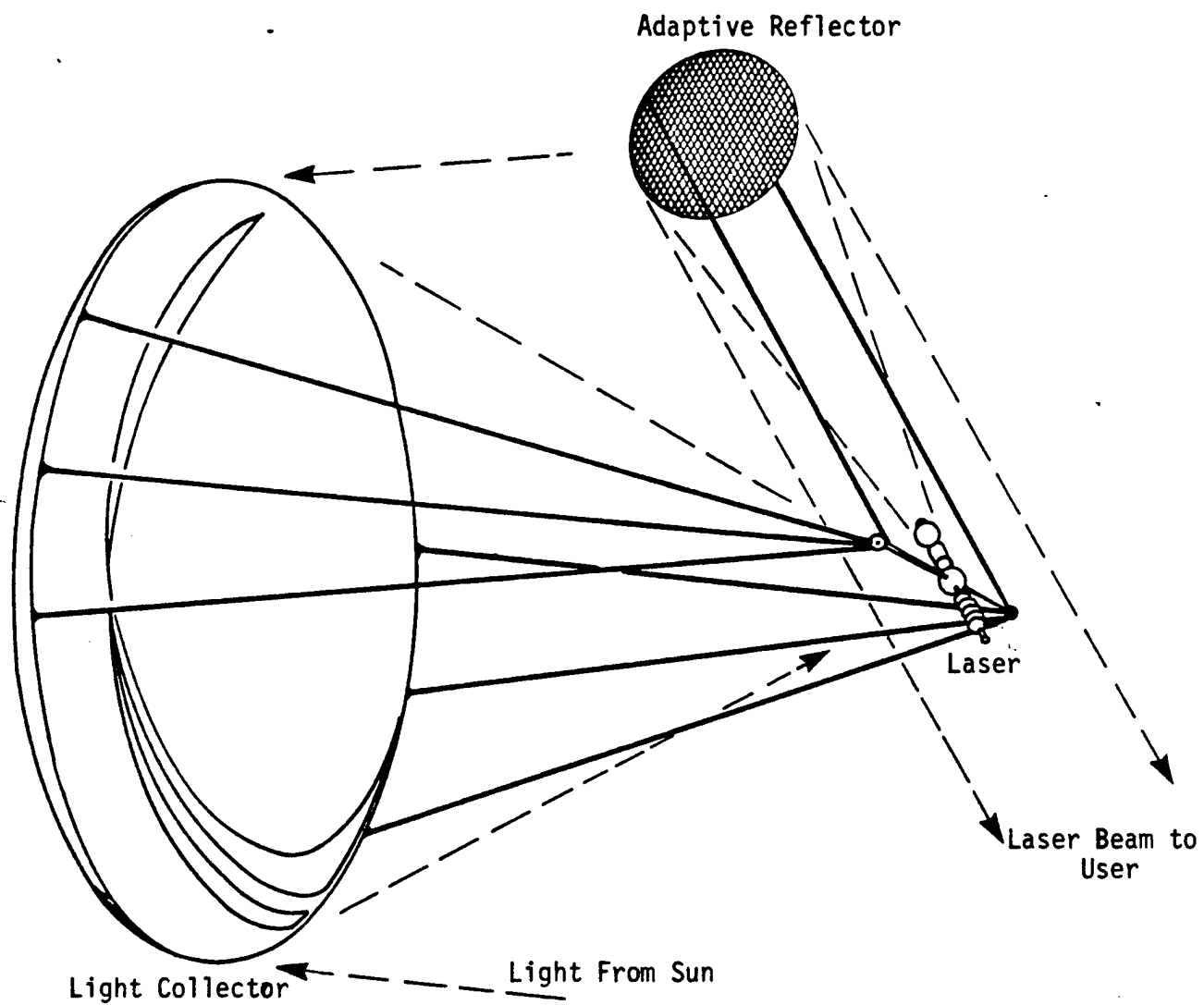


Figure 3. Level Scheme Of Photochemical Iodine Laser. Chemical Species n_1 Through n_6 Occur in The Laser [Ref. 9]



78 01887

Figure 4. Conceptual View of a Direct Solar-Pumped Laser [Ref. 9]

focal length/diameter of the collector) is used, a solid angle of only about 3 steradians of the laser tube is exposed to the incoming light, reducing the possible pumping from that of the full solid angle of 4π steradians. Furthermore, the high intensity from a spherical focus at low f number is obtained only with a small circular image which then must be used to pump a long laser tube (see Figure 5).

The major components of this system are:

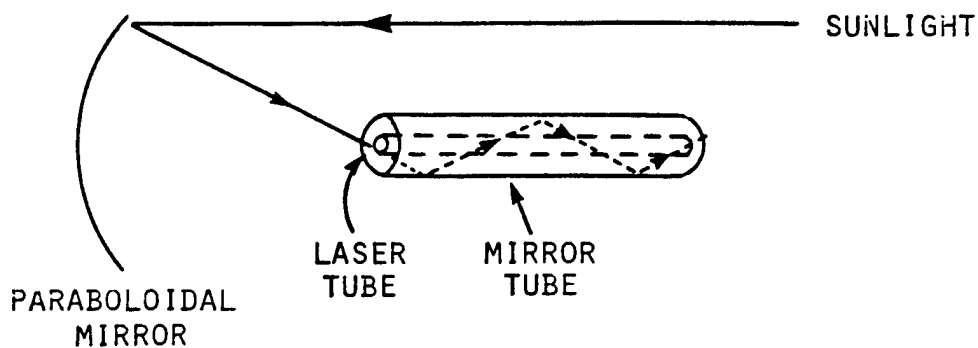
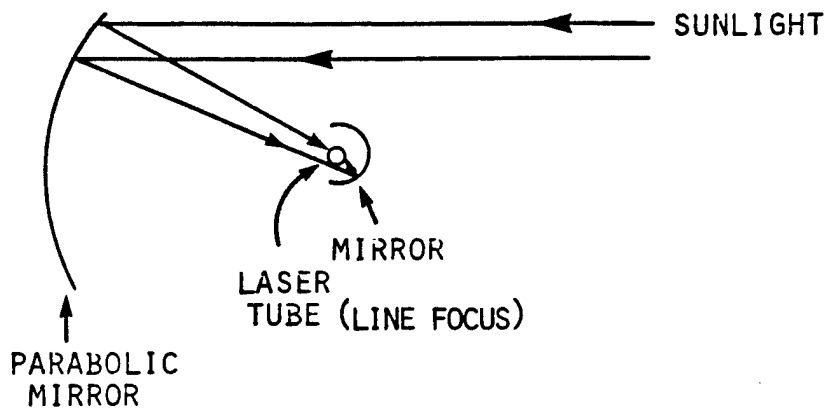
- Filter/collector
- Secondary focussing mirror
- Laser tubes, windows and cavity mirrors
- Cooling systems and power plant
- Waste heat radiator
- Gas make-up or purification system

The direct optically pumped laser is weighed on a self-consistent basis in Section 3 along with the other laser concepts analyzed in that section. Suffice it to say here that the chemical purity problem and large areas of collector are potential disadvantages of this system that are hard to overcome even with the most optimistic technological advances between now and 1990.

2.3 Indirect Solar Pumped Lasers

In order to help overcome the severe limitations of direct solar-pumped lasers a new approach has been suggested wherein concentrated solar radiation is absorbed and re-radiated via an intermediate black body. This body would be heated by focussed sunlight to a high temperature, and must be engineered to have small heat losses. In a static system, cooled laser tubes would be placed within the cavity (as shown in Figure 6) to be pumped by the cavity radiation. Alternatively, the lasing gas could be flowed through the black body into a laser cavity where it would then be caused to lase via the introduction of catalysts

1. PARABOLIC MIRROR PLUS SECONDARY CONCENTRATING MIRROR



2. PARABOLIC MIRROR/FILTER PLUS MIRRORED CAVITY

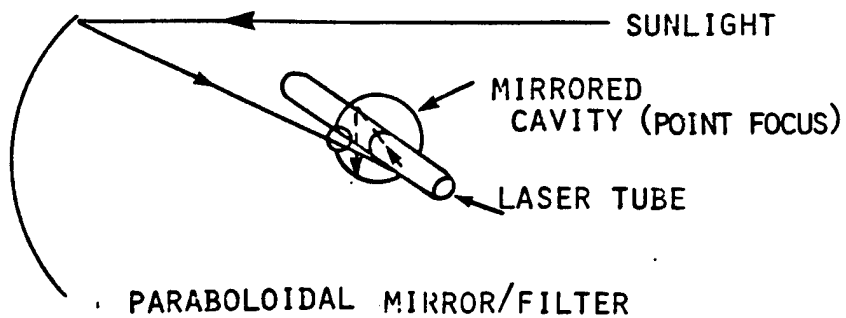
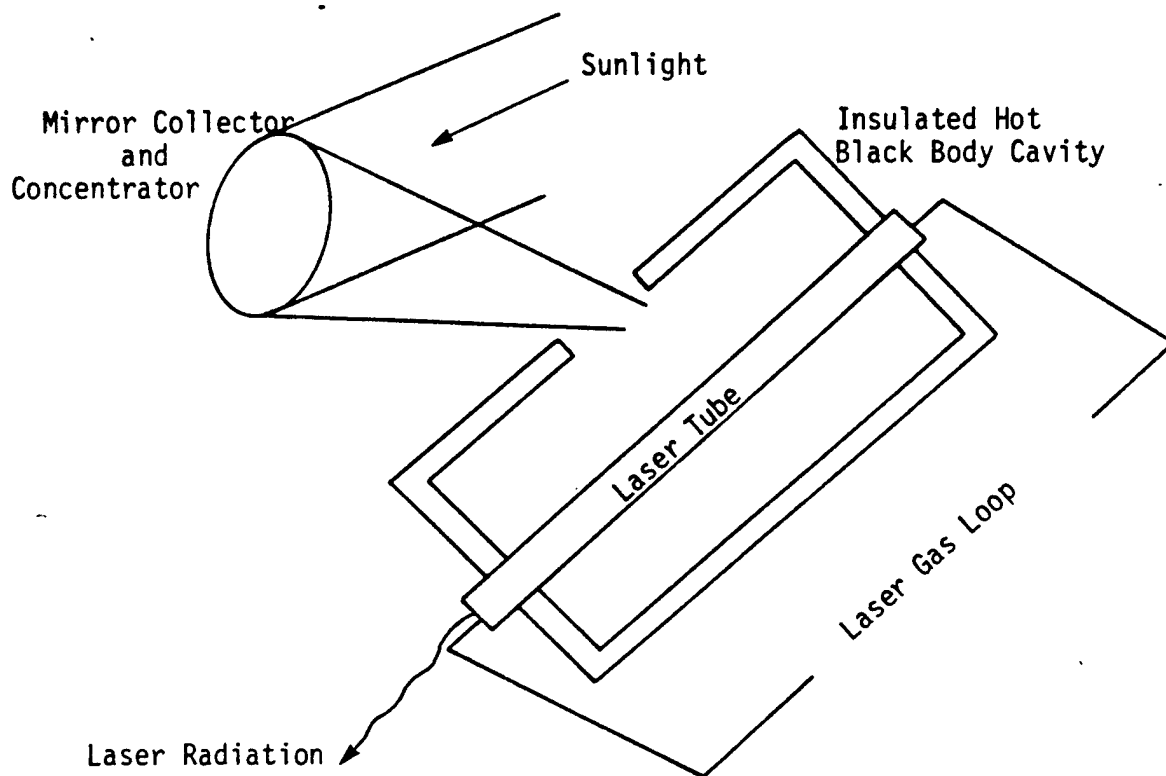


Figure 5. Solar Collection/Concentrator Schemes for Direct Optical Pumping

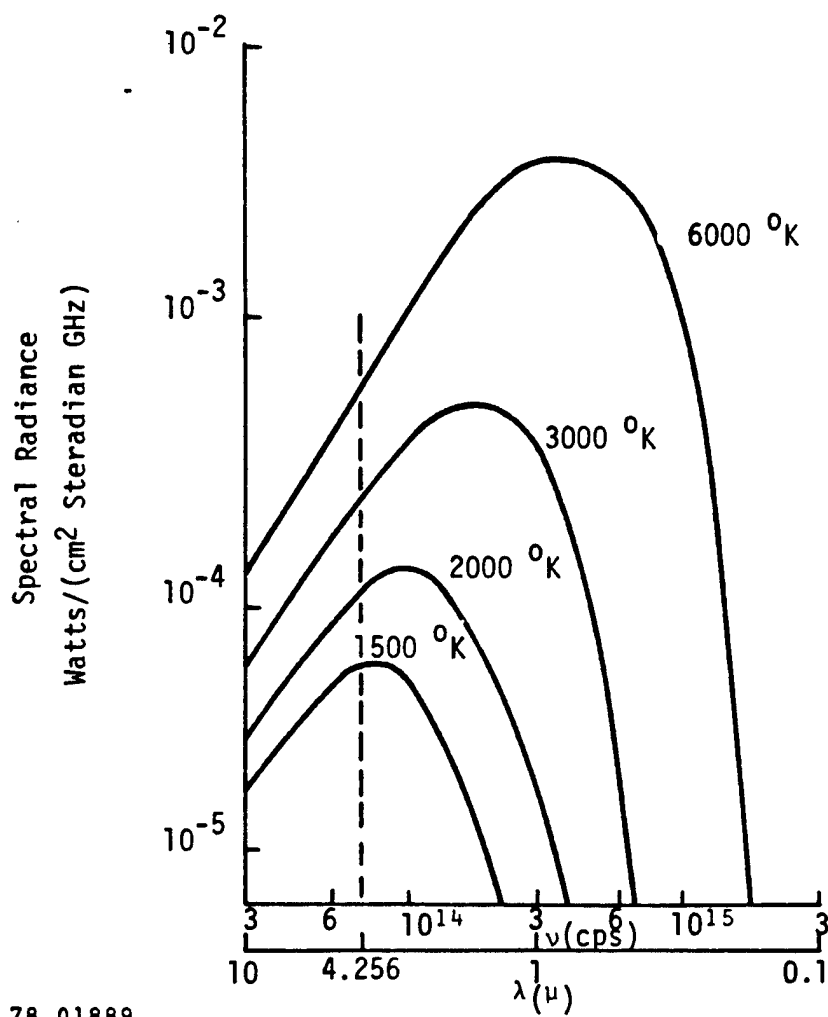


78 01888

Figure 6. Indirect Pumping Via An Intermediate Black Body

and/or resonant transfer of energy to other lasants. In either case, black body temperatures (T_B) of 2000°K to 3000°K seem possible if carbon is used as the cavity material. The advantage of such a system is that in order to maintain a black body spectrum, radiation will be continuously remitted at any frequency which has been depleted due to the selective absorption of the lasant gas. Any radiation not absorbed by the lasant can then be reabsorbed by the cavity walls and used to fill in the absorption hole, rather than being wasted as in the direct absorption case. The efficiency of the black body-method of excitation is primarily a function of the ratio of the laser medium absorption to the black body heat losses, and could in principle be many times that of a directly pumped solar laser.

An examination of Figure 7 reveals that at $T_B = 2000^{\circ}\text{K}$ to 3000°K the black body spectral intensity in the visible region is greatly reduced from that of sunlight ($T_B \sim 6000^{\circ}\text{K}$). The reduction in the infrared (IR) region is not so drastic, however. At 5μ , for example, the spectral intensity at 3000°K is 38 percent of that at 6000°K , whereas at 0.5μ it is less than one percent of the 6000°K radiation. Since the solid angle of exposure of the lasant gas approaches 4π in the indirect pumping scheme (rather than being limited by the f number, as in direct pumping) this reduction in the intensity of the IR pumping radiation can be compensated for by the increased solid angle of exposure of the gas. Thus, optical pumping in the IR region ($\lambda > 1.5\mu$) may be better when accomplished via an intermediate cavity. The lasants shown earlier in Table 3 are possible candidates for this approach. The successful application of this concept may be the best way of achieving high efficiency for solar pumped lasers.



78 01889

Figure 7. Blackbody Spectral Distribution at Selected Temperatures. The fundamental absorption band of CO₂ is indicated on the wavelength scale at 4.256 μ .

2.3.1 Definitions of Efficiencies

The solar radiation spectrum outside the earth's atmosphere is well approximated by a black body distribution function in which the characteristic temperature is about 5785 °K.⁴² There are some minor irregularities in the spectrum, but these anomalies affect the main part of the energy spectrum very little. At earth orbit, the solar flux is well known to be about 0.14 W/cm,⁴³ which ultimately provides the energy source with which to pump the solar laser system. One can easily compute the necessary collector size for any laser power (P_L) once the overall efficiency (η) of the complete laser system is known, using the expression

$$A = P_L / \eta S \quad (9)$$

where S is the solar flux at earth orbit, and A represents the projected area of the collector. As S and η are relatively small numbers, large collector dimensions are required for powerful laser systems. For this reason it is extremely important to seek high overall efficiency to reduce the collector dimensions and cost. The overall efficiency is a product of component efficiencies, each of which must be estimated, so that the resultant product can be maximized.

The system efficiency, η , may be defined as follows:

$$\eta = (\eta_R \cdot \eta_B \cdot \eta_L \cdot \eta_{DIFF} \cdot \eta_S) \quad (10)$$

where

$$\eta_R = \text{cavity efficiency} = \frac{\text{net power delivered to black body}}{\text{solar power entering the black body}}$$

$$\eta_{\text{DIFF}} = \text{reflector/efficiency} = \frac{\text{solar power entering the black body} + \text{aux. power}}{\text{solar power intercepted by the reflector}}$$

$$\eta_B = \text{spectrum utilization efficiency} = \frac{\text{absorbed power in laser medium}}{\text{net power delivered to black body}}$$

$$\eta_L = \text{laser efficiency} = \frac{\text{laser power out}}{\text{absorbed power in laser medium}}$$

$$\eta_S = \text{component efficiency} = \frac{\text{power entering the black body}}{\text{power entering black body} + \text{aux. power}}$$

Assuming for the moment that η_S is nearly one, η_R will be determined by the interaction of the focussed sunlight with the black body cavity. In particular, the balance between the amount of sunlight admitted through the black body aperture and the flux re-radiated through the aperture must be considered. The aperture number, f , controls the degree to which the sunlight can be concentrated for use in solar pumping; η_{DIFF} depends upon the diffuseness of the edge of the solar intensity distribution, and will be discussed further in Section 3.1.

For an ideal paraboloidal mirror, the maximum value of \bar{F}_{FS}/F_S is 1/4, occurring at rim angle, $\theta_m = 45$ degrees (where F_S and \bar{F}_{FS} are the average flux of radiation at the sun's surface and at the focal spot area A , respectively).¹³ For this value of θ_m , $f = 0.6$. Aperture

numbers less than this are unnecessary as they result in aberrations thereby preventing further concentration of light. Larger f numbers pose no optical problems, but the resultant solar flux at the focal spot is decreased.

2.3.2 Heat Losses

Unwanted heat losses in the system are: (1) re-radiation heat losses through the holes in the black body cavity (e.g., insertion point for the solar flux), (2) heat losses from the outer walls of the intermediate cavity to space, and (3) undesirable absorption in the laser medium and its containment walls. The first can be minimized by a high concentration of sunlight via low f -number optics, and low intermediate black body temperature. Assuming black body re-emission, the heat lost through the coupling hole is $A\sigma T_B^4$, where T_B is the intermediate body temperature. The efficiency η_c can then be taken as

$$\eta_R = \frac{P_{in} - P_{re-emit}}{P_{in}} = 1 - \frac{A\sigma T_B^4}{\bar{F}_{FS}A} \quad (11)$$

Using equation (11) and taking the maximum value of $\bar{F}_{FS} = \frac{1}{4}\pi T_s^4$ gives the optimum reflector efficiency,

$$\eta_R|_{opt} = 1 - 4 \left(\frac{T_B}{T_s} \right)^4 \quad (12)$$

These results are given in Table 4.

At a cavity temperature equal to 3000°K , the re-radiation loss becomes significant, while for lower temperatures, the re-radiation losses are quite small. If this were the only loss mechanism, the utilization of the sun's energy for pumping could be as high as 98 percent for $T_B = 1500^{\circ}\text{K}$.

The heat lost to space via heat conduction or other radiation losses can be controlled by using effective insulating material and radiation shields. Preliminary calculations using carbon felt as an

insulating agent together with an external boundary at an emissivity of 0.1 shows that 20 to 30 cm of felt will reduce the conduction heat loss to well below re-radiation losses associated with η_R . Further reduction is possible with more insulation. Carbon felt is very light and is not a serious weight penalty.

Table 4
Optimum Coupling Efficiency vs. Body Temperature

T_B	3000°K	2500°K	2000°K	1500°K
$\eta_R _{\text{opt}}$	0.712	0.862	0.944	0.982

The third loss mechanism is absorption in the walls of the laser tubes. For the static gas system, this loss will be in the walls of the laser cavity itself, and would result in two significant effects: (1) it reduces the efficiency of the indirect approach by wasting energy, and (2) it causes heating of the laser tube and hence the gas mixture, requiring that a coolant be flowed through the system. The same effects manifest themselves in the flowing system with two principal modifications: (1) the premature lasing of some of the gas before reaching the laser cavity will result in additional losses even if the duct to the laser cavity is highly reflective, and (2) the laser gas containment walls are cooled by the flowing gas itself. In either case, additional demands will be made upon the heat rejection system. In order to minimize these demands, materials which are highly transparent to the radiation in the black body cavity must be found. Figure 8 shows the transmission curves of thin samples of some possible optical materials. (By "thin" it is meant that bulk absorption of the passed radiation has not become an important effect). Alkali metal salts have very desirable optical properties (being transparent through the entire range of useable wavelengths) but they are rather difficult to handle. Sapphire and MgO

suffer from the opposite problem, being very sturdy but optically inferior, while ZnSe is rather strong and moderately transparent. The fractional heat lost through absorption can be estimated by assuming complete absorption beyond a transmission cut-off frequency or wavelength (λ_c^1) and comparing it with the flux over all wavelengths. At long wavelengths, this gives the approximate expression, using the Rayleigh-Jeans formula for B_v

$$\frac{P_{\text{ABS}}^{\text{IR}}}{\text{Heat flux}} = \frac{\pi \int_0^{\nu_c} B_v d\nu}{\sigma T_B^4} = \frac{2\pi}{3} \frac{kc}{\sigma} \left(\frac{1}{\lambda_c^1 T_B} \right)^3 \quad (13)$$

This is nontrivial as it is a broadband loss. Fortunately, however, it is significant only in the far IR at which point the specific intensity is falling off quite rapidly. Just being able to double the wavelength at which absorption effectively occurs reduces the heat load by nearly an order of magnitude, a very desirable effect. Reflections and scattering by the laser tube represent no real losses to the system.

At the UV and visible wavelengths, absorption may also be a problem. In this case, it can be shown for wavelengths shorter than the visible cutoff wavelength, λ_c^v that the fractional absorption in the visible is

$$\frac{P_{\text{ABS}}^v}{\text{Heat flux}} = \frac{2\pi}{3} \frac{kc}{\sigma} \left(\frac{1}{\lambda_c^v T_B} \right)^3 e^{-X} \left[3 + \frac{9}{X} + \frac{18}{X^2} + \frac{18}{X^3} \right] \quad (14)$$

where $X = hc/\lambda_c^v kT$. Table 5 shows the sum total of the fractional absorptions for the materials shown in Figure 8 ignoring reflection effects.

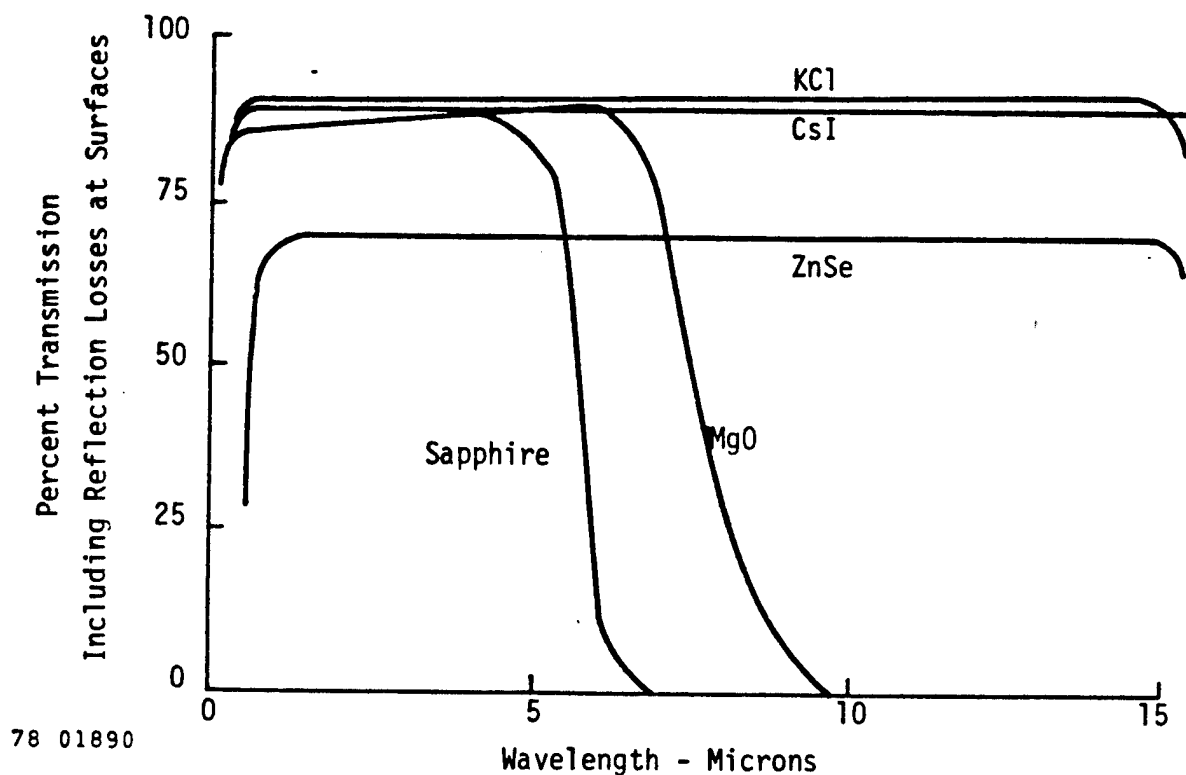


Figure 8. Transmission of Various Optical Materials

Table 5

Fractional Absorption Losses Associated with Transparent Materials
Versus Black Body Temperature

	$\lambda_c^I(\mu)$	$\lambda_c^V(\mu)$	3000°K	2500°K	2000°K	1500°K
Sapphire	6	0.25	0.0266	0.0461	0.0904	0.2116
ZnSe	16	0.55	0.0260	0.0096	0.0057	0.0112
KCl	20	0.25	$7.27(10^{-4})$	$1.28(10^{-3})$	$2.45(10^{-3})$	$5.64(10^{-3})$
CsI	48	0.35	$6.61(10^{-4})$	$1.6(10^{-4})$	$1.78(10^{-4})$	$4.23(10^{-4})$
MgO	8	0.55	0.0359	0.0269	0.0390	0.0881

2.3.3 Absorption Bandwidths of Laser Media

In contrast to bound-free transitions, bound-bound transitions are usually quite narrow. Considering CO_2 as an example, the net bandwidth due to a Doppler-broadened absorption spectrum can be estimated. Normal CO_2 has P and R branches about 15 lines/branch (every other rotational quantum number) giving rise to about 30 lines. For the static gas case, each line located at approximately 4.3μ is fractionally broadened to give a total effective bandwidth of about $4.4(10^{-4})\mu$. The fraction of the total flux/area that is useful in optical pumping is about

$$\frac{P_m}{\text{Heat Flux}} \approx \frac{\pi f B_v d\nu}{\sigma T_B^4} = 2.5(10^{-5}) \text{ at } 2000^\circ\text{K} \quad (15)$$

where P_m refers to the absorption in the laser medium. This is an extremely small fraction and indicates the need for an improvement as system losses may still dominate in line or band spectra. There are a number of ways to improve the effective bandwidth that should be considered. One way is to increase the pressure above 10 torr and thus collisionally broaden each line. At 1000 torr, for example, many IR bands would have approximately 100 times their Doppler-broadened line-width. Additional absorbers, either different molecules or isotopes of the same molecular system, may be used which can efficiently transfer their absorbed energy by collisions. These ideas are incorporated into the flowing gas laser system, which has a calculated fraction of useful flux/area of

$$\frac{P_m}{\text{Heat flux}} \approx 0.01 \text{ to } 0.04 \text{ between } 2000^\circ\text{K and } 3000^\circ\text{K}. \quad (16)$$

Lastly, overtones and hot bands of molecular systems may contribute to the pumping.

In summary, suitable broadening mechanisms may exist to extend the effective band utilization of a black body radiation over that of a

simple Doppler-broadened system. Of course, the above suggestions apply equally well both to the conventional directly pumped case and to the indirectly pumped case.

2.3.4 Energy Balance and Potential Efficiency

The use of simple energy balances permits estimation of the potential efficiency of the system. Taking into account various forms of heat in the system gives for a heat balance

$$P_{in} = P_{Re-emit} + P_{cond} + P_m + P_T + P_{DIFF} \quad (17)$$

where P_{in} = power collected by the solar mirror

$P_{Re-emit}$ = re-emission from the black body at temperature T_B through the coupling hole area

P_{cond} = heat lost via conduction

P_m = the absorption by the laser medium

P_L = Laser power out

P_T = total power absorbed by optical materials, etc.

P_{DIFF} = Power lost due to the diffuseness of the edges of the focussed solar radiation

This may also be written in terms of efficiencies as

$$P_{in} = (1 - \eta_R \eta_{DIFF}) P_{in} + \alpha P_m + P_m + P_T \quad (18)$$

where α is the factor, P_{cond}/P_m . The quantity η_{DIFF} can be approximated by assuming a gaussian intensity distribution for the focussed radiation by determining the fraction of distribution that would be passed by a circular aperture of radius r centered at the maximum of the intensity distribution (see Section 3.2: Figure 19 illustrates schematically how η_R , η_{DIFF} and $\eta_R \eta_{DIFF}$ vary with r for the above assumptions). Defining an efficiency

$$\eta' = \frac{P_L}{P_{in}} = \frac{\eta_L P_m}{P_{in}} = \frac{\eta_L P_m}{\frac{1}{\eta_{diff} \eta_R} [(1 + \alpha) P_m + P_T]} \quad (19)$$

gives

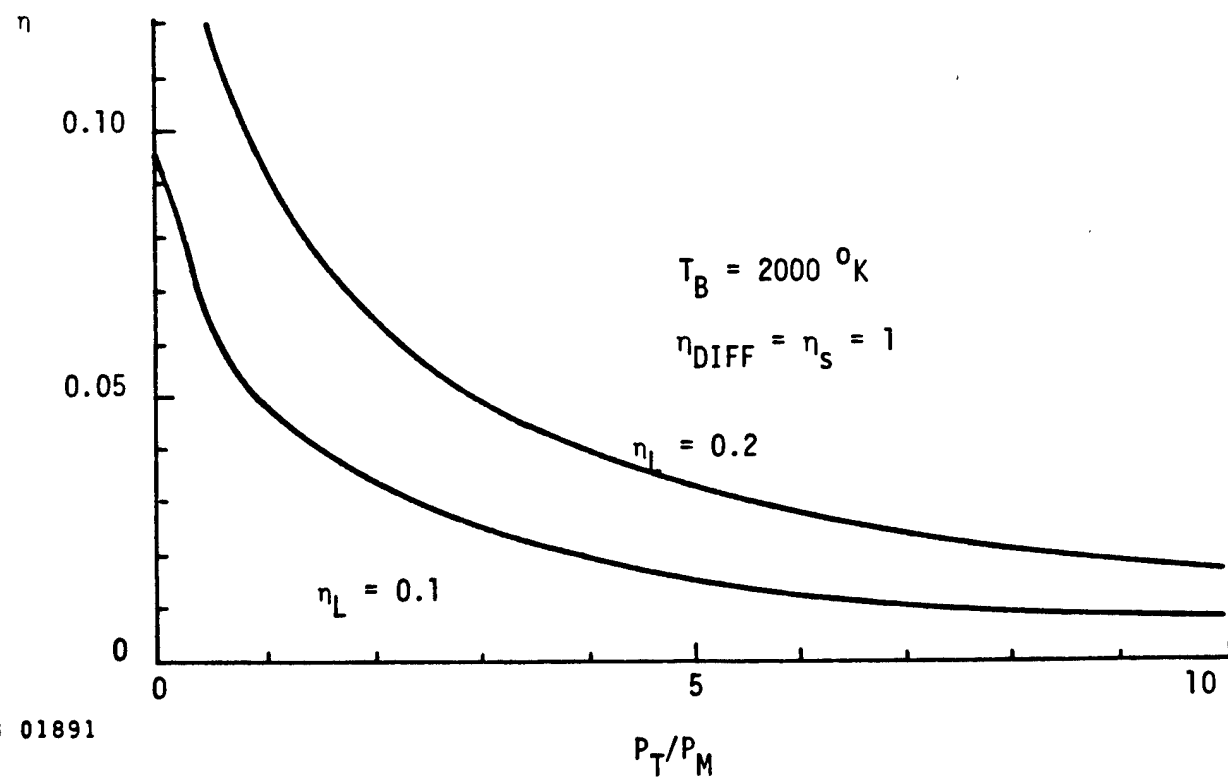
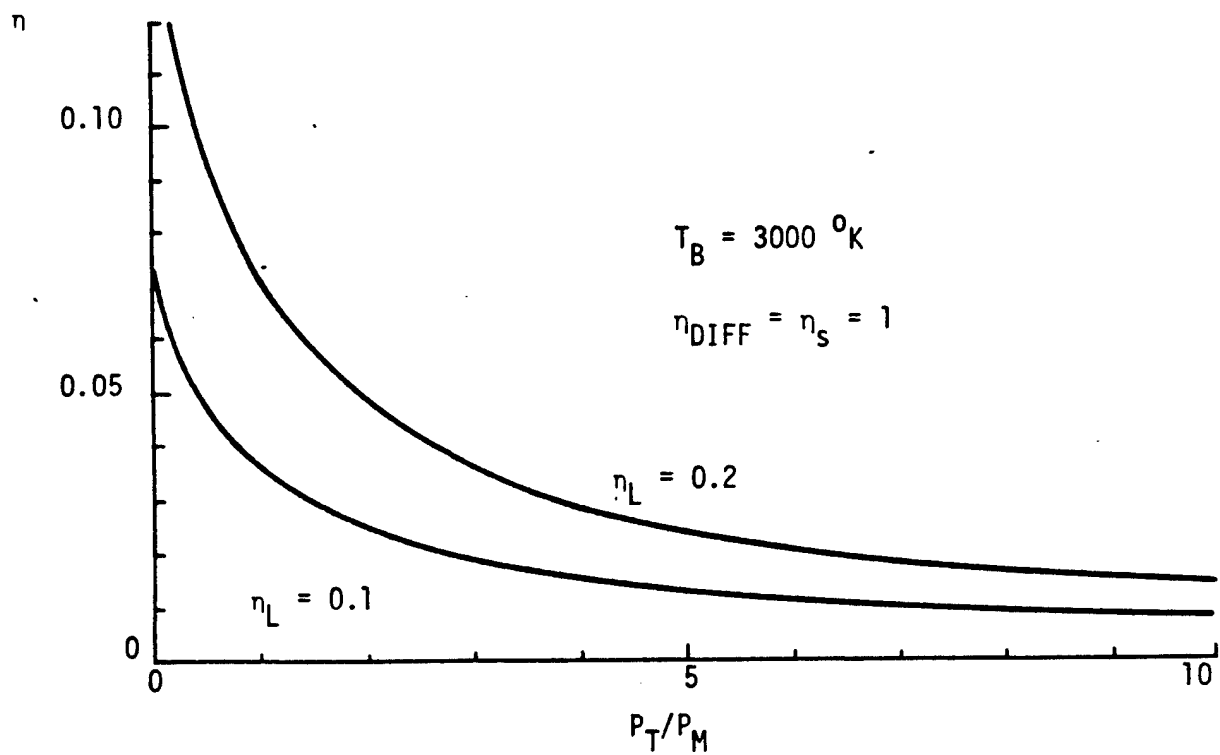
$$\eta' = \frac{\eta_{diff} \eta_R \eta_L}{(1 + \alpha) + P_T/P_m} \quad (20)$$

If α can be made negligible by thermal insulation, η' then becomes

$$\eta' = \frac{\eta_{diff} \eta_R \eta_L}{1 + P_T/P_m} \approx \eta \text{ if } \eta_s \approx 1 \quad (21)$$

It is immediately clear that the efficiency of the system will not only be determined by the collector and laser conversion efficiencies, but also by the ratio of the power absorbed by the laser gas containment walls to that of the medium. In other words, if the loss in these walls is the dominant absorption loss, the efficiency will be low as most of the energy is going to heat the walls. For this reason it is important to obtain very transparent optical wall material and arrange to have the laser medium absorb over as wide a range of bandwidths as possible. Figure 9 shows η as a function of P_T/P_m for two body temperatures and η_L 's. The difference between the two temperatures is due to the differences in η_R which was taken as the optimum case. One can readily see that if P_T/P_m can be on the order of one that η will be large. Even if $P_T/P_m = 10$, η may be on the order of one to two percent. As each laser system will be different, no concrete values of P_T/P_m are assigned. Because of the small bandwidth of the usual absorbers, it will be difficult to get small values of P_T/P_m although values near one may be obtainable.

The preceding calculations apply both for the static and flowing gas systems with the exception that the approximate equality between η' and η (Equation 21) would probably not be valid for the flowing system. The power delivered to the auxiliary equipment in the flowing gas system is probably a significant loss. The magnitude of P_m however, would also be expected to be larger in the flowing gas case, as was demonstrated previously. The balance between these two factors as well as detailed cooling and structural considerations will be investigated in Section 4.



78 01891

Figure 9. Efficiency vs P_T/P_M

By carrying out an energy balance on an optically pumped system without using an intermediate body, one can compare the improvements in performance of the system. For the conventional system,

$$P_{in} = P_m + P_T + P_{TR} \quad (22)$$

where P_{TR} = the power focussed through the system that is not absorbed and hence wasted. The overall efficiency of this system, η'' , is defined by

$$\eta'' = \frac{P_L}{P_{in}} = \frac{\eta_L}{P_{in}/P_m} = \eta_L \epsilon \quad (23)$$

where ϵ = the fraction of sunlight that is used in pumping the optical medium only. This is related to $\pi/B_v dv/\sigma T_s^4$ for a surface calculation. (Recall that for a simple system ϵ is on the order of 10^{-2} to 10^{-4}). Therefore

$$\frac{\eta'}{\eta''} = \frac{\eta_R \eta_L \eta_{DIFF}}{(1 + P_T/P_m) \eta_L \epsilon} = \frac{\eta_R \eta_{diff}}{(1 + P_T/P_m) \epsilon} \quad (24)$$

Since $(\eta_R \eta_{DIFF})$ is of the order of unity and assuming P_T/P_m is small, the improvement is seen to be $\frac{1}{\epsilon}$. As P_T/P_m may be sensibly larger than one, this ratio may not be obtained, but the combination of the factors may still be much greater than 1. The value of η_s should be approximately the same in either case.

2.3.5 Choice of Lasants

The use of an IR laser system is contingent upon the ability of the laser to reach threshold when indirectly pumped. The pure CO laser, the CO-CO₂ mixing laser, and the pure CO₂ laser systems are all well studied, and all show promise of meeting this criterion. In addition to reaching threshold the laser system chosen should have as large a gain and laser efficiency as possible. Calculations have therefore been performed for these quantities, the results of which will be presented below.

Pumping calculations for the lasant were performed for Lorentz and Doppler line shapes and two geometries (infinite slab and infinite cylinder). Results for the cylindrical geometry show slightly more uniform pumping throughout the volume of the gas; however the differences from the slab geometry were not great. Therefore, for calculational ease the slab geometry was used to find the best possible thickness. All calculations assumed that $T_{\text{gas}} = 300^{\circ}\text{K}$ and that the black body radiation incident from all 2π steradians passes through every point on each surface of the slab. An integral over frequency was then performed for the product of the black body energy spectrum (minus any energy previously absorbed) and the absorption coefficient of the medium under consideration. The calculation accounted for the absorption at each point along the path of each ray from both sides of the slab, thus giving rise to the values tabulated in Table 6.

Table 6
Absorption of Black Body Radiation by Lasants

Partial Pressure in Torr of:			Slab Thickness L(cm)	Blackbody Temperature $T_B(\text{k})$	Number of Isotopes	P_{abs} (watts/cm ³)	
CO	CO ₂	He				Edge	Center
72 ⁽ⁱ⁾	4	0	3	2000	6-1	0.754	0.172
72	4	0	10	2000	6-1	0.722	0.0807
10*	0	0	1	2000	1	0.064	0.0044
0	10	0	1	2000	1	0.627	0.030
0 ⁽ⁱⁱ⁾	12	12	1	2000	12-1	0.831	0.268
0	12	12	1	3000	12-1	1.761	0.569
760	0	0	3	2000	6	5.25	1.36

*Doppler-broadened (all other cases Lorentz-broadened).

Using the information in Table 6 and assuming saturation of the lasant, the gain per meter (g_0) and laser efficiency (η_L) were computed for the cases labeled (i) and (ii) above.

Case (i) $g_0 = 0.03/\text{m}$ $\eta_L = 25$ percent

Case (ii) $g_0 = 0.067/\text{m}$ $\eta_L = 35$ percent

The cases finally considered for the actual laser systems are not always identical with those tabulated above. There are relatively simple methods for obtaining the appropriate quantities when the pressure, number of isotopes or T_B is changed, however. Increasing the pressure results in collisional broadening of the absorption lines, which increases the volumetric pumping rate. The difference between absorption by CO_2 at 10 torr and 1000 torr, for instance, is a factor of 100. The effect of changing T_B is to change the intensity of the black body radiation at frequency ν , B_ν , and thereby change the amount of power being absorbed by a factor of $\frac{B_\nu(T_B)}{B_\nu(T_0)}$ from the original absorption at T_0 . The effect of introducing a number of isotopes was assumed to be a simple scaling of the absorbed flux with that number. The use of 12 isotopes of CO_2 results, under this assumption, in 12 times the power being absorbed by a single isotope. Although the possibility of overlapping spectral lines makes this assumption not quite valid, overtones (which are not explicitly considered) should compensate for any overestimates made in this calculation. Almost all of the numbers used in the calculations to follow are derived from those of Table 1 in accordance with the procedures outlined above except in the case of the pure CO system at $3/4$ atm and $T_{\text{gas}} = 125^\circ\text{K}$. In this case, a laser efficiency of $\eta_L \approx 50$ percent was assumed on the basis of EDL results. This case was not originally considered to be a competitive system due to its low operating temperature, and was added to the systems under consideration only after it became apparent from preliminary calculations that it is roughly as competitive as the mixing gas system. The mixing gas system was also chosen to have an efficiency

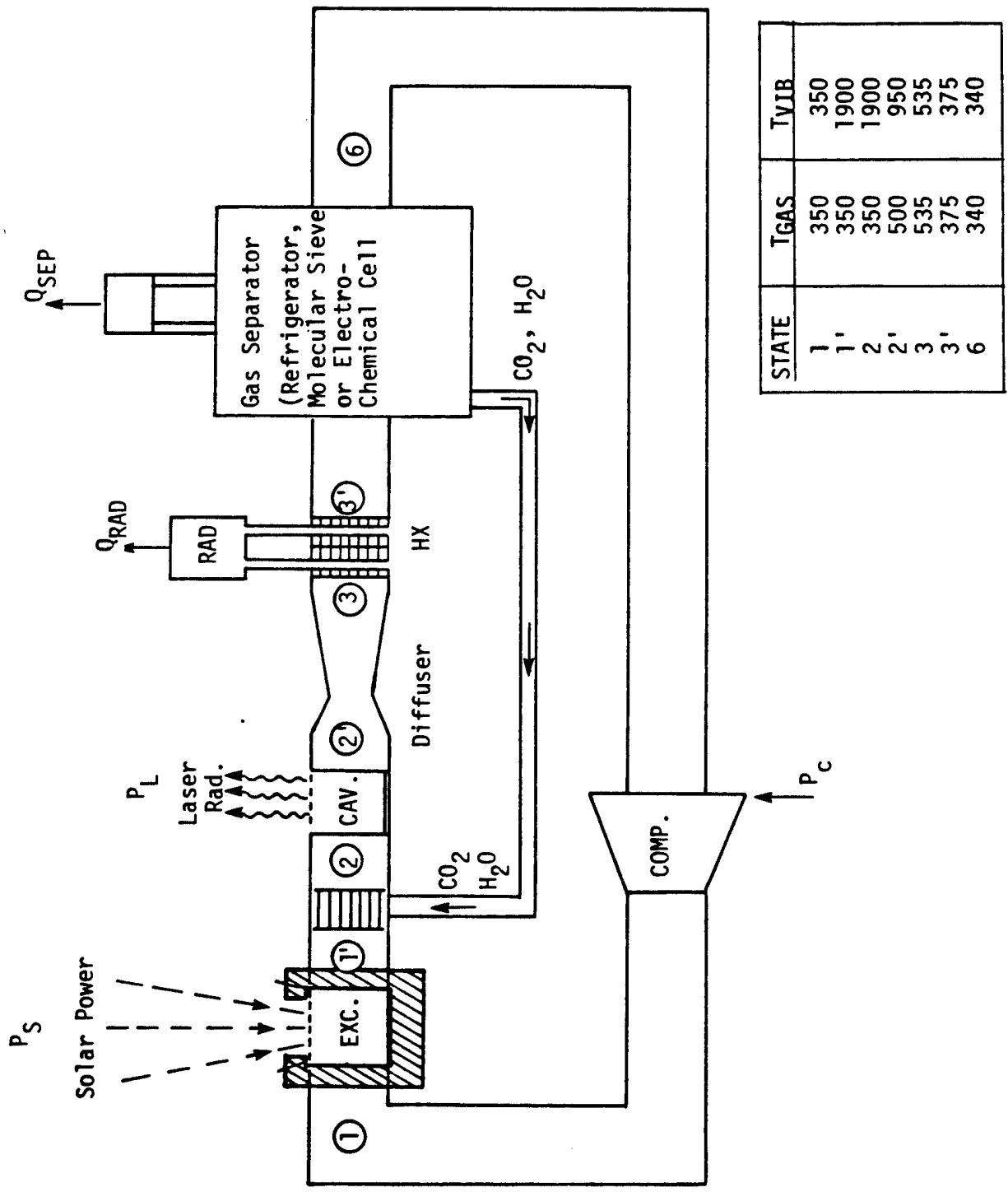
of $\eta_L = 30$ percent, and is assumed to operate at $\sim 3/4$ atm and at $T_{\text{gas}} \sim 350^\circ\text{K}$. The CO_2 static laser is assumed to operate at 36 torr with 18 isotopes of CO_2 , some of which are radioactive with long half lives. This system has an approximate efficiency of $\eta_L = 30$ percent, too.

2.3.6 Three Laser Concepts

Before discussing specific components of the individual laser systems under consideration the difficulties associated with active cooling of lasants should be mentioned. The use of refrigerators has been contemplated since several of the competing systems operate at very low temperatures or use cryogenic gas purification procedures. The major problem with active refrigerators is the fact that the refrigerator sizes contemplated for these systems are large even by terrestrial standards. An estimate was made for the mass of a Stirling cycle refrigerator of the Philips type which would handle 2×10^6 watt of cooling between 125°K and 350°K . This refrigerator would have a mass of between 10^4 and 2×10^4 Kg according to the estimates made, and would require approximately 5×10^5 watts to power it.⁴⁴ A Lockheed estimate for a similar system provides an estimate of 2.5×10^4 to 4×10^4 Kg⁴⁵ with comparable efficiency. Turbine systems were also considered, however they are very inefficient over the required temperature range. The probability of actually constructing such a system, even in a 1990 time frame, is not great. A more realistic approach would be to place a number of smaller refrigerators in a series to form a cascade system, except that such systems are prone to failure. If twenty 10^5 watt refrigerators were used, for instance, each one having a 95 percent chance of running for three years without failure, there would be only a 36 percent chance that the entire system would run for three years. In view of these difficulties it was decided that passive cooling of the system is desirable.

2.3.6.1. CO_2 Mixing Gas Laser

The mixing gas laser system (Figure 10) is the most complicated of the systems to be considered. In this system CO gas is excited by



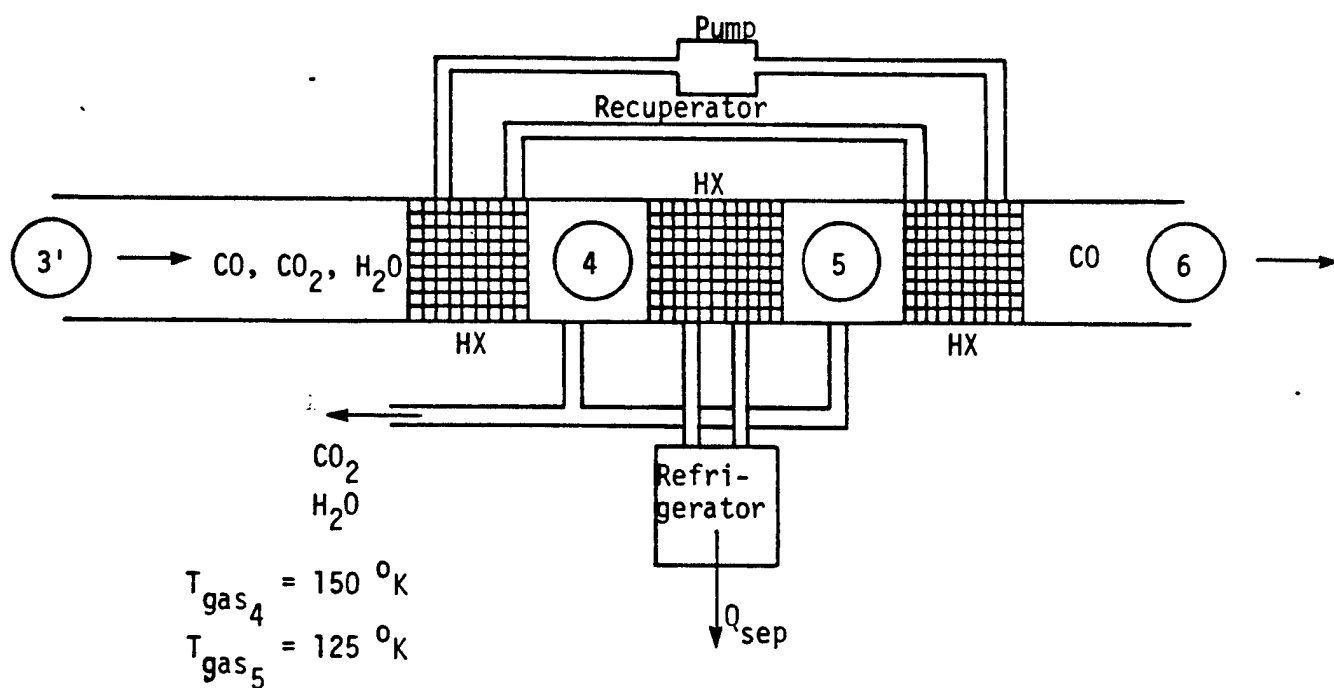
78 01892

Figure 10. Solar Pumped Mixing Laser

flowing it through the black body. After emerging from the black body, the gas is mixed with CO_2 and H_2O catalyst, the excitation energy is transferred to the CO_2 , and the gas mixture is transferred to a laser cavity where it lases. After lasing the CO_2 and H_2O catalyst must be removed from the CO gas before the CO can begin the cycle anew. There are three feasible means of accomplishing this separation; refrigeration (active or passive) absorption beds, and electrochemical cells.

Most of the difficulties with active refrigeration have been mentioned previously. Since it is necessary to obtain a gas temperature of 125°K in order to obtain the required gas purity, passive refrigeration requires very large radiator areas. This increases the danger of meteorite damage and the mass of the radiator (see Section 3); however, it is extremely simple and reliable if properly shielded. A recuperator may be used to decrease the cooling requirements (Figure 11).

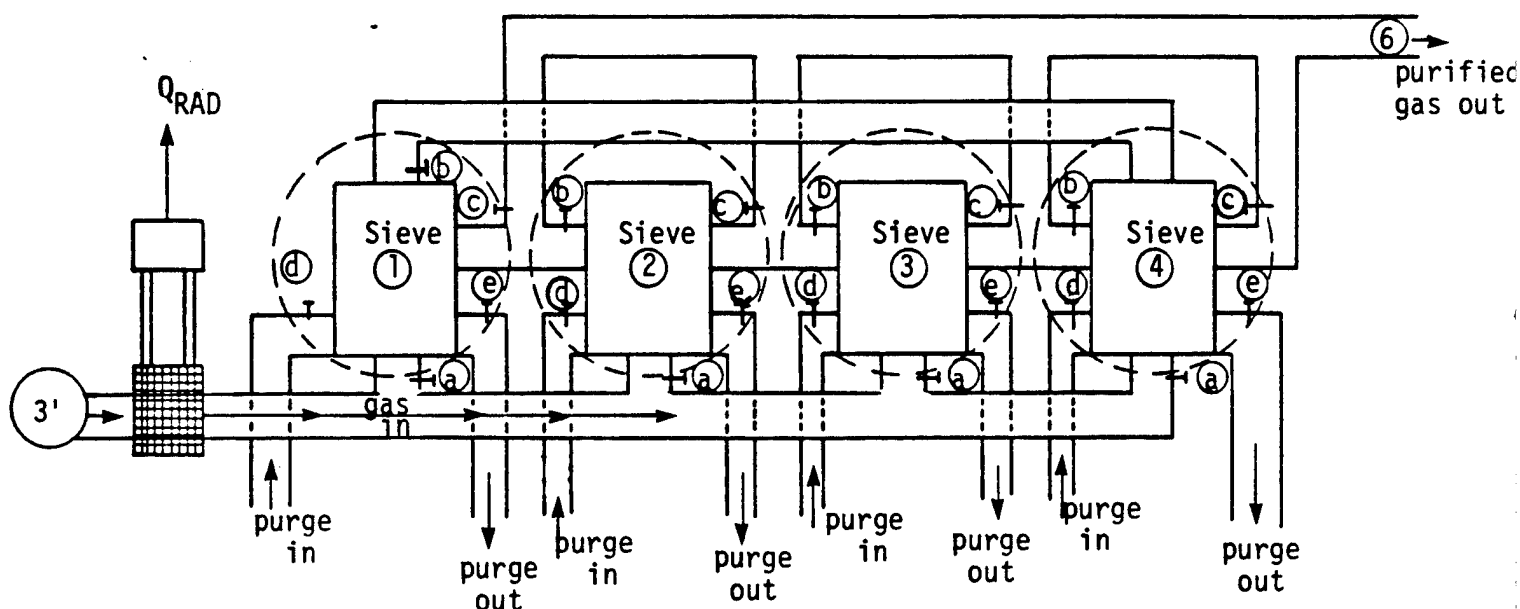
The absorbent bed approach has a number of uncertainties associated with it. The most important of these is the question of how quickly a bed may be purified for reuse. Calculations involving four Linde molecular sieves (Type 4-A) in the configuration depicted in Figure 12 indicate that a mass of approximately 1.5 mt of sieve is required, where \dot{m} is the gas flow through the black body and t is the amount of time required to purify a sieve from 28 torr partial pressure of CO_2 and 1.4 torr H_2O to 0.01 torr of each. Larger fractions of CO_2 and H_2O would cause serious de-activation of CO before it reaches the laser cavity. For values of $\dot{m} \approx 20$ kg/sec, $t \leq 100$ sec yields acceptable masses if molecular sieves are used to purify the water and CO_2 out of the CO stream. This system would eliminate the necessity of a regenerative heat exchanger as well as the inconvenience of handling solid CO_2 and ice. In order to purify the beds they could be heated with gas from Stage 3 of Figure 10 and then be pumped down. If t must significantly exceed 100 sec, the mass of the sieves will probably be prohibitive.



78 01893

Figure 11. Recuperated Refrigeration Scheme for CO_2 , H_2O removal

The use of an electrochemical cell⁴⁶ is also a possibility. The use of such a cell introduces a number of complications to the system (Figure 13), however the possibility of recovering some of the energy needed for the gas separation as electrical energy makes this penalty less severe. This system requires O_2 to be circulated with the CO_2 and H_2O , and still requires a dessicant for water removal from the CO stream. This dessicant would weigh much less than the molecular sieves of the previous paragraph, but could still be quite massive. It is difficult to estimate the mass and effectiveness of this system as it is still in the developmental stages.



Stage 1 = 5.17% CO_2 + .0031% H_2O (by weight)

Stage 2 = $C_1\%$ CO_2

Stage 3 = $C_2\%$ CO_2 (Note: $C_2 = 0$ may be required for cooling time)

Stage 4 = cleansing cycle

		Stage 1	Stage 2	Stage 3	Stage 4
78 01894	$0 < t < \tau$	Sieve 1	Sieve 2	Sieve 3	Sieve 4
	$\tau < t < 2\tau$	Sieve 2	Sieve 3	Sieve 4	Sieve 1
2	$2\tau < t < 3\tau$	Sieve 3	Sieve 4	Sieve 1	Sieve 2
3	$3\tau < t < 4\tau$	Sieve 4	Sieve 3	Sieve 2	Sieve 1

τ = time required to cleanse a sieve

$M_{\text{Total}} = 38.8 + \text{pipes and valves}$

Figure 12. Cascaded Molecular Sieves for H_2O , CO_2 Removal

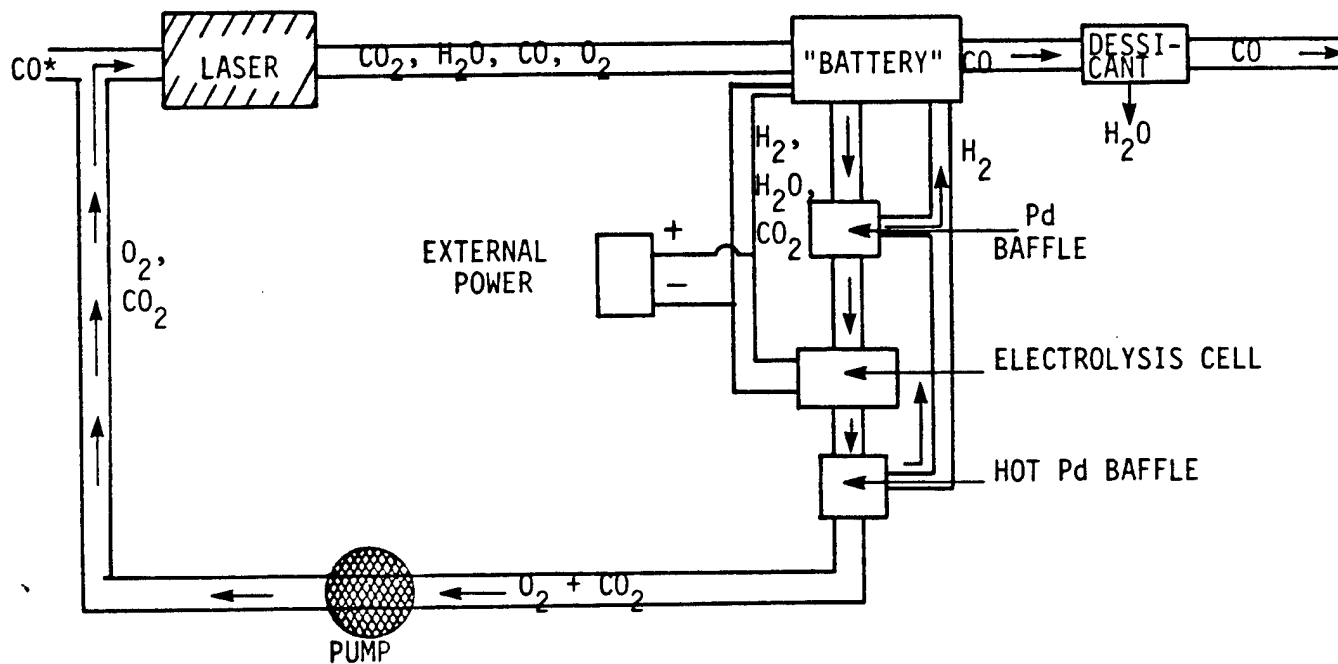
In addition to the gas purification apparatus, the mixing laser requires a mixing system and a method for rapidly transferring the mixed gas into a laser cavity. These processes both involve pressure drops in the system and an increase in pumping requirements. The laser cavities themselves may either be placed directly after the mixing nozzles (in which case there will be many cavities) or sufficiently far down stream that the cavities may be consolidated into one or a few.

The black body itself and the methods for containing the gas in it will be discussed in later sections.

2.3.6.2 CO₂ Static Laser System

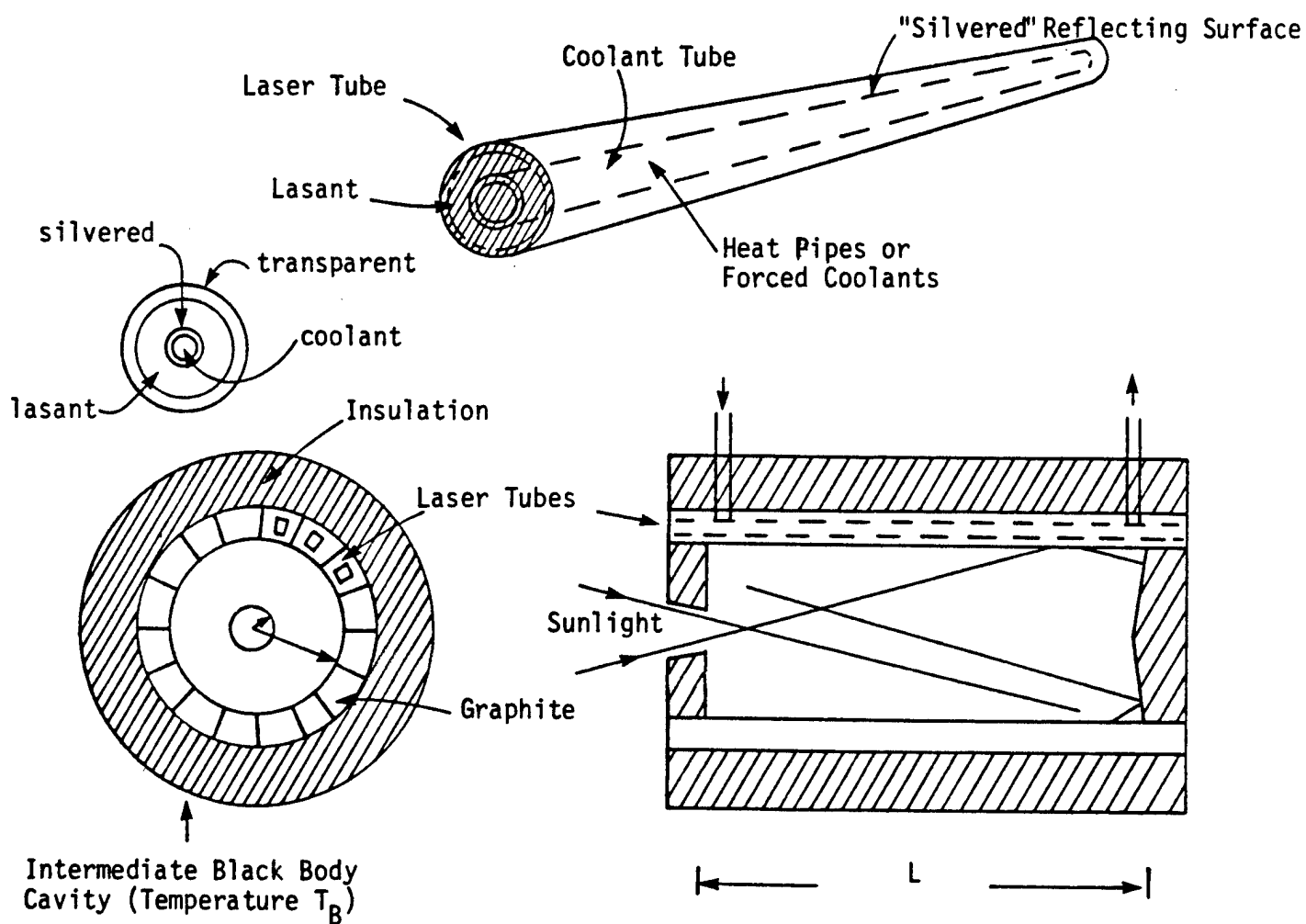
The use of a static lasant gas is the simplest approach to black body mediated pumping. In this scheme the laser cavities are placed inside the black body (see Figure 14). The gas inside the laser tubes is pumped by means of the radiation in the black body (characterized by a temperature T_B) and the laser radiation from each laser tube cavity emanates from the end of that cavity after first passing through an annular lens. The laser light is focussed through a very small hole in the black body wall, and collected again by an identical lens outside the black body cavity. A coolant must be circulated down the center of the laser tube to insure that the gas furthest from the coolant is adequately cooled (Figure 14). The coolant could be a liquid or gas circulated through the center pipe; the center pipe could also take the form of a "heat pipe."^{47,48} In addition to this, a very slow flow of the lasant gas could be produced, or a slow rotation could be imparted to the satellite. This would cause axial convective cooling in the former case, or azimuthal convection in the latter, thus increasing the heat transfer rate and keeping the gas cooler.

If CO₂ is used as the lasant, the gas can be kept at 350 to 400°K. This decreases the radiator area required for cooling considerably if the



78 02175

Figure 13. Electrochemical Cell for H_2O , CO_2 Removal



78 08583

Figure 14. CO₂ Static Solar-Pumped Laser System

heat transfer coefficient between the gas and the coolant is large (meaning that the coolant need be only a few degrees cooler than the desired gas temperature). The most critical aspect of this system is the laser tube walls. Since there is no, or very little, gas flow to cool the walls, they must be very transparent to the incident radiation in order that high temperatures are not developed due to absorption. The walls may be extremely thin in this case, since the CO_2 gas is at very low pressure, which will aid in keeping the walls transparent.

2.3.6.3 CO Flowing Gas Laser

This laser system is similar to the mixing laser system, except that the lasant is now pure CO gas which must be maintained at a temperature of $\sim 125^\circ\text{K}$. There is no need in this system to remove any impurities from the lasant, which reduces the complexity of the system considerably in comparison to the mixing gas system. Furthermore, the laser tubes in this system can be inside the black body itself, as in the static laser case. The pressure of the lasant will be assumed to be $3/4$ atm, and the temperature of the gas will be restricted to the range between 125 and 150°K . The CO gas must remain in the laser tubes for a time sufficient for lasing, then must be flushed out for cooling back to 125°K . Cooling is the critical process in this system, since radiation at 125°K requires large radiator areas.

SECTION 3

COMPARISON TO OTHER LASERS

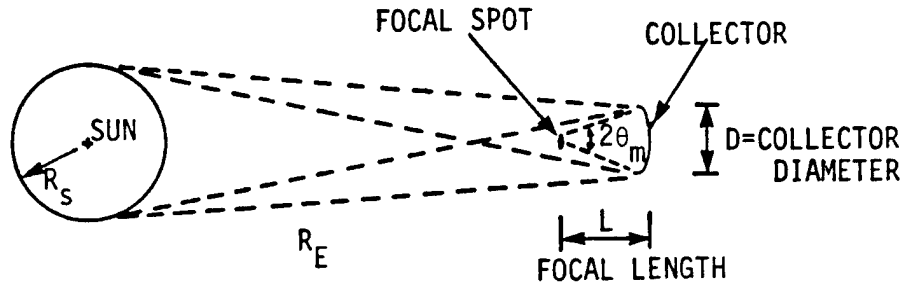
In order to evaluate all three types of laser on an equal basis approximate designs for the collector-concentrator, absorber cavity, heat exchangers, power unit and waste heat radiator are developed below and applied uniformly to each type of laser. These components and the laser system components are also weighed on a uniform basis. Because a choice of specific technology leads to particular weight characteristics, a sensitivity analysis has also been carried out to determine the influence of key components such as the radiator weight and the collector-concentrator weight on the total system weight for each type of laser. The status of current technology required for the three laser types is presented along with an identification of critical areas needing further development.

This section concludes with a comparison of the feasibility and cost-effectiveness of each of the laser types. The CO₂ GDL proves to be the heaviest and most expensive system and the indirect optically pumped laser (IOPL) is the lightest and least expensive. The solar IOPL also employs an acceptable level of technology within the 1990 time frame. For these reasons it has been chosen as the best laser and the conceptual design is selected from those candidates presented in Section 2.

3.1. Collector-Concentrators:

The geometry of the collector is shown in Figure 15. Balancing the energy flux at earth orbit (assuming a collector reflectivity, η_M) leads to⁴³

$$S\pi\left(\frac{D}{2}\right)^2 = F_s \left(\frac{4\pi R_s^2}{4\pi R_e^2} \right) \frac{D^2}{4} = \frac{F_{fs} A}{\eta_M} \quad (25)$$



78 01862

Figure 15. Geometry of Solar Radiation Collector and Optics

where X is the radiation flux at the collector, F_s is the average radiation flux at the sun's surface, F_{fs} is the average radiation flux at the focal spot (area A), D is the diameter of the collector, R_s is the sun's radius and R_e is the earth-sun distance. The focal spot area of a perfect paraboloid collector is ⁴³

$$A = \frac{\pi}{4} \left(\frac{4LR_s}{R_e \cos \theta_m (1 + \cos \theta_m)} \right)^2 \quad (26)$$

where θ_m is the run angle of the collector. Solving for F_{fs}/F_s gives

$$F_{fs}/F_s = \frac{\eta_M D}{16L^2} \cos^2 \theta_m (1 + \cos \theta_m)^2 \quad (27)$$

The aperture number is given by

$$f \equiv \frac{L}{D} = \frac{1 + \cos \theta_m}{4 \sin \theta_m} \quad (28)$$

Thus,

$$F_{fs}/F_s = \eta_M \left(\frac{\sin 2\theta_m}{2} \right)^2 \quad (29)$$

For a simple paraboloid the maximum value of F_{fs}/F_s is $\eta_M/4$ occurring at $\theta_m \approx 45$ degrees. For this value of θ_m , $f = 0.6$. Aperture numbers less than this result in aberrations which prevent further concentration of light. Larger f numbers pose no optical problems, but the resultant solar flux at the focal spot is decreased.

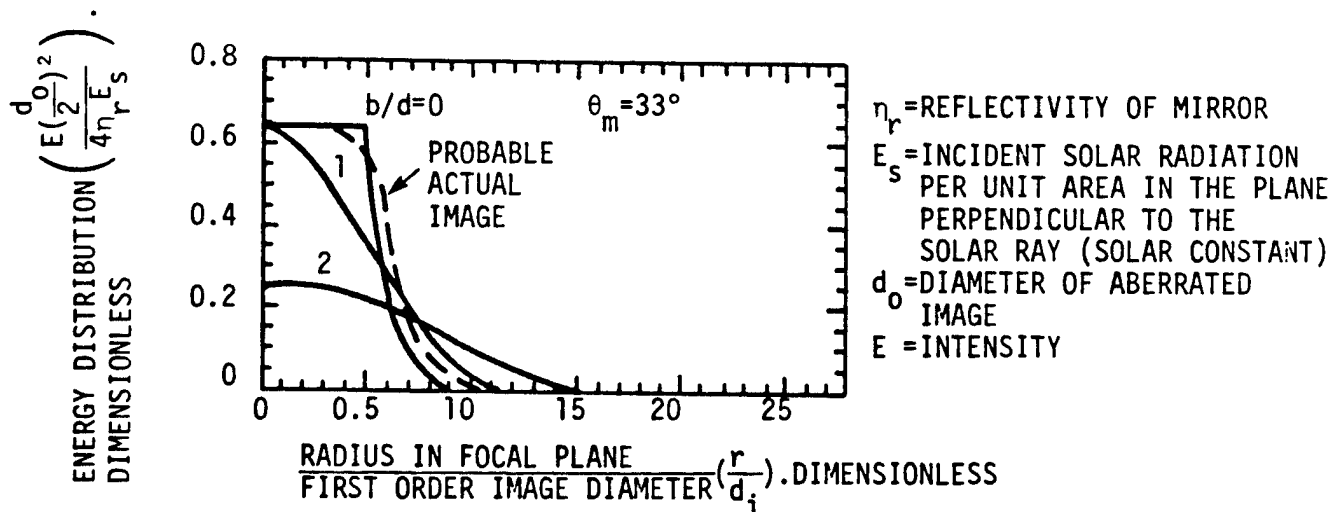
The foregoing analysis applies to a perfect paraboloid and the intensity distribution at the focal plane is shown in Figure 16 for $b/d = 0$. In practice imperfections in the collector surface will broaden and diffuse the intensity distribution at the focal plane, with the consequence that a given size absorber (or cavity aperture) will receive less energy from the collector compared to the perfect case. To compute this effect, consider the maximum angle of deviation of a reflected solar ray from the direction of propagation of the same ray reflected from a perfect parabolic mirror (see Figure 17):

d_i is the size of the first order image, ϕ is the angular diameter of the sun and θ_m is the rim angle of the mirror. Then the ray will be incident upon the focal plane a distance

$$\frac{b}{2} = \frac{2\alpha d}{\phi \cos \theta_m \cos(\frac{\theta_m}{2})} \quad (30)$$

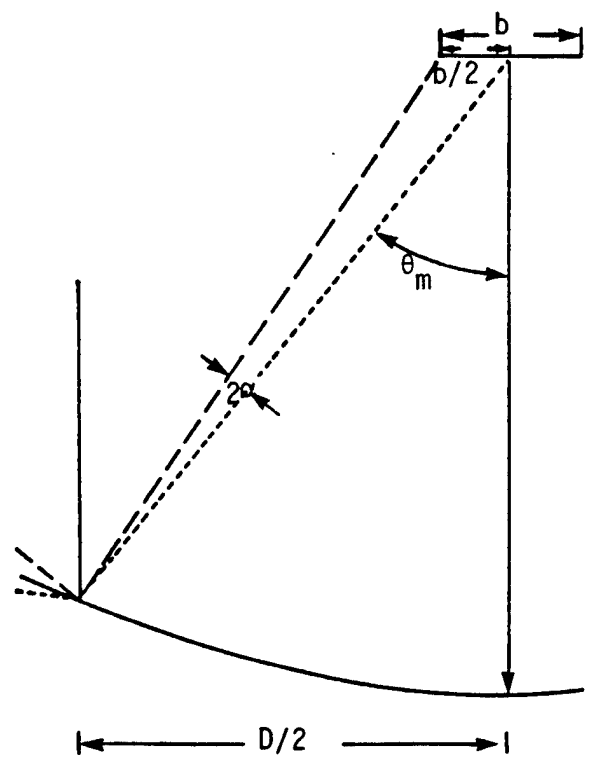
from the center of the first order image (Figure 17).

The deviation of the mirror from a perfect paraboloid may occur due to facetting or distortions resulting from imperfect construction of the mirror. While the quantity $\frac{b}{d_i}$ can be made much smaller than 1 it



78 01883

Figure 16. Energy Distribution Versus Radius in Focal Plane⁴³



78 01884

Figure 17. Geometry of Mirror Imperfections of Order α for Rim Angle, θ_m , and Mirror Diameter, D .

will not be possible to make it zero. This will result in an energy distribution similar to $\frac{b}{d} = 0$ in Figure 16 but rounded to begin approaching the $\frac{b}{d} = 1$ case. If this shape is approximated by a gaussian, efficiency calculations may be carried out in closed form.

Assuming a gaussian with width parameter "a" (Figure 18) the finite aperture-diffuse image losses can be quantified by means of the quantity

$$\eta_{\text{diff}} = \frac{\text{flux into aperture}}{\text{total flux reflected from mirror}}$$

With a gaussian peak, this becomes (where r is the aperture radius)

$$\eta_{\text{diff}} = \frac{\int_0^{r/a} e^{-\frac{1}{2}\left(\frac{x}{a}\right)^2} \left(\frac{x}{a}\right) dx}{\int_0^{\infty} e^{-\frac{1}{2}\left(\frac{x}{a}\right)^2} \left(\frac{x}{a}\right) dx} \quad (31)$$

Since

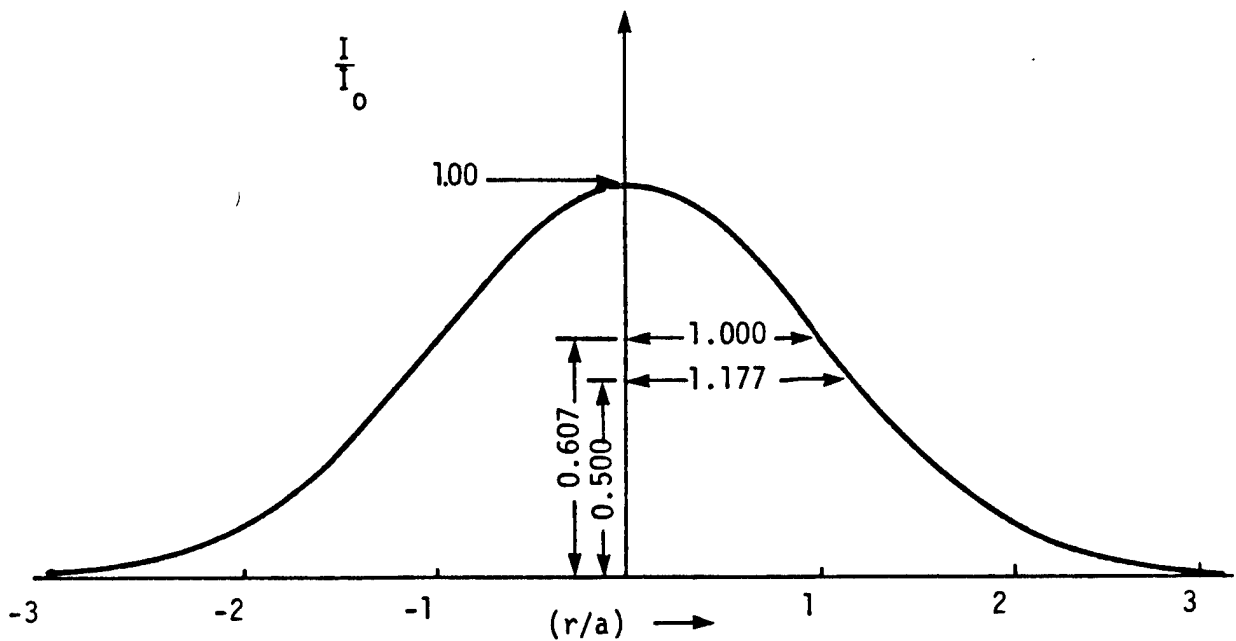
$$\int_0^{y_0} e^{-y^2/2} y dy = 2 \int_0^{\frac{1}{\sqrt{2}} y_0} e^{-v^2} v dv = \int_0^{\frac{1}{2} y_0^2} e^{-z} dz \quad (32)$$

or

$$\int_0^{y_0} e^{-y^2/2} y dy = \left[1 - e^{-\frac{1}{2} y_0^2} \right] \quad (33)$$

Equation (31) becomes

$$\eta_{\text{diff}} = \left[1 - e^{-\frac{1}{2} \left(\frac{r}{a}\right)^2} \right] \quad (34)$$



78 01885

Figure 18. Gaussian Intensity Distribution as a Function of Radius, r , and Gaussian Parameter, a .

As early as 1962 it was possible to manufacture a deployable collector/concentrator of 12 meters diameter which had a mirror quality of $\alpha = 3 \times 10^{-4}$ radians.⁴⁹ Comparing this to the sun's angular diameter of 10^{-2} radians suggests from equation (30), that b/d can be as small as 0.01 even in a larger collector where individual facets making up the total mirror are manufactured in the size and with the tolerance of the 1967 mirror.

It is also evident from this discussion that the collector-concentrator, because of its considerable size (at least 10^4m^2 for a ten percent efficient solar laser), will require a combination of deployment and assembly in space using facets of the type described above. A rigid but lightweight frame to support and align each of the facets will be required, plus a control network and servo-mechanisms for turning the facets.

The alternative approach is to construct a much simpler and less precise reflecting surface, trading off the weight and complexity of the former scheme for a more dispersed intensity distribution at the focal plane. There is an obvious need to develop lighter weight collector technology and a variety of authors have discussed materials and structures for accomplishing this goal. Material properties are summarized in Table 7, showing their mass densities and reflectivities.

In some instances, the mirror profiles are attained in flat facets made from an extra-light weight reflecting "skin" of metallized plastic stretched by springs across a rigid framework. In order to achieve a surface quality of $b/d = 0.01$, approximately 10^4 flat facets would be required, each properly aimed.

The choice of mirror quality is in part determined by the temperature of the absorbing body. In the case of a high temperature

Table 7. Collector-Concentrator Materials and Properties (Ref. 80)

Materials	Properties (3 to 6 g/m ²)
Kapton*	Plasma Etched 7.6 μ m to 2 μ m thick Chemically Etched
Mylar	
Ciba-Geigy B-100	2 μ m thick
Ciba-Geigy P-100	Similar to B-100 but better high temperature (up to 400°C) performance
Electrocast Poly-Amides	Less than 1 μ m thick

*Any of these materials can be coated with 1000 Å of Aluminum giving a net reflectance of 88 percent or better; 125 Å of Chromium also insures a high emittance (>0.6).

absorber (e.g., black body cavity or high temperature Brayton cycle receiver), the re-radiation losses are exacerbated by large apertures and so the incoming radiation intensity distribution should be as sharply confined as possible, requiring high mirror quality. For low temperature receivers, the mirror quality is not nearly so important. The combination of these two influences is discussed more in the next subsection.

For purposes of weighing laser systems on a comparable basis, we shall apply the Hughes study weights. These are intermediate between those chosen by Rather et al.⁹ for their very large collector areas, and those used by earlier studies. The Hughes study did not go into detail as to how the radiator weight was derived so that for an absolute weight some justification is still required. More will be said about the exact choice of radiator material and structure in the conceptual design of Section 4.

3.2. Cavity Absorbers

Cavity absorbers receive sunlight from the collector-concentrator and convert thermal power for the laser system. Two aspects of cavity absorbers are important to solar powered lasers. These are the radiation losses at the receiving aperture and the upper temperature limits imposed by materials, in the cavity walls, heat exchanger tubes and coolants. In the case of indirect solar pumped lasers only the black body cavity walls pose a direct limitation since there are no heat exchangers or high temperature coolants used. However, all of the laser concepts will require auxiliary power which we assume to be provided by a solar Brayton cycle. In this case all three material categories impose limits on cavity absorber performance.

The re-radiation losses can be quantified by means of

$$\eta_R = 1 - \frac{\text{Power Re-radiated}}{\text{Power collected}} .$$

For $0 \leq \frac{b}{d} < 1$, the maximum intensity of the focused radiation is one-fourth the solar flux where $\eta_M = 1$ (i.e., 100 percent reflectivity) (Ref. 13, 43). Thus in the case of a Gaussian distribution of intensity at the cavity aperture, the power collected is

$$P_{\text{coll}} = \frac{1}{4} \sigma T_s^4 \int_0^r \int_0^{2\pi} e^{-\frac{1}{2} \left(\frac{r}{a}\right)^2} r dr d\theta = \frac{\pi}{2} a^2 \sigma T_s^4 \int_0^{r/a} e^{-\frac{1}{2} y^2} y dy \quad (35)$$

where T_s = the equivalent black-body temperature of the sun = 5785 °K
The power re-radiated is given by $\pi r^2 \sigma T_B^4$, so that

$$\eta_R = 1 - \frac{2\pi r^2 \sigma T_B^4}{\pi a^2 \sigma T_s^4} \left[\int_0^{r/a} e^{-\frac{1}{2} y^2} y dy \right]^{-1} \quad (36)$$

or

$$\eta_R = 1 - 2 \left(\frac{r}{a}\right)^2 \left(\frac{T_B}{T_s}\right)^4 \frac{1}{1 - e^{-\frac{1}{2} \left(\frac{r}{a}\right)^2}} \quad (37)$$

Combining equations (37) and (34) gives

$$\eta_c = \eta_R \eta_{\text{diff}} = 1 - e^{-\frac{1}{2} \left(\frac{r}{a}\right)^2} - 2 \left(\frac{r}{a}\right)^2 \left(\frac{T_B}{T_s}\right)^4 \quad (38)$$

η_c is plotted versus $\left(\frac{r}{a}\right)$ for four values of T_B in Figure 19. The maximum value for η_c is given by

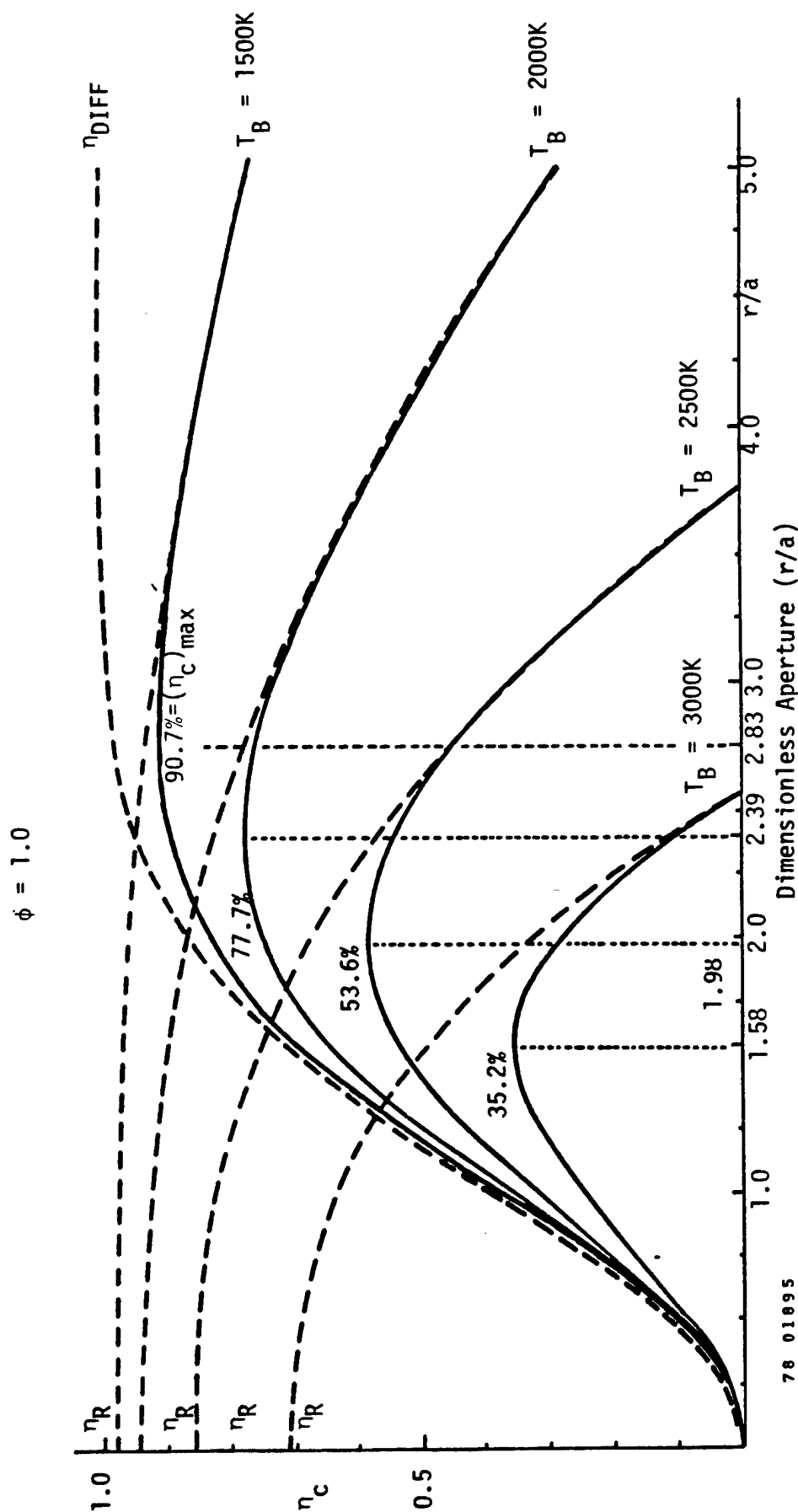


Figure 19. Gaussian Cutoff Efficiency, η_{DIFF} ; Re-radiation Efficiency, η_R and the Product Collection Efficiency, $\eta_c = \eta_R \eta_{DIFF}$ as a Function of Cavity Aperture (r/a) for Different Cavity Temperatures, T_B

$$\frac{d\eta_c}{d\left(\frac{r}{a}\right)} = \left(\frac{r}{a}\right)_0^{-\frac{1}{2}} \left(\frac{r}{a}\right)_0^2 - 4\left(\frac{T_B}{T_S}\right)^4 \left(\frac{r}{a}\right)_0 = 0 \quad (39)$$

or

$$\left(\frac{r}{a}\right)_0 = -2 \ln \left[4\left(\frac{T_B}{T_S}\right)^4 \right] \quad (40)$$

The values of $\frac{r}{a}_0$ and $\eta_{c_{\max}}$ are indicated in Figure 19 for each of the values of T_B . Clearly, low values of T_B permit high efficiencies of energy utilization. The impact of this effect has been included in the discussion of indirect solar-pumped lasers in Section 4. It is also incorporated in the computation of solar powered Brayton cycle efficiencies and materials choices presented in the next subsection.

The technology of cavity absorbers has recently received increased attention due to the national solar thermal power R and D program sponsored by the U.S. Department of Energy. A selection of cavity receiver concepts developed for the power tower solar thermal scheme is shown in Figure 20. The peak operating temperatures and coolant materials are listed in Table 8. The temperature of these cavities is limited by the fact that the hot materials in the cavity are in contact with air allowing oxidation to occur. Higher temperatures could presumably be employed with these cavities if they were operated in a neutral atmosphere or in the hard vacuum of space. However, the limit of heat exchangers still would require peak temperatures to be kept below 1700 °K. Recent ceramic heat exchanger research by the Garrett AiResearch Corp⁵⁰ and others^{51, 52} for combustion gases has shown that 1900°K is feasible for the heat exchanger material itself (i.e., Silicon Nitride) and that peak coolant temperatures of 2100 °K may be achieved. Because of weight and heat transfer requirements

Table 8. Materials and Temperatures for
Cavity Absorber Examples [†]

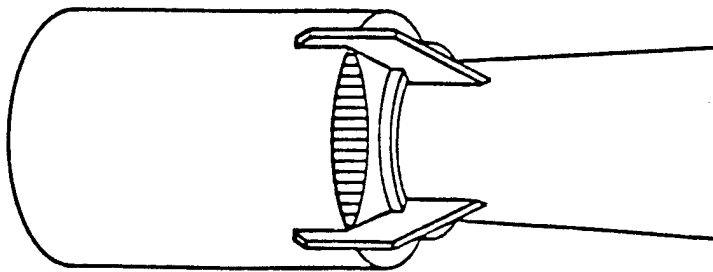
Cavity	Construction	Temperature/Pressure
Honeywell	Vertical Cavity Water/Steam	510° C/10.0 MPa
McDonald Douglas	External Absorber Water/Steam	510° C/10.1 MPa
Boeing*	Vertical Cavity	816°C/3.4 MPa
Martin Maretta	Horizontal Cavity Water/Steam	510° C/9.3 MPa

[†] Ref. 81

* Ref. 82

we shall utilize liquid lithium as the coolant in our design for space power plant. The lithium carries heat from the cavity absorber to a second heat exchanger where it heats up the gaseous working fluid in the Brayton cycle power units. This constitutes the conventional design approach.

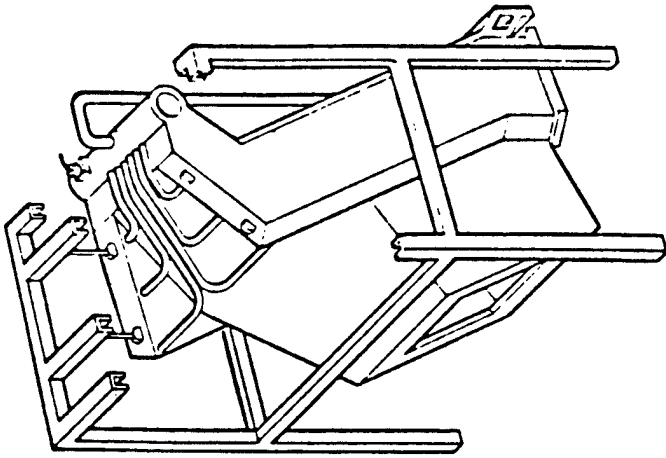
A more advanced cavity design, suggested by A. Hertzberg⁵³ has also been considered for a higher efficiency power cycle design, as shown in Figure 21. The high temperature potential of the volume-heated, cooler wall absorber cavity in Figure 21 is on the order of 2000 °K to 3000 °K. The walls are cooled by transpiration of the working fluid (e.g., potassium) through the walls into the central heating region. There the focussed solar radiation is absorbed by the pressure broadened lines of the working fluid (e.g., see Figure 22) and the highest temperature gases are exhausted into the power unit. No heat exchanger is required in this device so that all of the wall and window materials are kept well below the peak temperatures of the working fluid, thereby avoiding many of the more conventional limitations. The window design shown in Figure 21 is an attempt



HONEYWELL



MC DONNELL
DOUGLAS



MARTIN MARIETTA

78 01914

Figure 20. Possible Cavity Absorber Designs for the Brayton Cycle Power Units

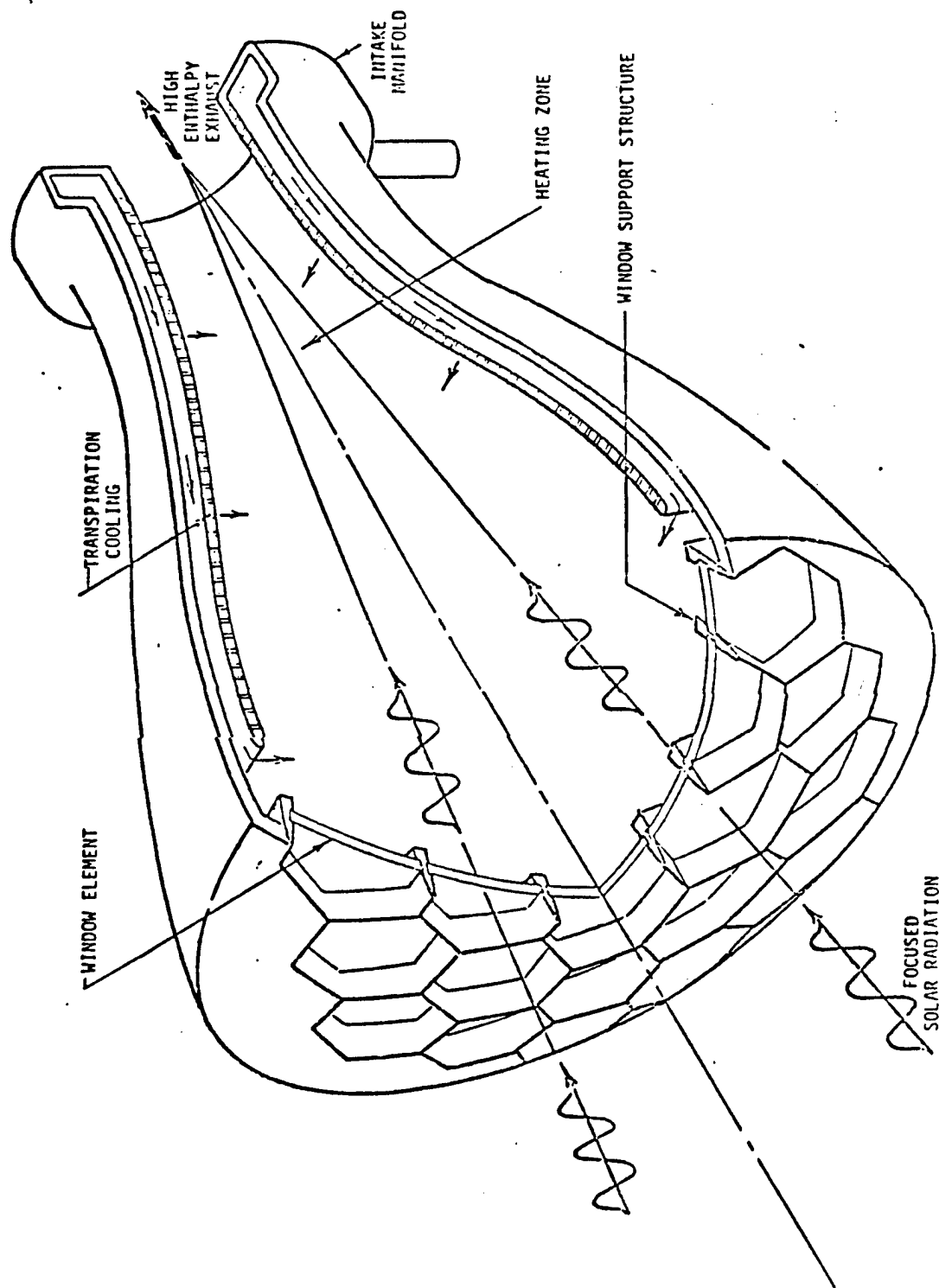


Figure 21. Solar Radiation Boiler-Receiver Solar Radiation from the Collectors in Focussed (at left) on the Transparent Window and Absorbed in the Heating Zone by the Driver Gas. The High Temperature Gases are Exhausted (at right) to the Energy Conversion System. ⁵³

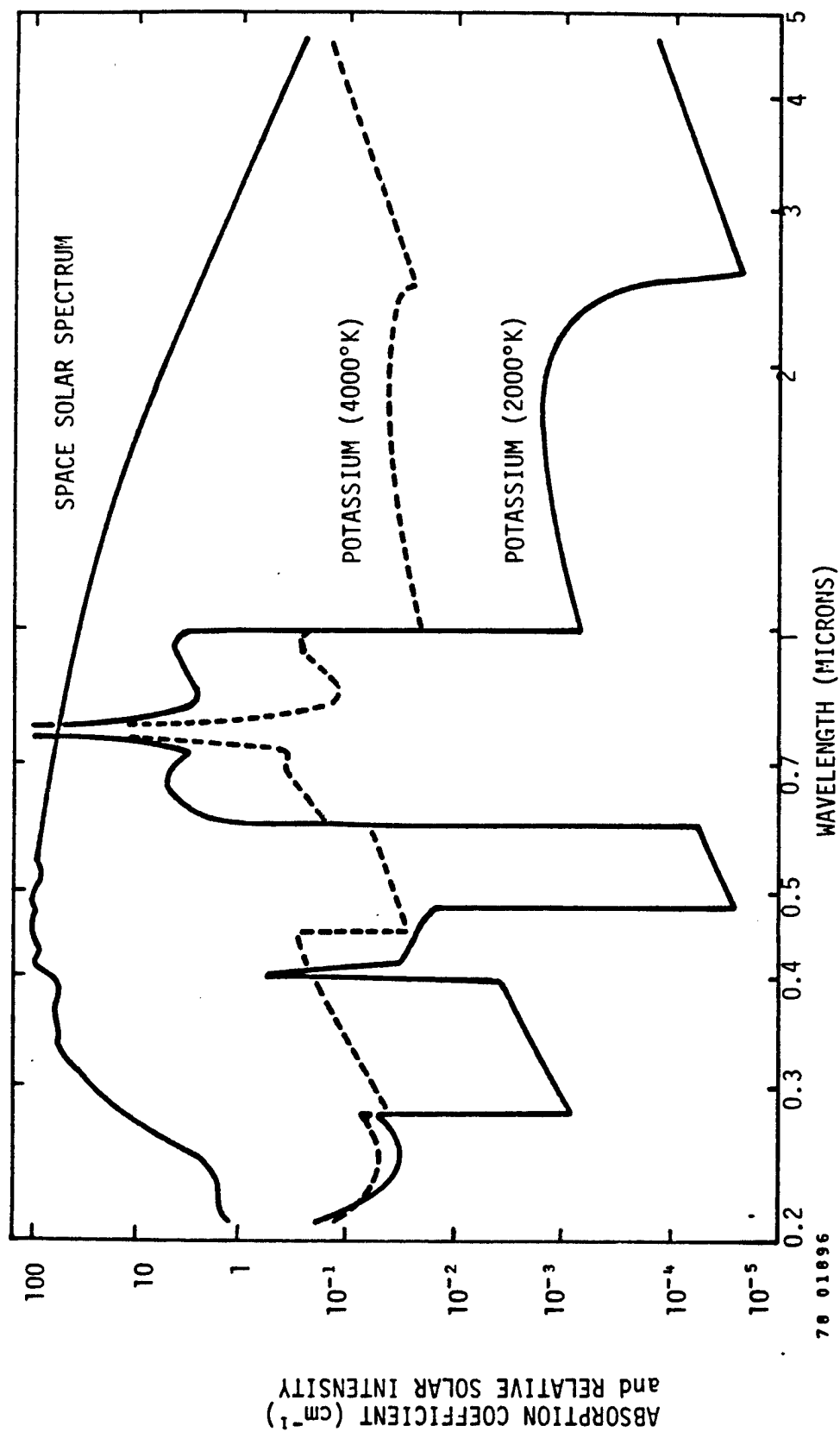


Figure 22. Space Solar Spectrum and Potassium Absorption Spectrum for $p = 1$ atm. 53

to use high temperature quartz or other materials pre-stressed by the window framework to avoid leakage. The window can also be designed to face convex inwards so that the higher pressure working fluid will place the window materials under compression. A mosaic structure is used so that the window flats can be thin and lightweight yet sufficiently strong. The framework is made highly reflecting to avoid being heated.

Each type of cavity absorber unit must be well insulated to decrease radiative losses from the walls. However, insulating materials are generally lightweight. The heaviest portion of such cavities will be the heat exchanger (if any) or glass tubes (in the case of the black body cavity). Hence, the cavities used with the Brayton cycle power units will be weighed as if they were just heat exchangers and individual designs will be used for weighing the black body cavities of indirect solar pumped lasers. In the case of the advanced cavity, the weight is estimated on the basis of pressure vessel technology instead of heat exchanger technology. Rather good precedents exist for the advanced absorber cavity in the development of liquid fuel rocket nozzles such as those used for the Saturn series of rockets in the Apollo space program.

3.3 Brayton Cycle Power Units

Brayton cycle space power plants have been studied extensively.⁵⁴⁻⁶¹ Most of the earlier design efforts were for relatively low output power on the order of 50 kW^{54, 55}. More recently with the interest in solar power satellites, thermal power plants in the multi-megawatt range have been considered^{58, 60}. A summary of a selection of these Brayton cycles is given in Table 9. A plot of the specific power versus absolute output power, shown in Figure 23, quickly reveals that an economy of scale exists which favors large units. The largest single design modules are 250 MW from the Boeing studies of the SPS (Ref. 58). Since their specific power does not fall on the line shown in Figure 23 we presume that the scale effects might

Table 9. Selected Brayton Cycle Space Power Units

Brayton Cycle Solar & Nuclear References	Thermal Eff., n%	Peak Temp. (turb. inlet)	Min. Temp.	Peak Press.	Turbine Press. Ratio	Work. Fluid	Weight	Total Elec Power
Tonelli & Secord	30	1500 °F	1900 °F 140 °F	67.2 psia	1.95	Argon	3640 lb* 4570 5865 whole system	18 kw* 27 40
Seikel & Nichols L. D.	22.5	1500 °K	1176 °K turb. exit.	10 atm	1.67 ea of 2 turbines	Neon + Cs or Xe	3.5-5 kg/kw 7.7-11 lb/kw	10 MW
Gregory, D. L.	45.4	1620 °K				Helium	100x10 ⁶ kg	300 MW
Southam, D. L.	30.5	1080 °K	300 °K	32.2 psia		Argon	3997 lb whole system	20 kw
Coombs & Norman	34.6	1111 °K (2000 °R)	292 °K (525 °R)	22.4 psia	1.72	Xe=44% He=56%	2812 lb whole system 1115 lb less nuclear heat source	7.25 kw
Hoodcock & Gregory								10,000 MW for \$13x10 ⁹
NASA TH-X-73344 November 1976	36.4	1300 °K				Argon	10 ⁶ kg	22.64 MW per module

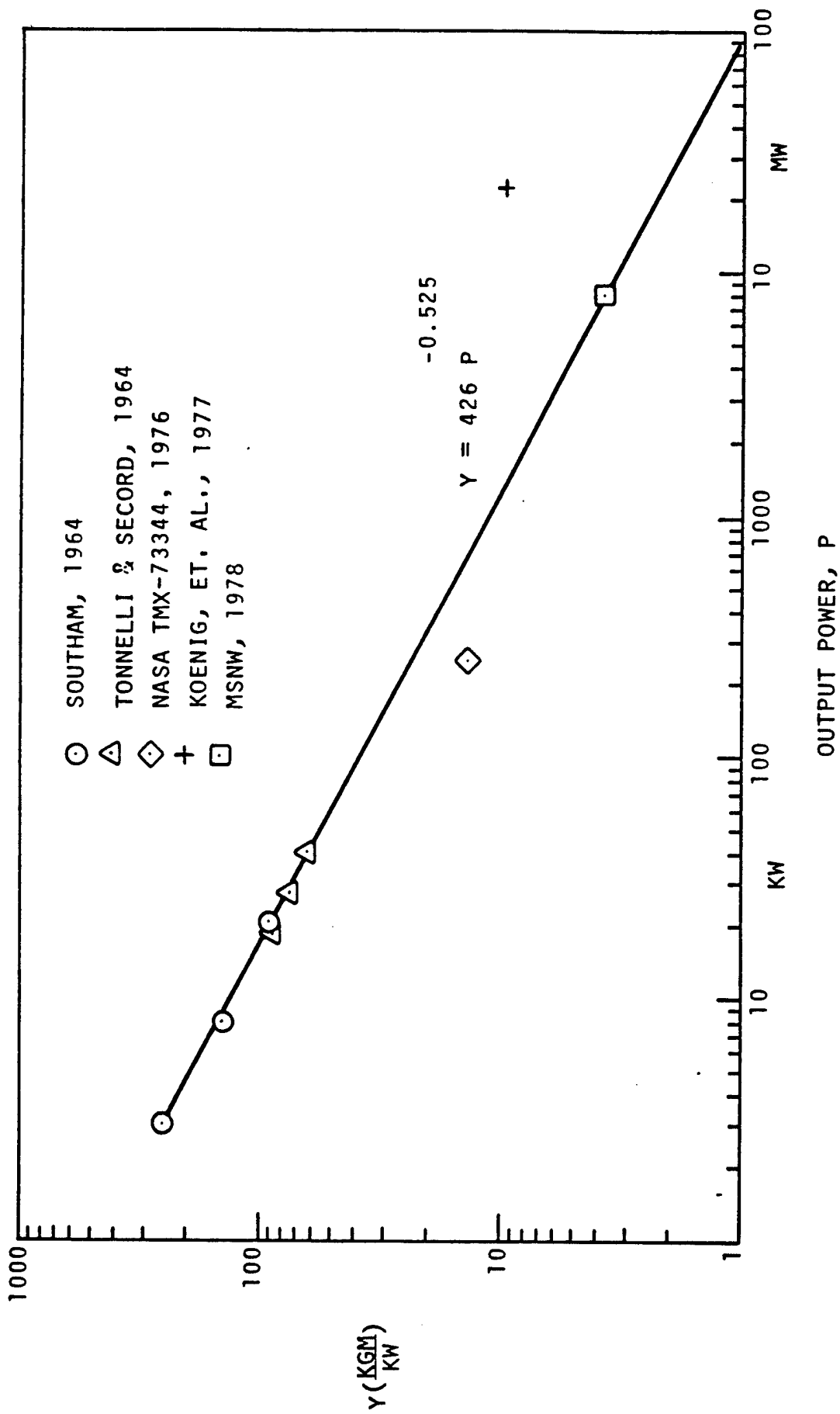


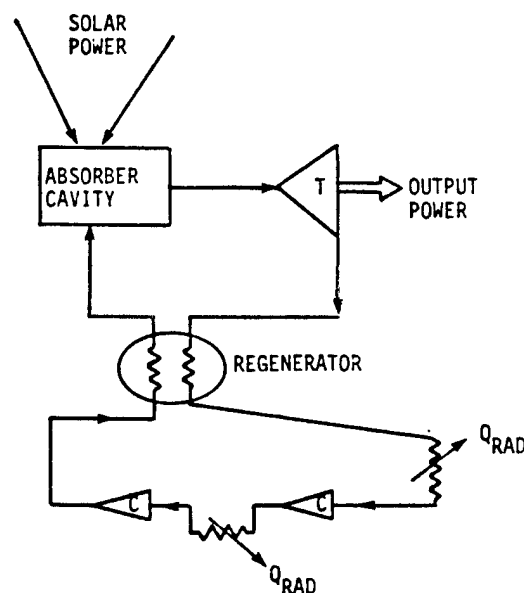
Figure 23. SOLAR BRAYTON SYSTEMS

78 01585

cease after a module size of approximately 10 MW. These designs generally are conservative in form, using low enough cycle temperatures to guarantee reliable performance over a many year lifetime. As a result the operating efficiencies are on the order of 25 percent. We shall adopt 25 percent for the conventional designs as a guideline for sizing the collector-concentrator, absorbing cavity and waste heat radiator serving the Brayton cycle power unit. A specific power of 2.55 kg/kW output will also be used.

In fact, the Boeing study^{58,60} utilized a thermo-electric topping cycle, Brayton bottoming cycle combination, to generate electricity at a higher efficiency than 25 percent. So it should be kept in mind that more advanced cycles do exist and that as a result the basic evaluation of the laser system weight may be on the conservative side. We shall discuss a high temperature advanced power cycle in more detail below.

A schematic of the conventional Brayton power cycle is shown in Figure 24, using an approach suggested by the AiResearch Corp⁶¹. The T-s cycle corresponding to Figure 24 is shown in the next Figure 25, where regeneration is



78 01097

Figure 24. Schematic of Brayton Cycle Power Unit with Regenerator and Intercooled Compressors

indicated by the hatched region. Hence, the absorber cavity must supply heat to this cycle in the temperature range of 638 °K up to 1600 °K. Rejected heat is radiated at 556 °K down to 380 °K. In the following subsection the question of the best radiator temperature will be addressed; it is only necessary to say here that the radiator and Brayton cycle temperatures can be chosen to optimize their combined performance. The cycle shown in Figure 25 has the following properties.

Turbine pressure ratio, $\pi_t = 6.2$

Peak turbine temperature = 1200 °K

Compressor pressure ratio, $\pi_c = 2.67$

Peak compressor Temperature, $T_c = 470$ °K

Working fluid, Helium/Xenon: $\bar{M} = 60$ (molecular weight)

Adiabatic turbine efficiency, $\eta_t = 0.93$

Adiabatic compressor efficiency, $\eta_c = 0.85$

Regenerator Effectiveness, $\epsilon = 0.9$

Pressure drop in Heat exchangers

and regenerator (per component), $\Delta P/p = 3$ percent

Specific net power output, $= 0.4 \frac{\text{kW}}{(\text{kg/sec})}$

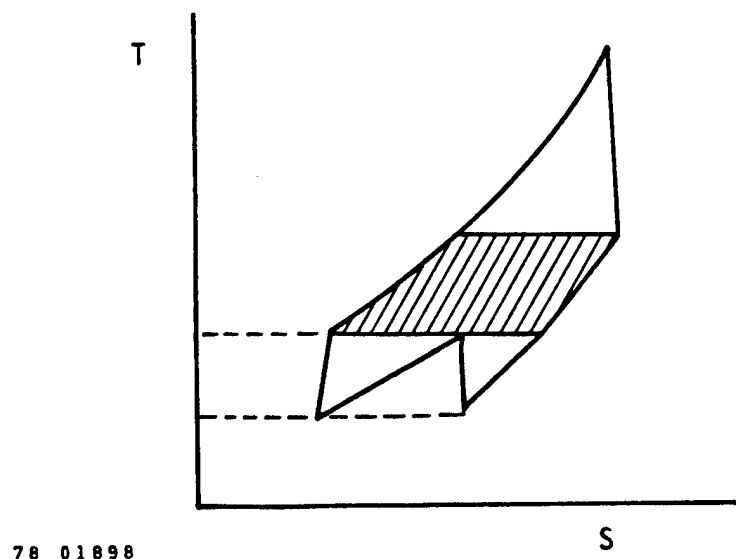


Figure 25. Temperature-Entropy Diagram for Brayton Power Unit Shown in Figure 24

An advanced energy exchanger/turbine power unit concept has also been developed by MSNW for a laser driven heat engine⁶² and by A. Hertzberg et al.⁵³ for a solar driven power system. The energy exchanger is a device which promises to increase substantially the thermal efficiency of turbine power generators. The energy exchanger is a compact device which transmits the work of expansion of a high temperature gas through a gas interface to a colder, lighter molecular weight gas which, in turn, drives a conventional turbine. Because this is a work transfer device, the overall thermal efficiency is determined by the high temperature of the driver working fluid and is independent of the temperature of colder, driven gas.

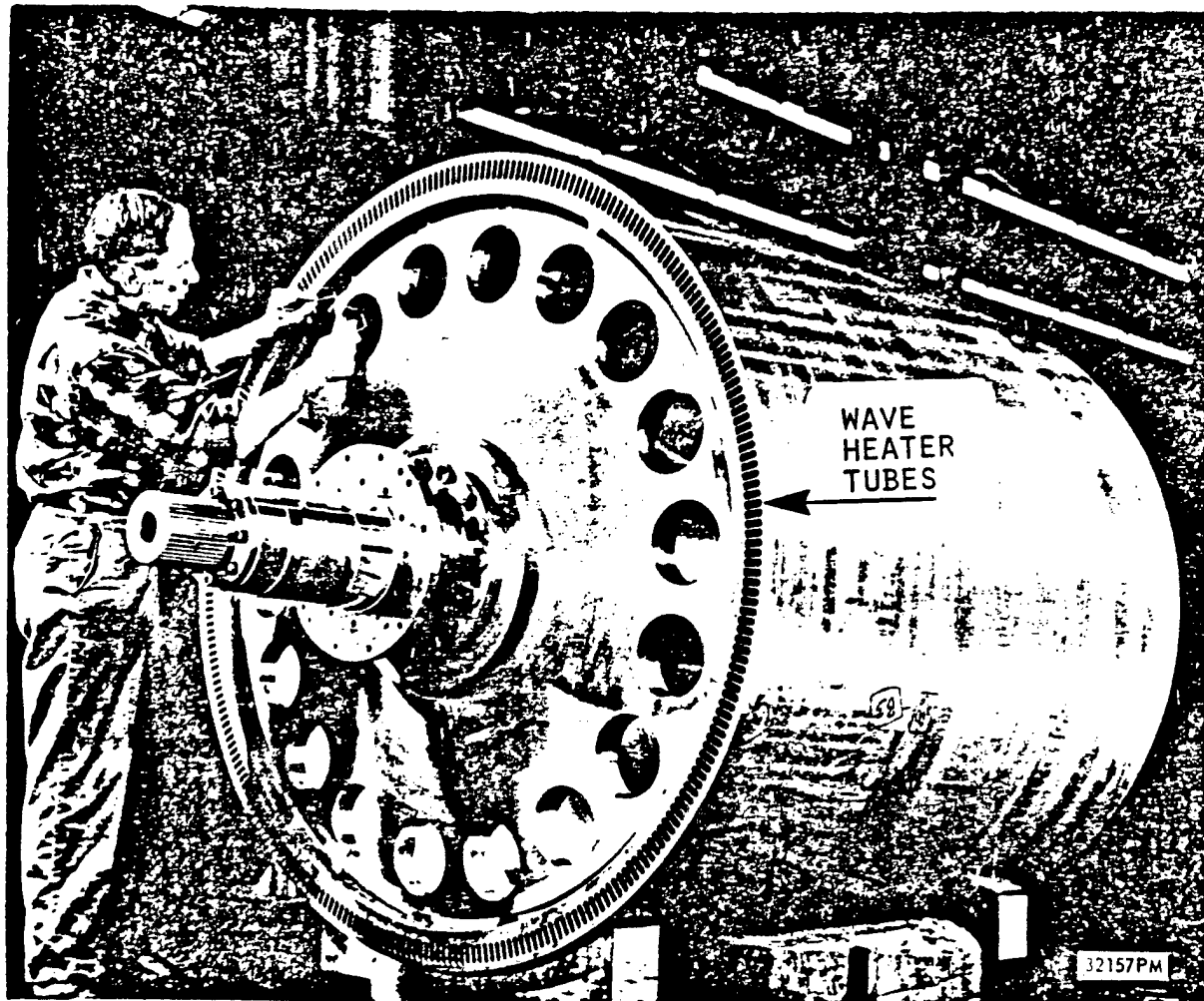
It can be shown that the transfer of energy across a gas interface by a compression wave is facilitated by a condition called impedance matching, which requires that no acoustic wave be reflected from the interface, i.e., the original wave be transmitted in full strength. In terms of the state of the two gases, impedance matching means that the specific heat ratio, γ , and the product of the density and sound speed, ρa , must be the same on each side of the interface. The combination of these two conditions guarantees that the ratio of the gas temperatures on either side of the interface is equal to the ratio of the molecular weights. That is, by choosing the molecular weight ratio of driver to driven gas (i.e., impedance matching), we can control within wide limits the temperature of the colder driven gas to be compatible with conventional turbine inlet temperature limits. Thus, a high efficiency thermal cycle can be designed using the energy exchanger to couple a high temperature source to conventional low temperature turbines. In the case of solar energy the advanced cavity shown in Figure 21 would provide the high temperature driver gas to the energy exchanger. The detailed operation of the energy exchanger is discussed in Reference 62.

Energy exchanger devices have been built and operated for large, high temperature (4500 °K) application and in small sizes (10 kwatt),

but these have not yet been optimized for high efficiency operation. Seippel,⁶³ of the Brown-Boveri Company, was the first to demonstrate an efficient gasdynamic energy exchanger, the "Comprex," in which gas compression was accomplished by shock processes. The Comprex transferred 69 percent of the available work of expansion through a compression ratio of 2.5. Later, independent research was carried out by Kantrowitz et al. at Cornell University, Berchtold at ITE and Zurich. At Cornell Aeronautics Laboratory (CAL, now CALSPAN), work continued on this type of machinery in the 1950s for propulsion, chemical processing, and a hypersonic wind tunnel. A prototype and a full-scale energy exchanger device called a "wave superheater" were constructed at CAL and operated successfully for wind tunnel applications over a five-year period.⁶⁴ Temperatures as high as 4500 °K, with air flows of 5 lbs/sec, were achieved in the full-scale wave superheater (Figure 26).

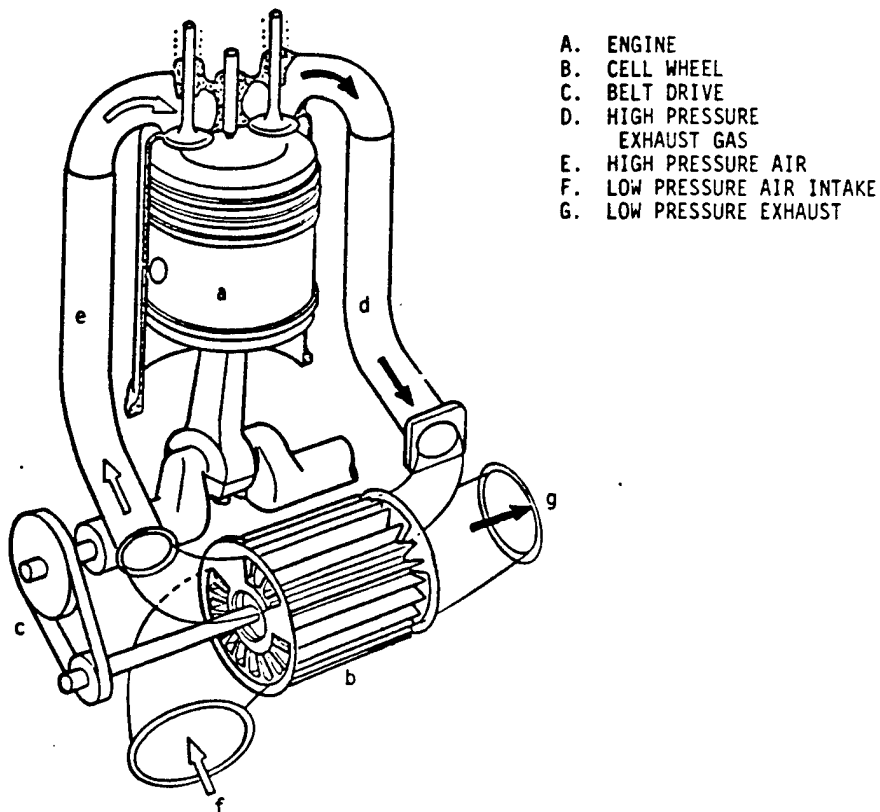
On a smaller scale (approximately 10 kW), Brown-Boveri has started manufacturing a Comprex-Supercharger for Diesel engines, shown schematically in Figure 27.⁶⁵ Test data by Brown-Boveri claim improvements in both power performance and economy over Seippel's original design, while also claiming beneficial effects on air pollution. In particular, the responsiveness of the Comprex-Supercharger system is outstanding. This device is the first entry of a wave machine into the commercial market.

The most recent study on energy exchanger technology, performed in 1977 at MSNW, explored the conceptual design, operation, material requirements, and peak cycle efficiency (on the order of 70 percent) for an energy exchanger used to boost the performance of an advanced fuels fusion reactor. The results of that study showed that the power conversion system employing an energy exchanger in a combined gas turbine/steam cycle would allow a relatively neutron-free fusion fuel to produce net electric power. No insurmountable technological



77 00917

Figure 26. Photograph of the Full-Scale Gasdynamic Wave Heater Drum Constructed and Operated at CAL



78 00918

Figure 27. Schematic of the Supercharging Application of the Comprex Waveheater Currently Being Marketed by Brown-Boveri Company

barriers to developing that power conversion system were apparent. The potential for an efficient "hands-on" fusion reactor in facilitating long-term energy needs is clearly impressive. MSNW is currently developing an efficient energy exchanger for power production under support from the Basic Energy Sciences Division of DOE.

From a consideration of ideal regenerated and intercooled cycles, it was found that the best configuration for the energy exchanger/turbine consists of three intercooled compressors, and one or possibly two turbines fed by an equivalent number of energy

exchangers, as shown schematically in Figure 28. The expression for the actual cycle efficiency is

$$\eta = \frac{K^{-1}(1 - \tau_{td}) - 3\tau^{-1}(\tau_{cd} - 1)}{1 - [\epsilon\tau_{td} + (1 - \epsilon)\tau^{-1}\tau_{cd}]} \quad (41)$$

where

$$K = \{\eta_{td}[1 - (1 - \eta_{cd})^{\frac{\gamma-1}{\gamma}}]\}^{-1} \quad (42)$$

represents the effects of the energy exchanger component efficiency (which is equal to $(\eta_{td}\eta_{cd})^{1/2}$), η_t and η_c are the turbine and compressor efficiencies for the D (driver) and d (driven) loops shown

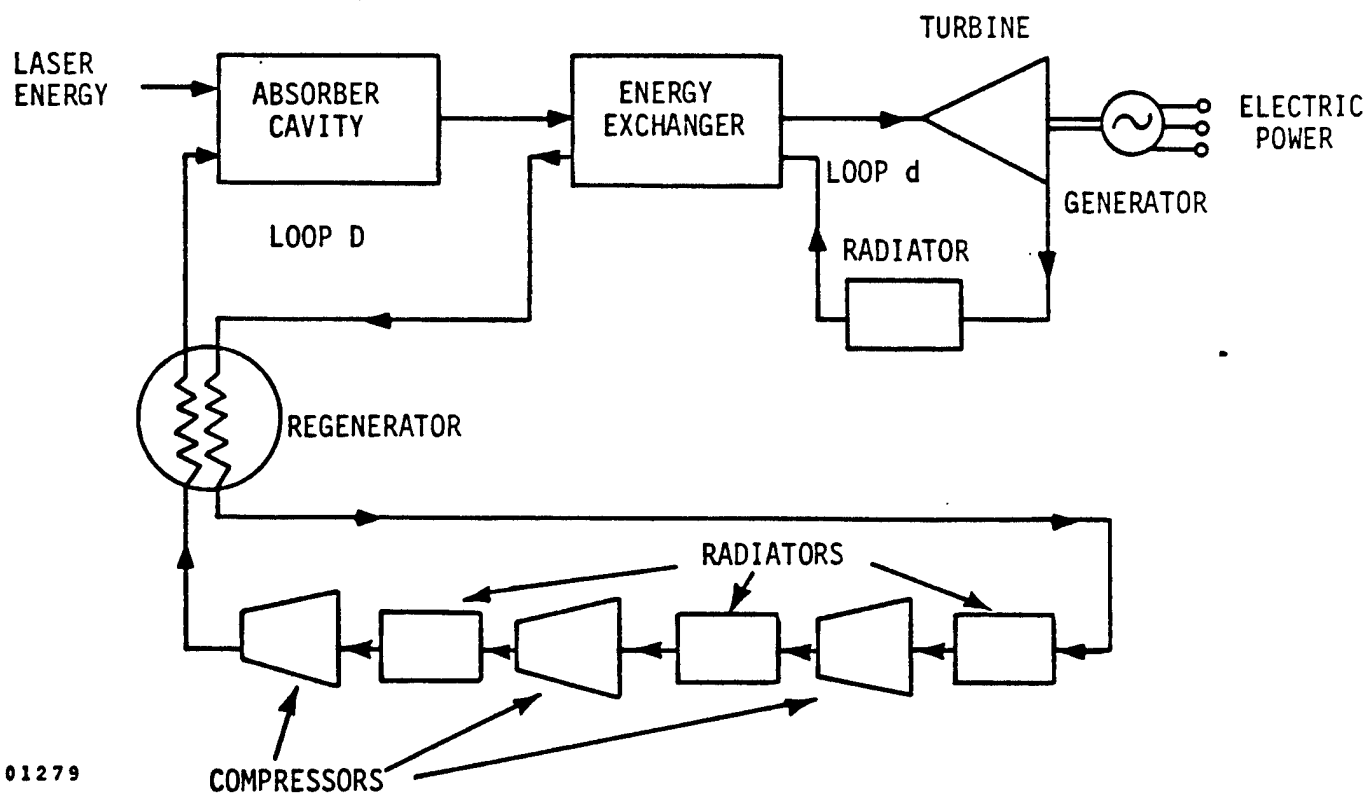


Figure 28. Schematic of Intercooled, Regenerated Brayton Cycle Utilizing an Energy Exchanger for High Efficiency Operation

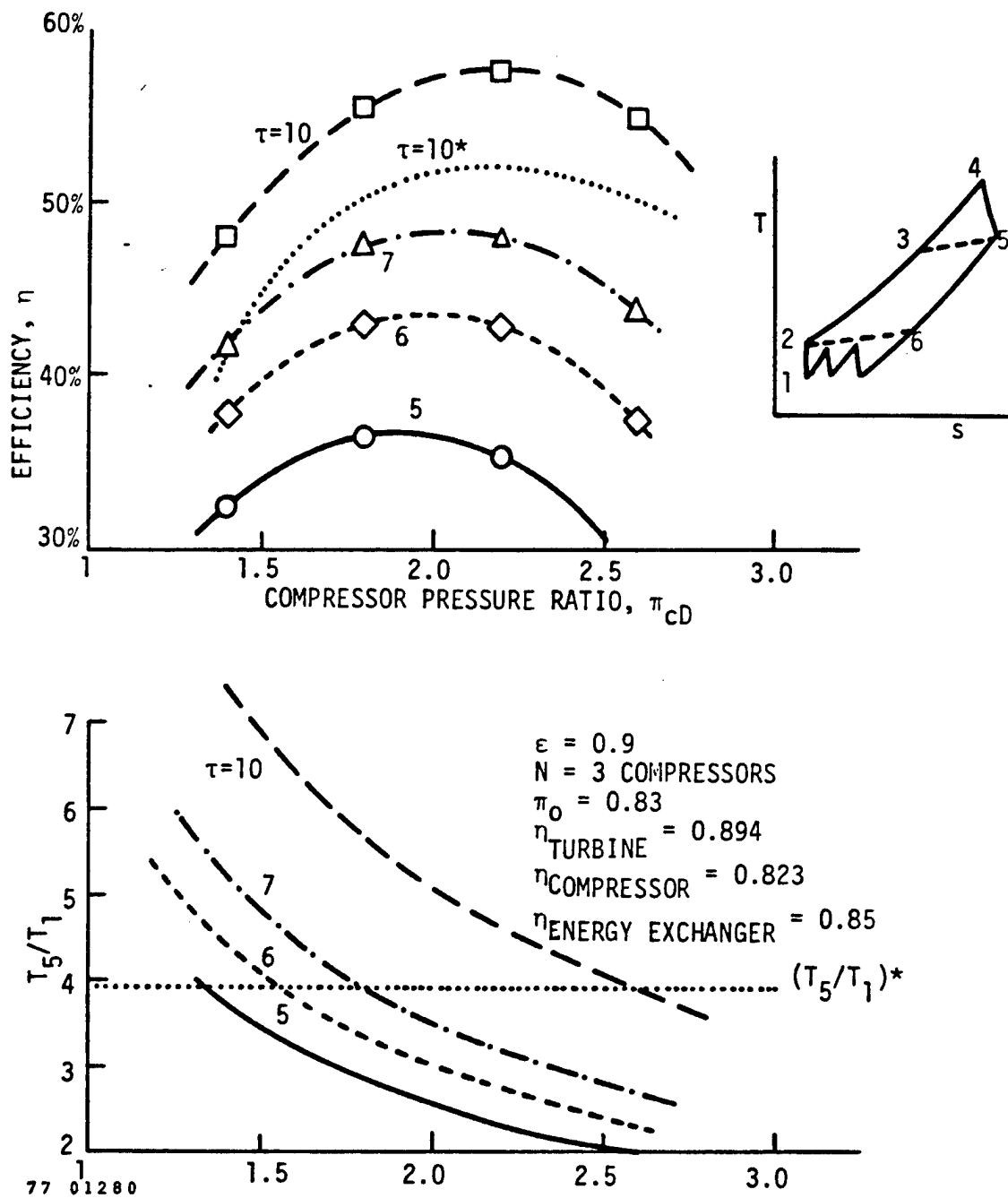
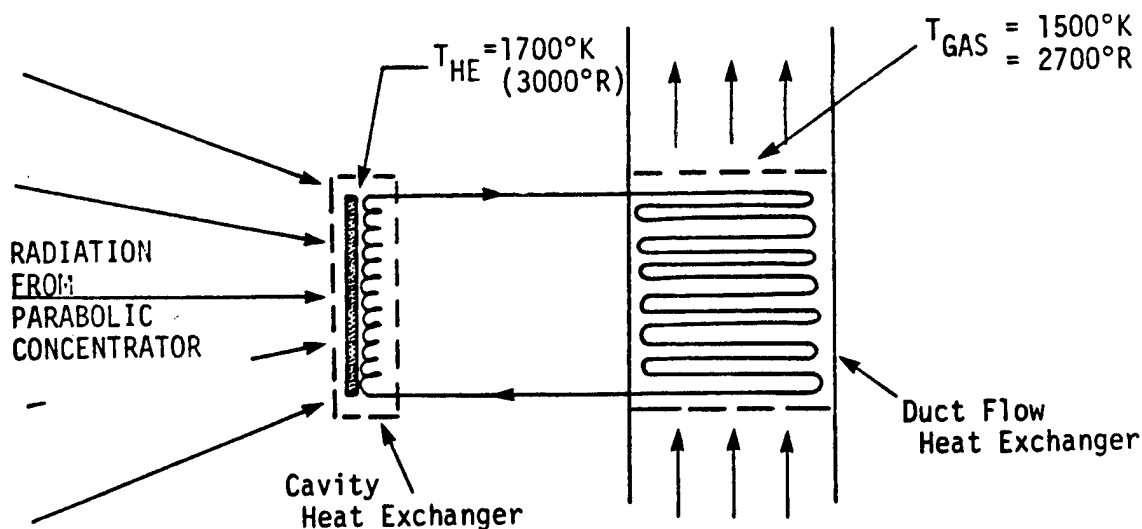


Figure 29. Energy Exchanger/Turbine Efficiency and Regenerator Peak Temperature (T_5/T_1) as Functions of Maximum-to-Minimum Temperature Ratio $\tau \equiv T_4/T_1$ and Compressor Ratio π_{CD} [$\tau = 10^*$ for $\eta_{EE} = 70\%$ instead of 85%; $(T_5/T_1)^*$ corresponds to $T_5 = 1170$ °K when $T_3 = 300$ °K]

in Figure 28 and ϵ is the regenerator effectiveness. The values of η_{tD} and η_{cD} are taken to be equal, and each is equal to the square root of the energy exchanger efficiency. The computation of the temperature ratios, τ_D and τ_d , and pressure ratio, π_d , can be obtained by prescribing the peak-to-minimum cycle temperature ratio, τ , and the pressure ratio, π_{cD} , for a single compressor. The results are shown in Figure 29. For example, if $T_1 = 300^\circ\text{K}$, $\tau = 10$ implies a peak temperature of 3000°K and a possible peak efficiency of nearly 60 percent for this system.⁶²

3.4. Heat Exchanger

The design of the cavity absorber and heat exchanger which delivers heat to this Brayton cycle is based on a black-body type cavity absorber with improved heat exchanger materials within the cavity itself to raise its coolant operating temperatures to the order of 1700°K (3000°R). A plan view of a finned tube heat exchanger in the Brayton cycle loop is shown in Figure 30; the cavity coolant tubes are shown schematically on the left. The number of tubes in the power unit heat exchanger can be determined by the amount of heat which must be delivered to the working fluid as well



78 01899

Figure 30. Heat Source Exchanger

as the liquid metal coolant temperature. This relationship is shown graphically in Figure 31 assuming 19 tubes across the duct on two-inch centers and each tube one inch O.D. (e.g. for the GDL application). The advantage of finned over unfinned heat exchangers is also illustrated. A reasonable number of the tubes in the downstream direction should not exceed 100 in order to keep the pressure drop reasonable. Hence a liquid metal temperature on the order of 3100 °R (1720 °K) has been chosen. A glance at the liquid lithium vapor pressure in Figure 32 shows that a pressure of about 2.5 atmospheres is required to prevent boiling.⁶⁷ Since this is a sealed unit, a small pump is required to circulate the liquid metal; a magnetic induction pump with no moving parts in the lithium stream should suffice.

The total tube wall area A_H in the absorber cavity can be computed assuming an aperture radius $r \cong 2.8a$ where a is the Gaussian half-width of the focussed radiation. This value of r/a approximately maximizes η_c , the collector efficiency, in the neighborhood of a cavity temperature, $T_B = 1500$ °K (e.g. see Figure 19). Also, we pick a collector rim angle of 45 degrees in order to reach the peak concentration ratios for paraboloidal mirrors. Under this condition the total radiation entering the cavity can be written as

$$\phi_{in} = 2I_{in} \left(\frac{a}{r}\right)^2 (1 - e^{-0.5(r/a)^2}) A_a \quad (43)$$

where $I_{in} = 0.25 F_s \eta_M$ and A_a is the cavity aperture area.

Simple energy balance between the power entering and leaving the cavity gives

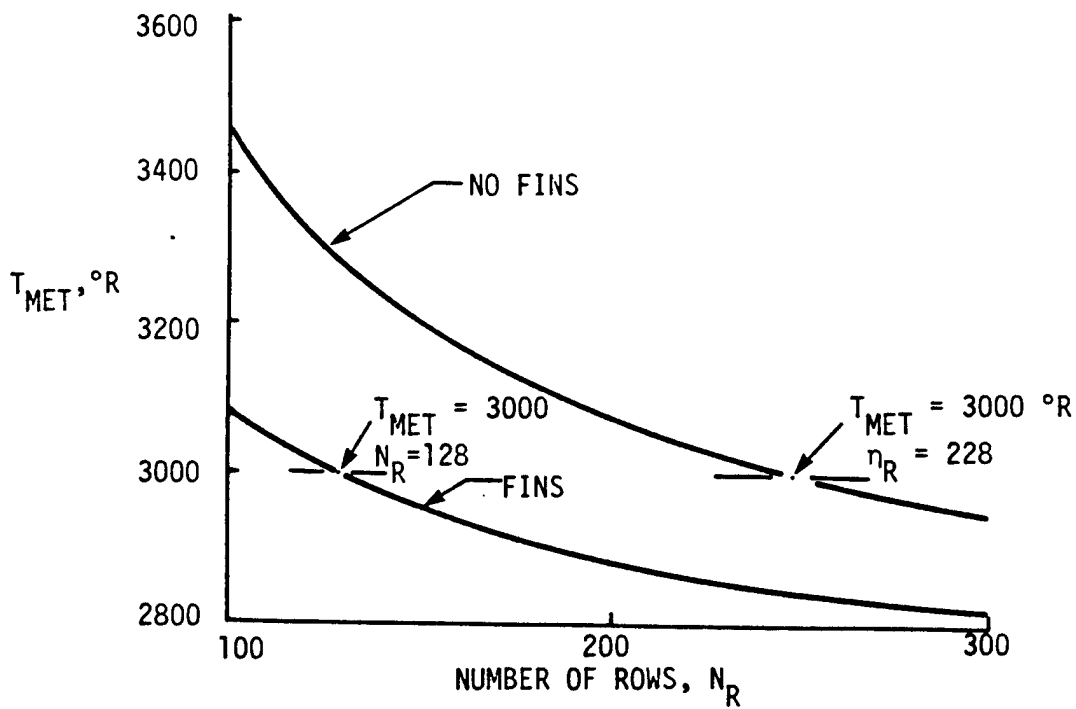
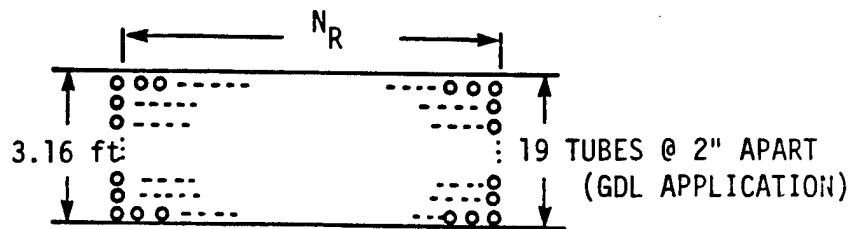
$$A_h h_f (T_B - T_f) + \epsilon \sigma T_B^4 A_a = \phi_{in} \quad (44)$$

where h_f is the heat transfer coefficient for a liquid metal,⁶⁸

$$T_{\text{MET}} \approx T_{\text{WALL}}$$

$$T_{\text{GAS}} = 2700^{\circ}\text{R} \ (1500^{\circ}\text{K})$$

$$h_{\text{c fins}} \approx 2 \times h_{\text{c no fins}}$$



78 01900

Figure 31. Heat Exchanger for Liquid Metal to Gas Heat Transfer

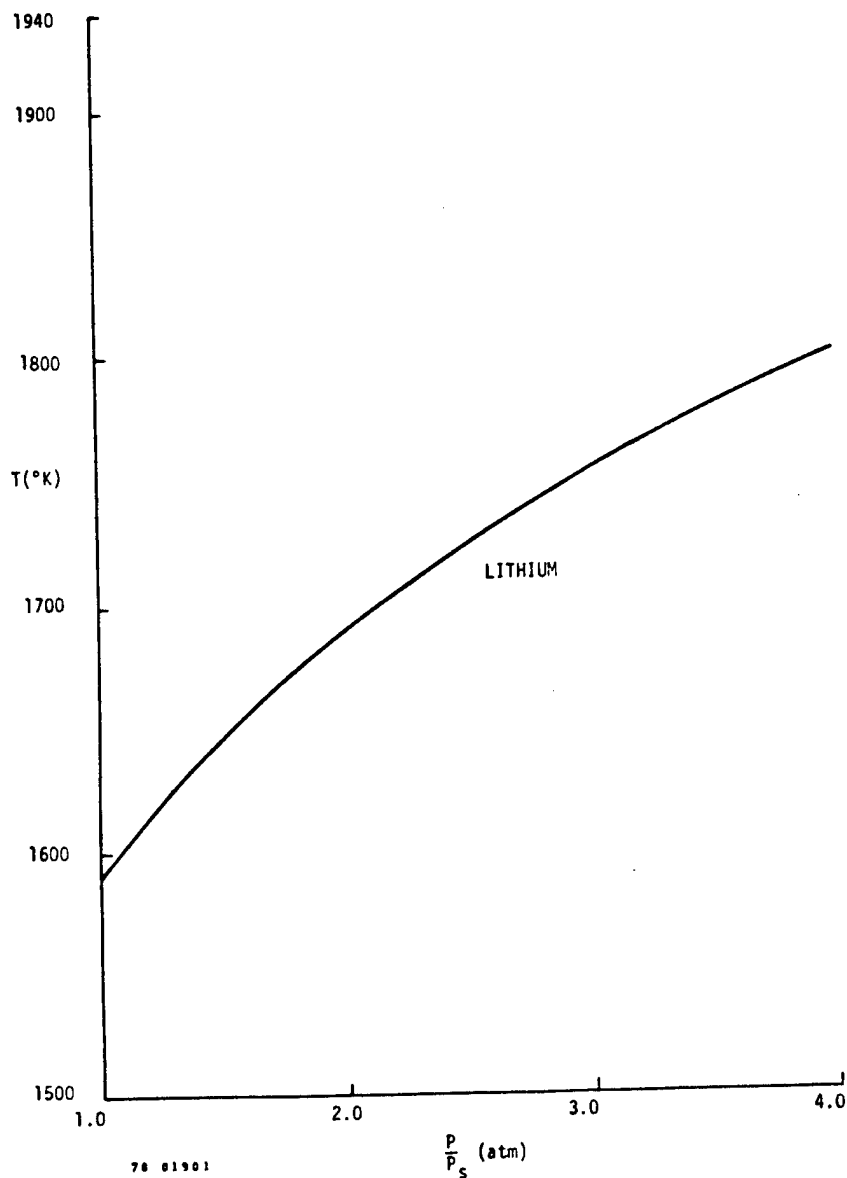


Figure 32. Variation of Boiling Point with Pressure

$$h_f = 0.625 C_p \rho v (R_e P_r)^{-0.6} \quad (45)$$

and T_f is the liquid metal temperature, 1720 °K. Solving (44) for A_h/A_a gives

$$\frac{A_h}{A_a} = \frac{0.5 \eta_m F_s \left(\frac{a}{r}\right)^2 \left(1 - e^{-0.5(r/a)^2}\right) - \epsilon \sigma T_B^4}{h_f (T_B - T_f)} \quad (46)$$

which is plotted in Figure 33 versus the cavity temperature, T_B . A choice of $T_B = 1700$ °K appears adequate to keep η_c high yet not have too large an area A_h (i.e., $A_h/A_a \approx 8$).

3.5 Waste Heat Radiator

Considerable difference exists in the literature for the design and weight of waste heat radiators. The Pratt and Whitney study used a separate liquid coolant in a finned tube radiator having a specific weight of 2.4 kg/kW of radiated power. The Hughes study assumed very approximately that a deployable radiator (i.e., unfolding, Teflon and aluminum structure) of the type designed for Sky Lab could be used with a specific weight of 0.23 kg/kW. Neither of these designs are armored against meteorite puncture.

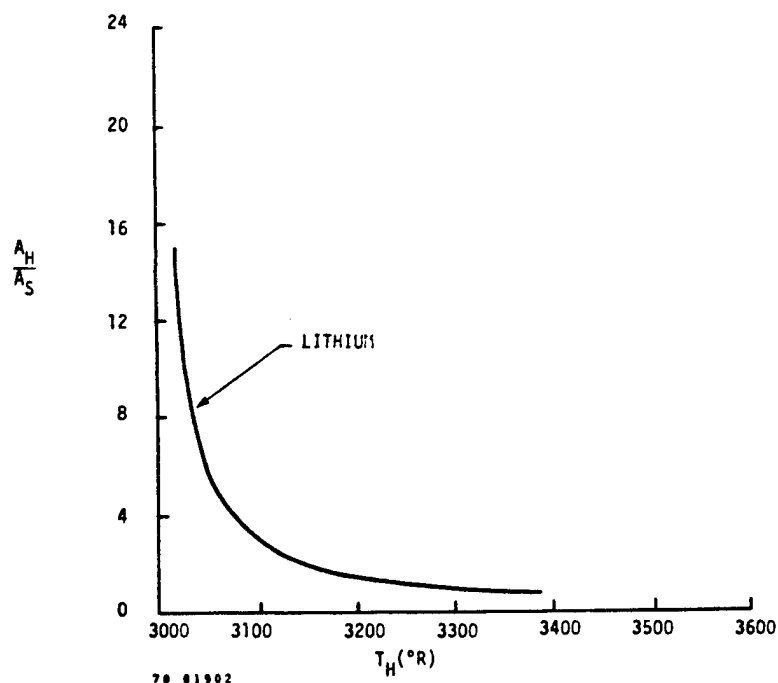
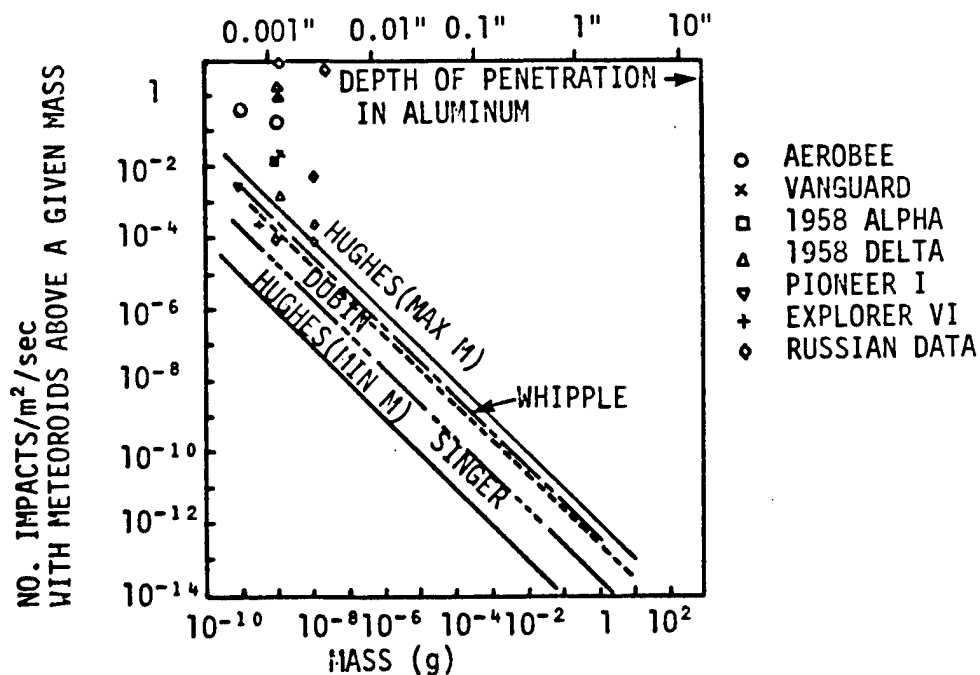


Figure 33. Ratio of Heat Exchanger Tube Area (A_H) to Aberrated Image Area (A_S) at Entrance to Cavity for Lithium Coolant as a Function of Temperature

Three factors influence the specific weight. First, the temperature and pressure of the coolant will affect the stress load on the radiator and hence the type of material to be used. If meteorite protection is desired, then armoring thickness will be the second factor influencing the weight. In this case the radiator mass will depend universally on the fourth power of the coolant temperature since more area is required to radiate a given amount of energy if it is available only at lower temperatures. Third, the particular design of the radiator structure will also affect the specific weight. These major influences are discussed below in an effort to arrive at a self-consistent basis for comparing radiator designs for each of the lasers being examined.

The figure of 0.23 kg/kW quoted by Hughes⁸ corresponds to a radiator density of $\frac{1}{3}$ kg/m² at 475 k, which is the areal density of an aluminum sheet 0.125 mm thick. According to Figure 34 there should then be around 10^{-5} meteoroid impacts per second with enough energy to penetrate a sheet of aluminum this thick.⁴³ Since radiator dimensions on the order of or

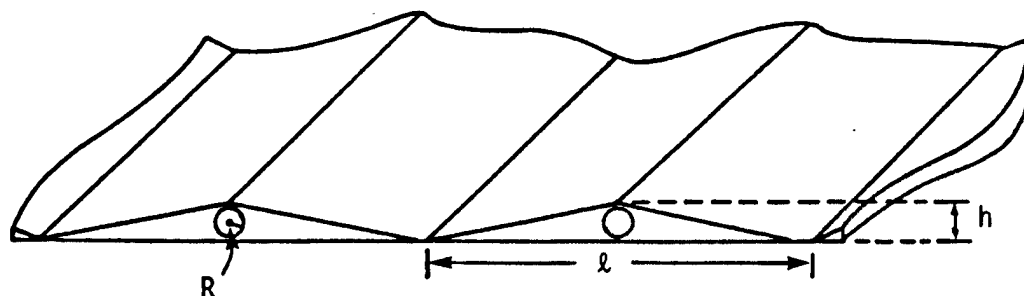


78 01903

Figure 34. Meteoroid Impact Frequency as a Function of Minimum Meteoroid Mass⁴³

larger than 10^5 m^2 are being contemplated in the design of this system, the number of potentially damaging impacts at $T_{\text{radiator}} = 475 \text{ }^\circ\text{K}$ is already appreciable if the radiator mass is kept at 0.23 Kg/Kw . Since each of the solar pumped laser systems considered are required to radiate at less than $400 \text{ }^\circ\text{K}$ their radiators would have to be both thinner and larger in order to radiate the required amounts of power, so that the potential for material damage increases rapidly with decreasing T_{rad} . For these reasons, some concern for the Hughes estimate of radiator masses may be justified. The Hughes estimate will be used initially in computing the radiator masses. However, this is done mainly to provide mass estimates consistent with those being made for competing systems. A more realistic radiator mass estimate will be made in this section to be used in the conceptual designs of Section 4.

An average areal density of 0.33 kg/m^2 is probably sufficient for an aluminum radiator to withstand the meteroid flux (it is the more critical fluid flow sections that are the thickest, see Figure 35). Below $475 \text{ }^\circ\text{K}$, however, the relationship between power radiated and radiator mass should probably be scaled by $\left(\frac{T_{\text{rad}}}{475}\right)^4$. In this way,



78 01904

Figure 35. Possible Radiator Design

the radiator thickness will remain constant up to $T_{\text{rad}} = 475 \text{ }^{\circ}\text{K}$ and increase above $475 \text{ }^{\circ}\text{K}$, providing adequate protection from meteroids at all temperatures (see Figure 36).

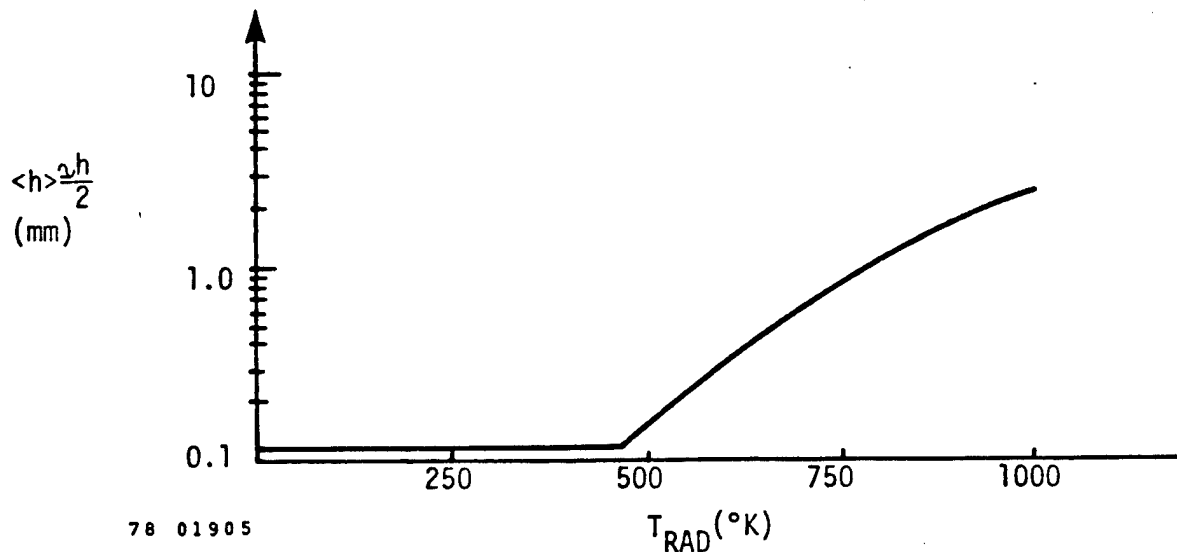


Figure 36. Average Radiator Thickness vs. Temperature

3.6. Solar Powered Gas Dynamic Laser

The closed cycle gas dynamic laser (GDL) analysis performed by Young and Kelch⁷ of Pratt and Whitney (P and W) serves as a basic design used in this evaluation. The GDL investigated for space application was developed in three versions in the original study; each GDL was powered by a nuclear reactor. The first version utilized a compressor to provide all of the heat to the lasant, as shown in the diagram in Figure 37. The second and third version applied conventional and advanced technology, respectively, to a regeneratively heated flow loop as shown in Figure 38.

The basic operation of all three versions depends on similar physics. The lasant is heated and then expanded so rapidly that the kinetic temperature drops below the vibrational temperature producing an inverted population of excited states which lase. The expansion is supersonic. In a closed cycle the gas must be slowed down and

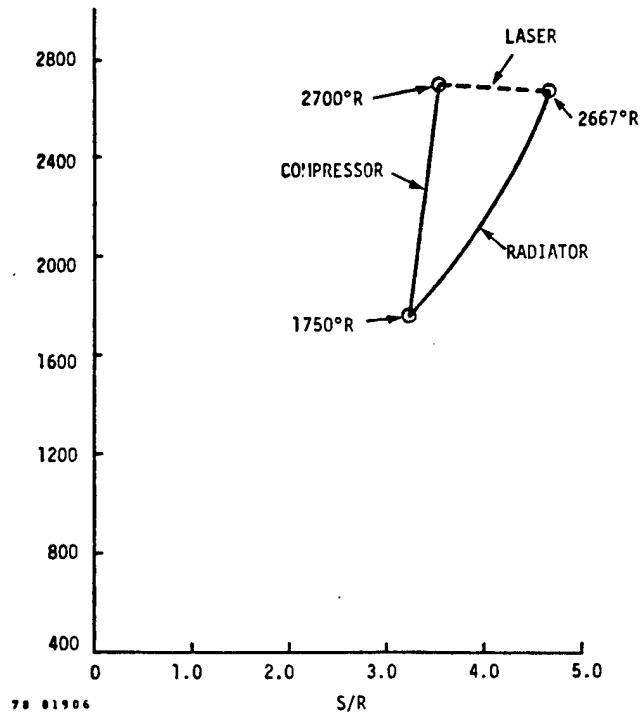


Figure 37. Temperature-Entropy Diagram of Non-Regenerated CO_2 GDL

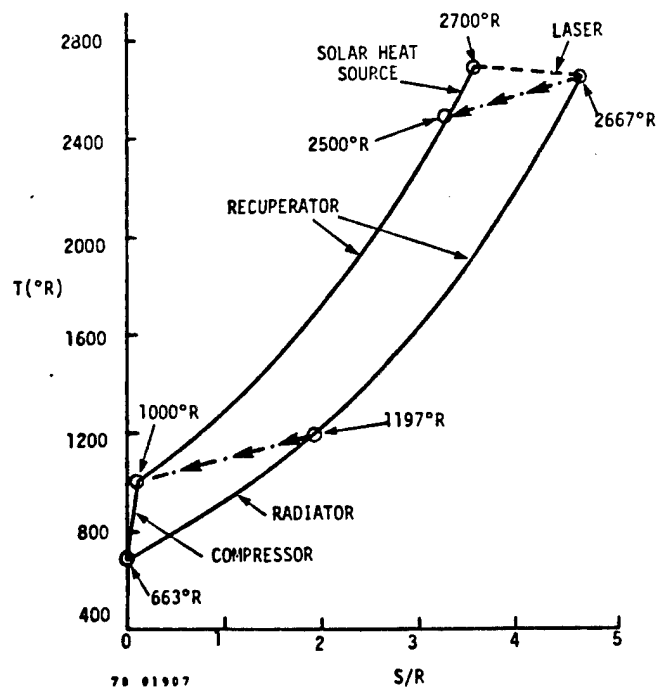


Figure 38. Recuperated CO_2 GDL (1 MW, $\gamma = 1.4$)

re-compressed to close the loop. A diffuser is used to decelerate the gas, recovering a good bit of the initial gas temperatures. In the first version most of this thermal energy is radiated as waste heat in the latter two versions some of the thermal energy is used to heat up the recompressed gas.

The principal differences between each version involves compressor technology, the first version requiring a high temperature compressor (presently unavailable and needing development) the second version relying on existing low temperature compressor technology and the third version depending on the development of a lightweight recuperator. We have adapted the second version of the GDL to a solar power source and have employed a waste heat radiator design consistent with all of the other laser types evaluated. The basic GDL parameters are summarized in Table 10 for the P and W 1 megawatt laser.⁷

The flow loop is diagramed schematically in Figure 39 where the dashed lines enclose the additions made to the Pratt and Whitney designs to provide solar power and to radiate waste heat. Solar energy must be supplied both to heat the lasant to 2700 °R and to drive the Brayton cycle power unit. The P & W design indicates that 6.6 MW of heat must be supplied at 2700 °R. Using the heat exchanger design discussed in Section 3.4 we see that a collector of ~ 100 m diameter is required as well as a cavity absorber to transfer the absorbed heat to the liquid lithium. The Brayton cycle must supply 8.8 MW of power to the laser loop compressor. Considering the weights discussed in Section 3.3 a specific weight of 2.55 Kg/Kw of output power is used. Similarly, the 14.4 MW of waste heat that must be radiated from the laser loop is available at 665 °K down to 380 °K.

A weight minimization similar to that conducted in the P & W study has been carried out here using a set of specific weights self-consistent with the Hughes study so that the two types of

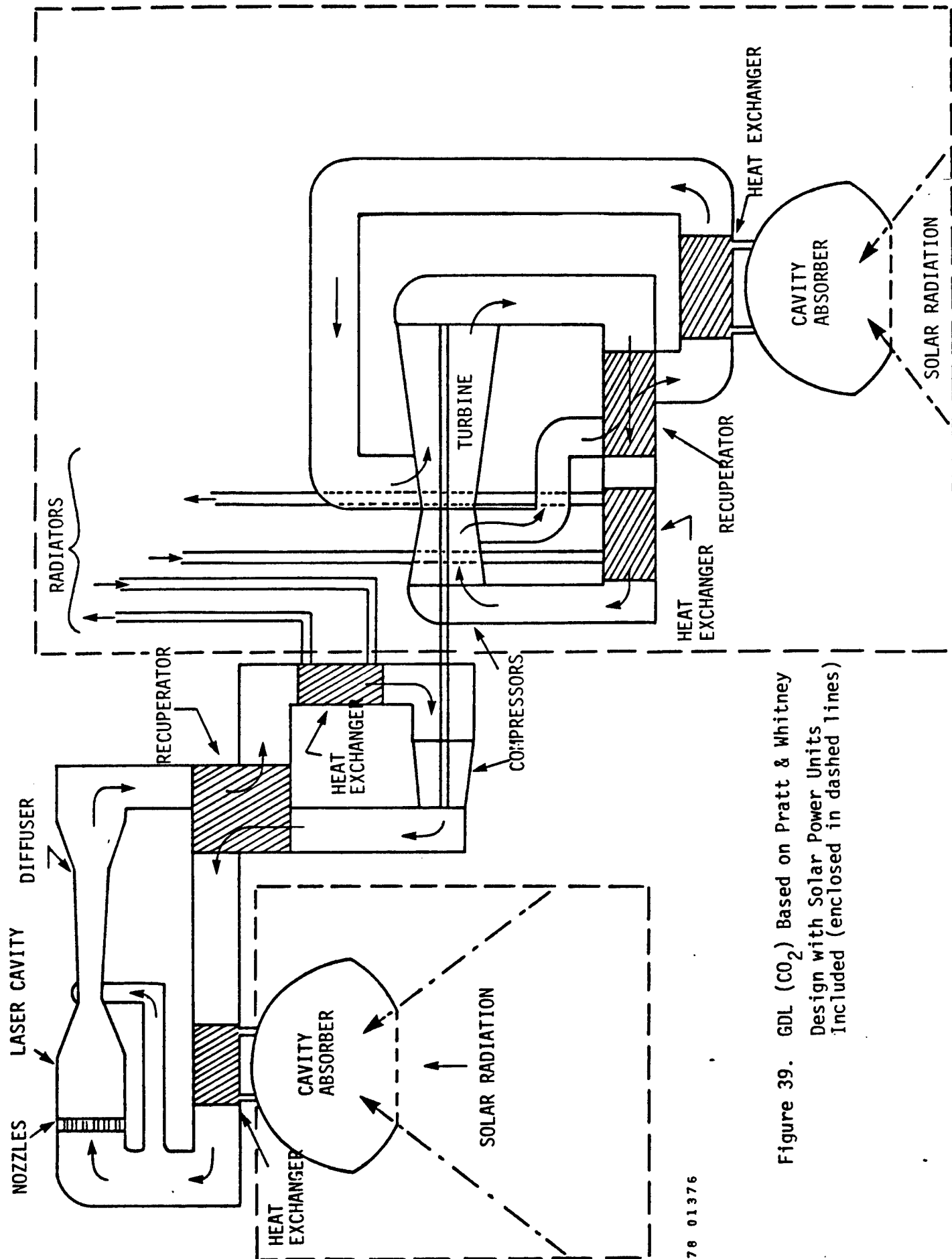
Table 10. Supersonic CO₂ GDL (1 MW)⁷

Parameters:

Laser Frequency (microns)	10.6
Gas Mix (N ₂ : CO ₂ : H ₂ O)	91:8:1
Stagnation Pressure (torr)	7755
Stagnation Temperature (°K)	1500
Nozzle Area Ratio	30:1
Mass Flow (kg/sec)	43.6
Cavity Width (cm)	14.86
Optical Configuration	2U0/3
Cavity Length (cm)	46
Cavity Height (cm)	13
Compressor Power (MW)	8.8
Heat Source (MW)	6.6
Heat Rejection (MW)	14.4

Weights (kg):

CNM	753
Diffuser	6,804
Recuperator	25,583
Heat Sink Heat Exchanger	6,083
Compressor	290
Aerodynamic Window	136
Heat Source Heat Exchanger	426
Ducts	3,606
Tanks	4,536
Optics	318
<hr/>	
Laser Subsystem	48,534 kg



78 01376

Figure 39. GDL (CO₂) Based on Pratt & Whitney Design with Solar Power Units Included (enclosed in dashed lines)

lasers can be compared on an equal basis. Those specific weights are listed in Table 11. The laser loop compressor exit temperature is the key variable in the weight minimization. This temperature can be phrased in terms of the compressor power, P_c , so that the total GDL weight is given by

$$W_{\text{total}} = W_L + W_{\text{sc}} + W_{\text{H1}} + W_{\text{RE}} + W_{\text{H2}} + W_{\text{RA}} + W_p + W_c \quad (47)$$

where W_{sc} = solar collector weight for laser loop, W_{H1} = absorber cavity weight for laser loop, W_{RE} = laser loop recuperator weight, W_{H2} = heat sink heat exchanger weight, W_{RA} = laser loop waste heat radiator weight, W_p = weight of solar Brayton power unit, W_c = weight of laser loop compressor, W_L = weight of remaining elements of the laser loop. The sum of

$$W_L + W_{\text{sc}} + W_{\text{H1}} = 8404 \text{ kg} \quad (48)$$

is constant throughout the minimization. For regenerator effectiveness $\epsilon_{\text{RE}} = 1$ (the most optimistic case), the weight equation becomes

$$W = 8404 + 0.56 [27.8(2667 - .12P_c)] + 0.109 P_c + \left(\frac{7.02 \times 10^{15}}{P_c^4} \right) P_c + 2.55 P_c + 0.098 P_c \quad (49)$$

where the order of terms is the same as in equation (47). Note the strong dependence on P_c due to the radiator temperature in the fourth term: here an optimistic assumption that $T_{\text{rad}} = T_{\text{exit}}$, the exit temperature of the compressor (i.e., inlet temperature for the radiator instead of the average radiator temperature). The minimum weight is

$$W_{\text{total}} = 64,626 \text{ kg at } P_c = 12,413 \text{ kW.} \quad (50)$$

Table 11. Specific Weights for Comparative Evaluation of Solar Lasers

Component	Coefficient	Scaling Variable	Reference
Ducts, Nozzles Optical Cavity, Diffusers	144 sec	\dot{M}_{LASER} (kg/sec) gas flow	Hughes (Ref. 8)
Radiators	0.23 (kg/kW)	P_{RAD} (kW)	Hughes (Ref. 8)
Turbines, Compressors	0.098 (kg/kW)	P_{OUT} (kW)	Hughes (Ref. 8)
Recuperator	0.56 (kg/kW)	P_{RECUP} (kW)	P & W (Ref. 7)
Collector	0.32 (kg/kW)	P_{COLLECT} (kW)	Hughes (Ref. 8)
Solar Brayton Power Unit	2.55 (kg/kW)	P_{OUT} (kW)	MSNW

This corresponds to a compressor exit temperature of 785 °K. The radiator inlet and outlet temperatures are 785 °K and 536 °K, respectively. These conditions vary considerably from those identified by P & W for the minimum weight conditions because lighter specific weights are used (to be consistent with the other lasers considered here) and because a solar power plant instead of a nuclear power plant was used. However, the higher temperature portion of the flow loop conditions are the same as the P & W study so that the nozzle, laser cavity and diffuser conditions are unchanged.

P & W has identified the critical technologies for the GDL as being the variable geometry diffuser design, heat exchanger and recuperator material development and optical system development. Improvements in present materials and design would allow a lighter more reliable laser to be built. The minimum weight computed above would require about 2.5 space shuttle loads (i.e., on the order of 27,000 kg each).⁶⁹

3.7. Solar Powered Electric Discharge Laser

The closed cycle electric discharge laser (EDL) analysis performed by Bailey and Smith⁸ of Hughes Aircraft Co (Hughes) is used as the basic EDL design in this evaluation. They examined both CO₂ and CO EDL's for CW space application assuming a solar power source. The CO₂ system was somewhat heavier than the CO system but this disadvantage was countered by a much better understood technology for the CO₂ system. A schematic of the flow loop for the subsonic CO₂ EDL system is shown in Figure 40 and the system parameters are reproduced in Table 12. The dimensions and possible configuration of an actual 1 MW CO₂ EDL is shown in Figure 41. The CO system has a similar flow arrangement with the major difference being that the CO laserant requires a very low operating temperature for good performance. The system best suited for this mode of operation was a supersonic CO EDL whose parameters are summarized in Table 13. As noted above

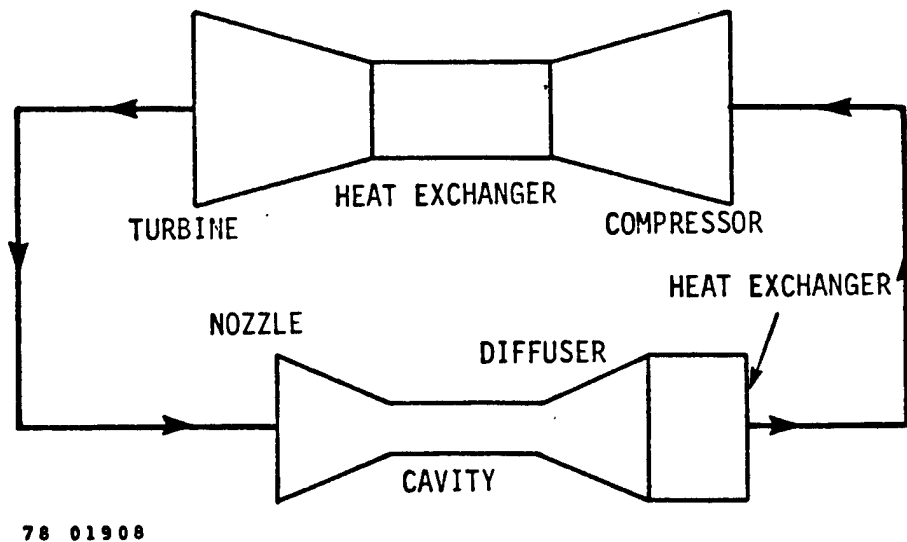


Figure 40. Refrigerator Laser Loop for Space Systems

Table 12
Subsonic CO₂ EDL (1 MW)⁸

<u>Parameters:</u>	
	10.6μ
Gas Mix He:N ₂ :CO ₂	8:7:1
Inlet Pressure (Torr)	450
Inlet Temperature (°K)	350
Inlet Mach Number	0.4
Mass Flow (kg/sec)	8.47
Cavity Width (cm)	75
No. Optical Passes	4
Output Coupling	90%
Cavity Length (cm)	4
Cavity Height (cm)	16
Sustainer Power (MW)	4.783
Net Turbo Power (MW)	1.699
Electron Beam Power (MW)	0.204
<u>Weights (kg):</u>	
Power conditioning	205
Inlet-cavity-diffuser	690
Electron guns	120
Optical Assembly	41
Duct work/structure	529
Heat exchangers	240
Compressor/gearbox	275
Turbine/generator	200
Exit window	42
Mirror cooling unit	240
Misc. (pumps, controls, etc.)	<u>258</u>
Laser System	2,840 kg

Table 12 (continued)

Laser system	2,840
Solar collector	8,600
Prime power	4,500
Radiator	<u>4,500</u>
Total	<u>20,400 kg</u>

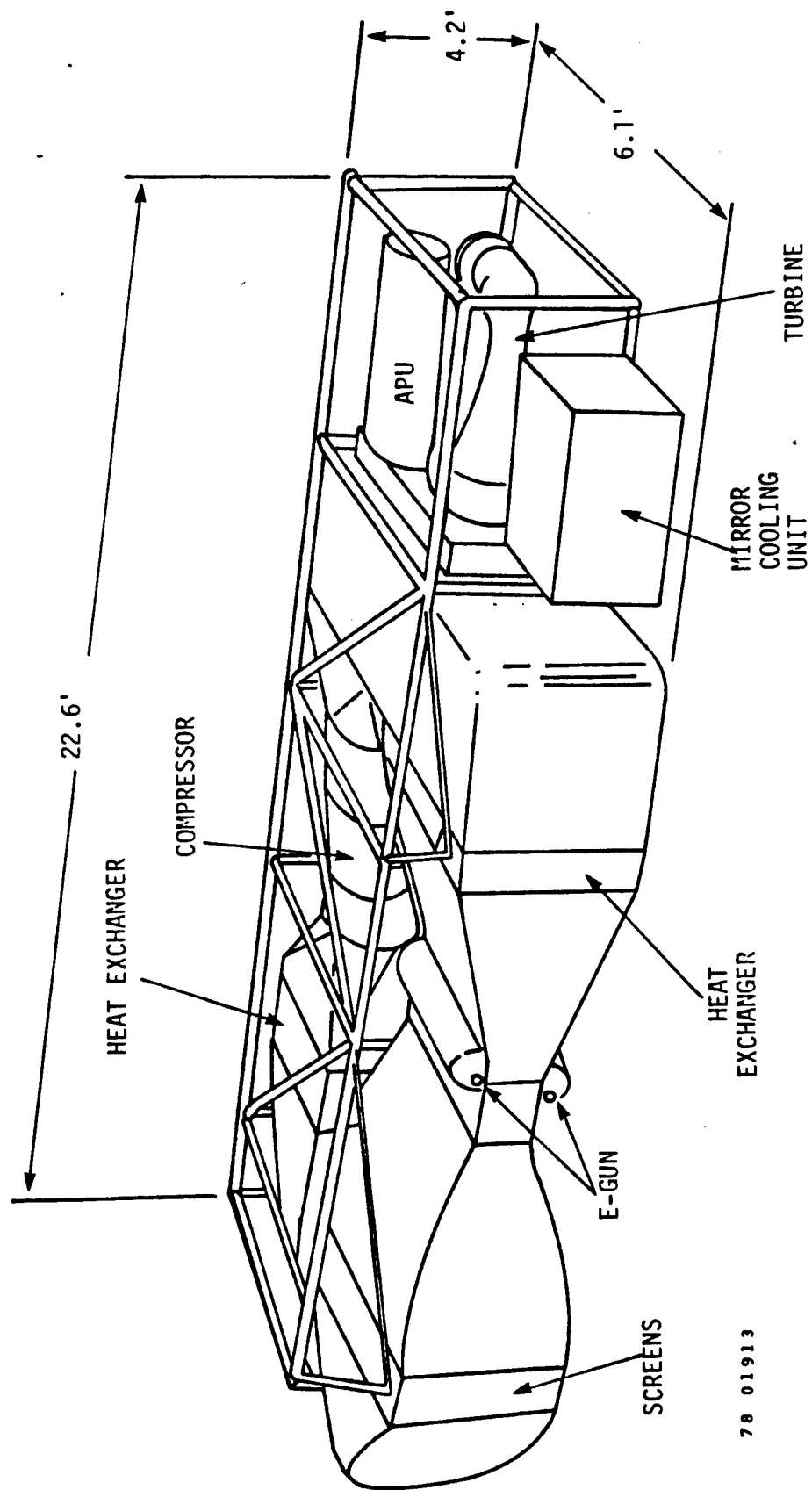


Figure 41. 1 Mwatt CO₂ Laser-Space⁸

78 01913

Table 13
Supersonic CO EDL (1 MW)⁸

Parameters:

Gas mix CO:Ar = 1:9
 Inlet mach no. = 3.58
 Inlet pressure = 65 torr
 Inlet temperature = 80 °K
 Cavity dimensions 5 x 10 x 60 cm
 Sustainer voltage = 1569 volts
 E-beam current density = 5.0 ma/cm²
 Sustainer power = 1.835 Mw
 Compressor power = 2.084 Mw
 Electron beam power = 0.455 Mw
 Estimated pump power = 0.025 Mw
 Total electrical power = 4.399 Mw
 System efficiency = 22.7%

Weights (kg):

Power conditioning	260
Inlet - cavity - diffuser	490
Electron gun	120
Optical assembly	32
Ductwork/structure	690
Heat exchangers	445
Compressor/gearbox	250
Exit window	42
Mirror cooling unit	200
Misc (pumps, controls, etc.)	<u>250</u>
Laser system	2,780
Solar collector	5,670
Prime power	4,350
Radiator	<u>4,163</u>
Total	<u>16,962 kg</u>

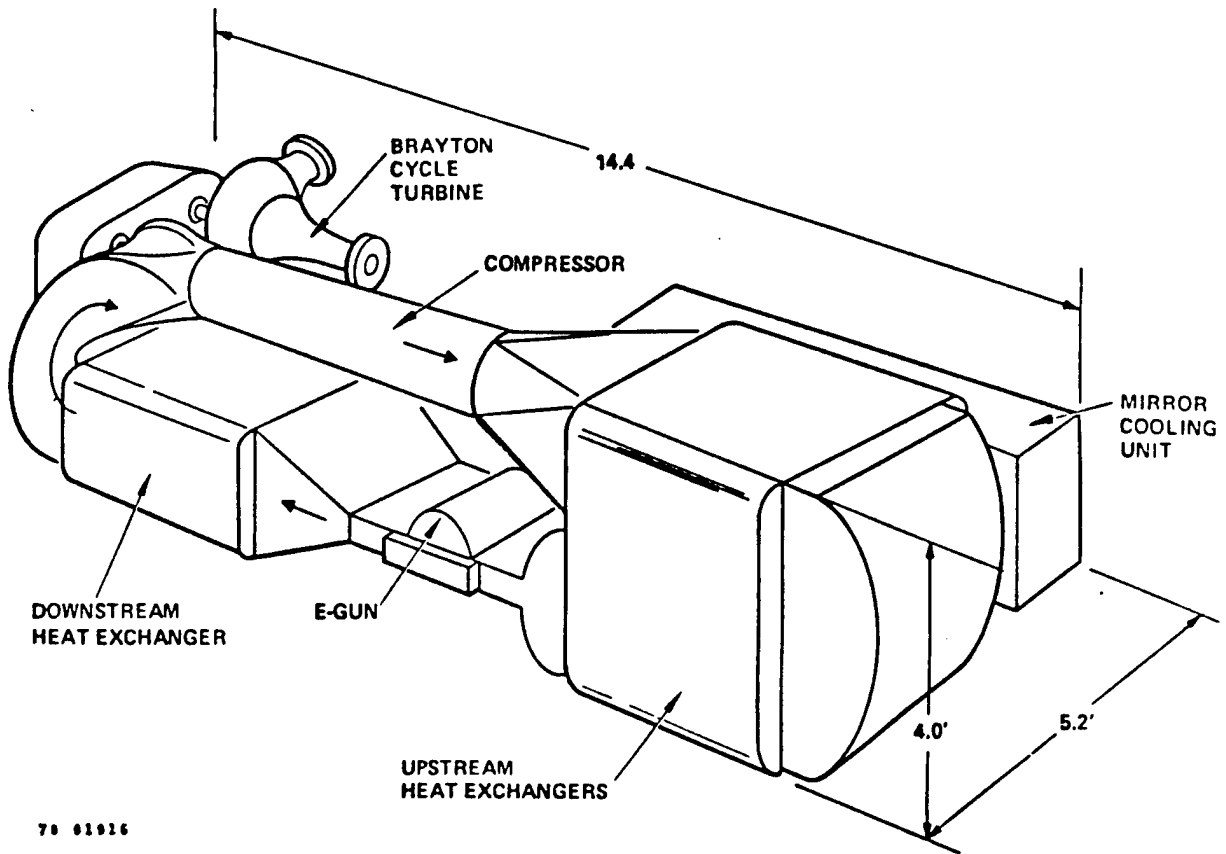


Figure 42. 1 MW CO Laser Space⁸

the CO EDL is lighter, at approximately 17,000 kg, compared to the CO₂ EDL, at approximately 20,000 kg. The dimensions and configuration of the CO EDL is shown in Figure 42.

3.8. Direct Solar Pumped Laser

Although no conceptual design for a direct optically pumped solar laser was developed, the weight of the CF_3I laser suggested by Rather et al.⁹ is estimated as a basis for comparing this laser to the others studied here. If we assume, as in Section 2.2, that the laser filter efficiency is 2.6% and the laser (quantum) efficiency is 21% then $P_{\text{RAD}} = 3.8 \text{ MW}$, $P_{\text{COLL}} = 183 \text{ MW}$. The weights of these two elements alone amount to

$$\begin{aligned} W_{\text{RAD}} + W_{\text{COLL}} &= (0.23) 3.8 \times 10^3 + (0.32) 183 \times 10^3 \\ &= 874 \text{ kg} + 58,560 \text{ kg} = 59,434 \text{ kg} \end{aligned}$$

An additional 600 kg is assigned to laser tubes, mirror, etc. and 250 kg to gas purification units. The critical technologies for this device are the threshold pumping power, the transparent laser tubes and the scheme for chemical reprocessing of the lasant.

3.9. Indirect Solar Pumped Laser

As a comparative example we choose the static CO_2 laser. A simple way of estimating the weight of this type of laser is developed here; the results are justified by the more detailed conceptual designs presented in Section 4.

The theory of these lasers discussed in Section 2.3 suggests that for $T_B = 2000 \text{ }^\circ\text{K}$, a laser (quantum) efficiency of 20 percent, and $P_T/P_m \cong$ that the overall system efficiency may be on the order of 10 percent. That is, for a 1 Megawatt laser output, 10 Megawatts of solar energy must be collected and 9 Megawatts rejected as waste heat. Furthermore, we assume that the static laser is cooled passively with heat pipes which require no gas circulation. Thus, with a black body cavity (plus laser tubes) weight of about 3000 kg the total approximate weight is

$$\begin{aligned} W_{\text{RAD}} + W_{\text{COLL}} + 3000 \text{ kg} &= (0.23) 9 \times 10^3 + (0.32) 10 \times 10^3 + 3000 \text{ kg} \\ &= 2070 + 3200 + 3000 = 8,270 \text{ kg} \end{aligned}$$

The critical technologies (discussed further in Section 4) for this class of lasers includes in order of priorities the laser tube materials, black body cavity, and, depending on the type of IOPL, either heat pipe radiators and/or solar Brayton cycle technology.

3.10 Comparative Analysis

The uniform weight estimates for each of the lasers are compared in Table 14. Clearly for the weight coefficients used, the indirect optically pumped solar laser is the lightest system and the GDL is the heaviest. In order to assess the robustness of this comparison, a sensitivity analysis of the total weights was made by varying first the collector specific weight and then the radiator specific weights as shown in Figures 43 and 44. The values used in Table 14 are identified by the vertical dashed line in both figures. The impact of this analysis is to verify the correctness of the conclusion drawn from Table 14 that the indirect optically pumped laser is the lightest over a considerable span of radiator and collector weight characteristics. Only at the extreme limit of low collector weight might the direct optically pumped scheme be preferable in terms of weight. Such low collector weights do not appear achievable in the 1990 time frame, in any case.

If one assumes that the capital cost of the laser system is roughly proportioned to the weights then similar conclusions are reached regarding the economic choice of the best laser. An overall summary of the comparative analysis, which includes the most critical technology in each case, is shown in Table 15. This table reinforces the choice of the indirect optically pumped solar laser as the proper subject for carrying out the conceptual design. These designs follow in Section 4.

Table 14. Solar Laser Weight Comparison
(1 MW Laser Output)

Components	Laser Type				Direct CF ₃ I	Indirect Static CO ₂
	Supersonic CO	EDL *	Subsonic CO ₂	GDL *	Supersonic CO ₂	OPL *
Laser Loop						
Ducts, Nozzle, Diffuser, Cavity, Mirrors, Window Cooling Subsystem	1,574		1,662	6,292	600	600
Radiator and Heat Exch.	445		240	5,023	874	2,070
Flow Loop Compressor	250		275	1,216	250	(N/A)
Gas Make-up Purification	250		258	(N/A)		(N/A)
Recuperator	(N/A)		(N/A)	18,330	(N/A)	(N/A)
Collector and Heat Exch.				2,112		
Power Source:						
Turbine/Recuperator/Compressor	4,350		4,700	7,199	(N/A)	(N/A)
Radiator and Heat Exch.	4,163		4,500	8,565		
Collector/Concentrator/Cavity Absorber	5,670		8,600	15,889	58,560	3,200
Power Conditioner	260		205	(N/A)	(N/A)	(N/A)
Black Body Cavity	(N/A)		(N/A)	(N/A)	(N/A)	2,400
Total Weight (kg)	16,962		20,440	64,626	60,284	8,270

*EDL = Electric Discharge Laser

GDL = Gas Dynamic Laser

OPL = Optically Pumped Laser

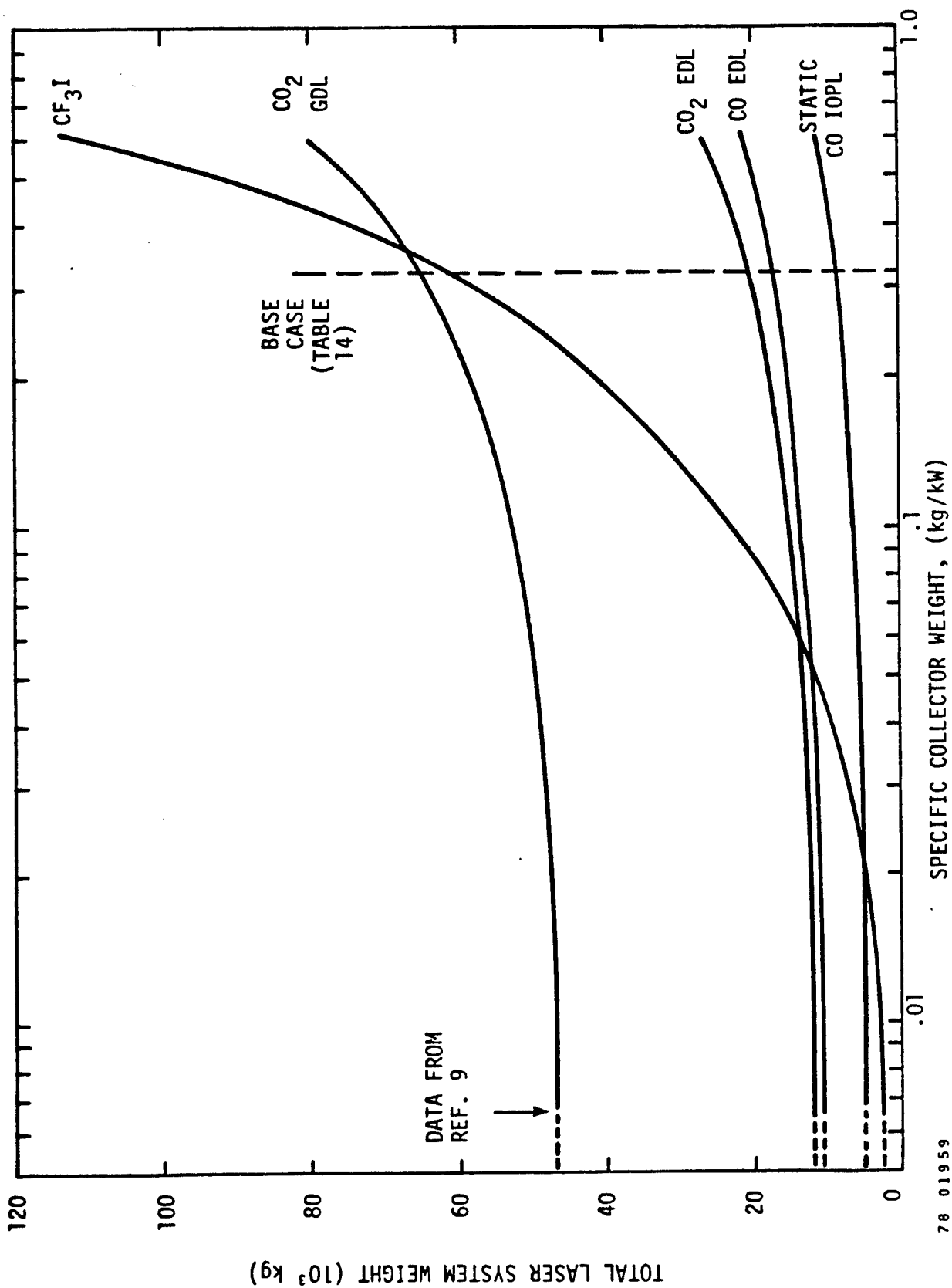
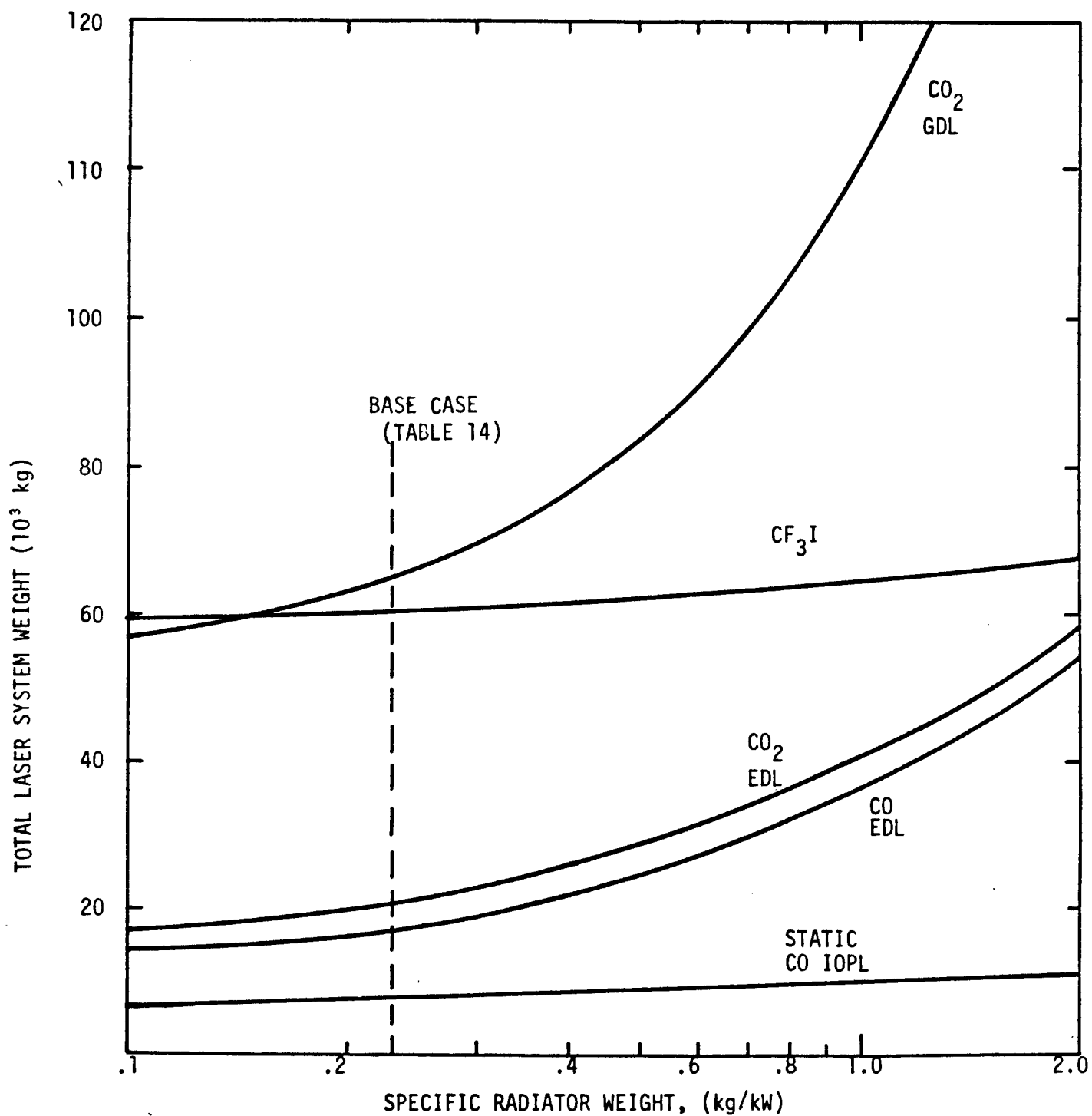


Figure 43. Total Solar Laser System Weight as a Function of Specific Solar Collector Weight



78 01960

Figure 44. Total Solar Laser System Weight as a Function of Specific Radiator Weight

Table 15. Summary of Solar Laser Comparison

Laser Type	Weight (kg)	Cost	Critical Areas	Experience
EDL (CO, CO ₂)	17,000-20,000	Medium	Chemistry	High
GDL (CO ₂)	65,000	High	None	High
Direct OPL(CF ₃ I)	60,000	High	Threshold Pumping Power; Chemistry	Modest
Indirect OPL (CO ₂)	8,000	Low	Optical Materials	Modest

SECTION 4

PRELIMINARY CONCEPTUAL DESIGNS OF THE INDIRECT SOLAR PUMPED LASER

The three indirect optically pumped schemes outlined in Section 2 are examined in more detail below to determine a basic conceptual design for each solar laser system and to evaluate the optimum performance condition for each in terms of efficiency and weight for a given power output.

Before discussing the masses of the systems under consideration it should be understood that the techniques used for estimating component masses in this work are characteristic but approximate. Estimates have been made for radiators, for instance, which include both constant area density estimates (i.e., 6.6 kg/m^2) and constant mass per watt estimates (i.e., 0.23 kg/kW). Areal density estimates for reflectors also vary dramatically, ranging between 0.45 kg/m^2 (Hughes) and 0.003 kg/m^2 .⁹ The Hughes estimates are used for consistent comparisons between competing systems. Computations using more realistic estimates for the radiator masses are presented in Section 4.4

4.1. Mixing Gas Laser System

The black body cavity in a solar pumped laser system must satisfy constraints imposed by the pumping time of the laser gas, the overall mass requirements of the system, and the temperature requirements of the laser gas. The simplest mixing laser geometry which seems capable of satisfying these demands is the layered tube configuration depicted in Figures 45 and 46. In this arrangement the CO pumping gas is exposed to the black body radiation emanating from the walls of the cavity and the carbon sheets between the tube layers. The pumped CO is then rapidly mixed with the CO_2 and H_2O and transferred into a

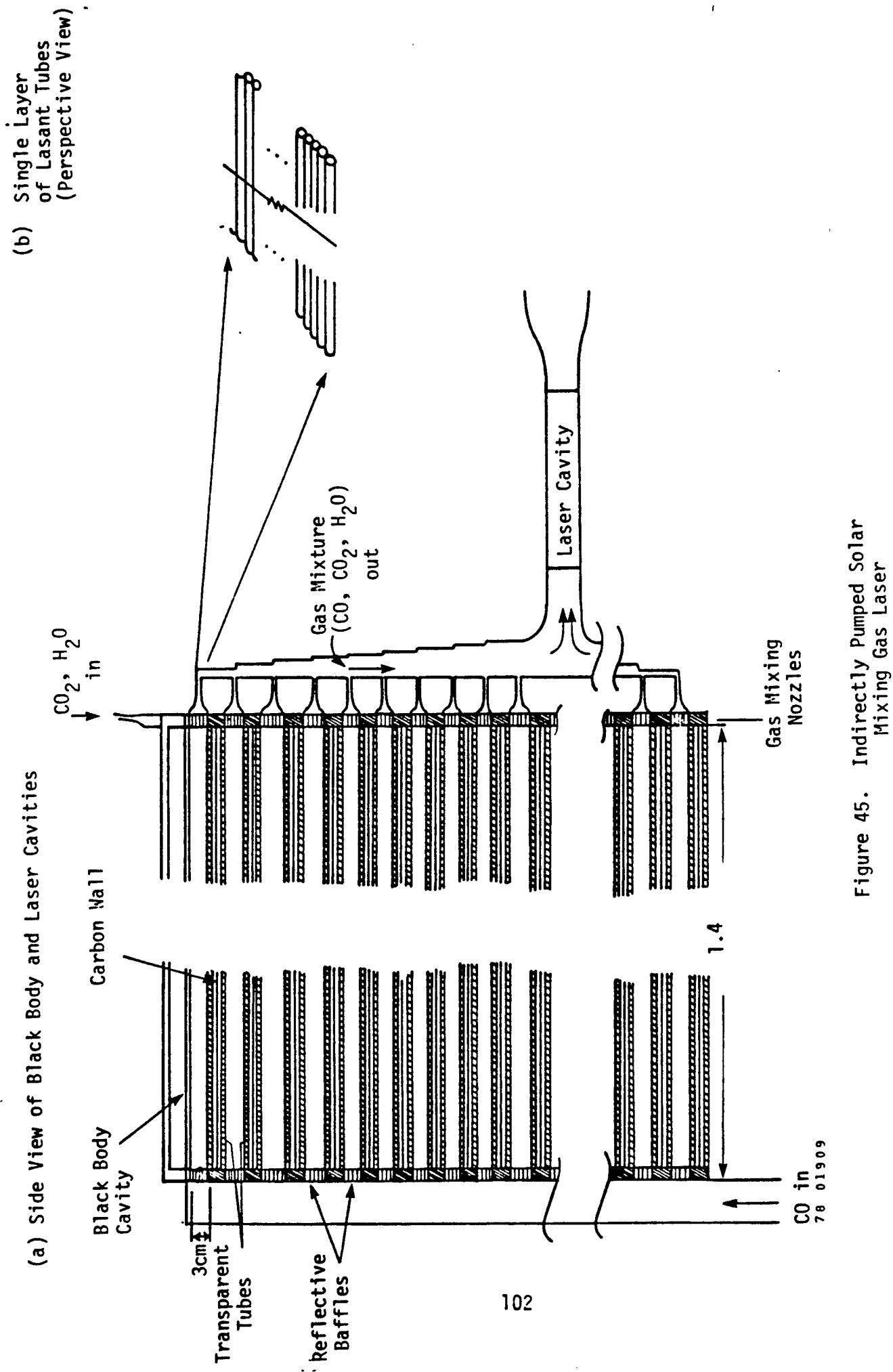
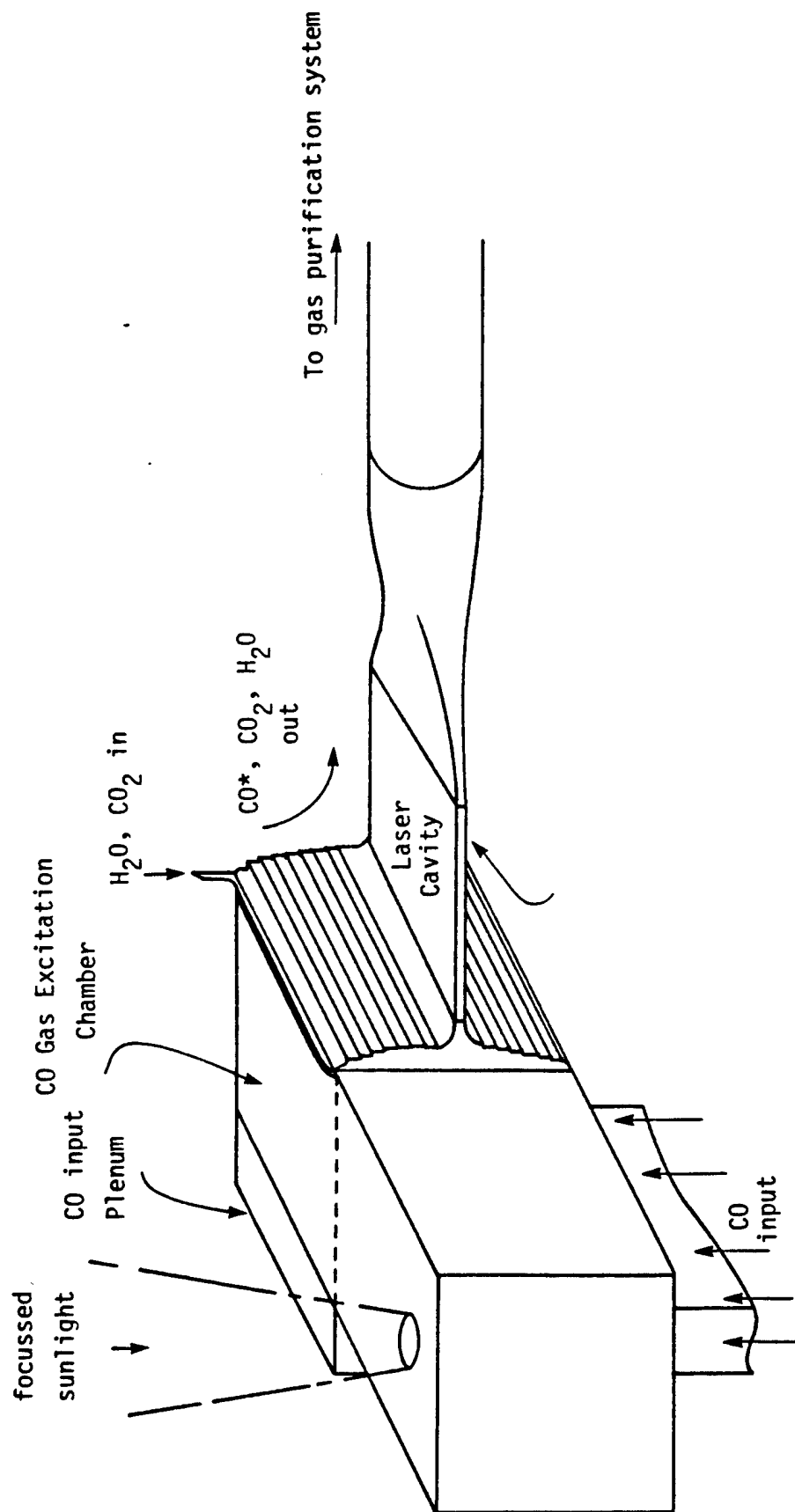


Figure 45. Indirectly Pumped Solar Mixing Gas Laser



78 01910

Figure 46. Black Body Excitation Chamber and Laser Cavity

laser cavity. After lasing, the CO_2 and H_2O must be removed from the CO stream, and the CO gases returned to the beginning of the cycle.

The meanings of symbols used in this section are defined below:

A = area

B_ν = spectral intensity at frequency

C_p = specific heat

F_A = flexural apparent limit

f_{ABS} = fraction of incident back body radiation absorbed

\bar{h}_c = unit convective heat conductance

h_ℓ = latent heat

ℓ = length of the transparent tubes

\dot{m} = mass flow of laser gas

M_T = mass of transparent tubes

N = number of layers of tubes

p = pressure of the laser gas

P_T = Prandtl number

P_{ABS} = power absorbed in the tube walls

P_{EXC} = power going into gas excitation

P_{HX} = heat flow in the heat exchanger

P_{IN} = total power intercepted by the solar reflector

P_L = laser power

P_{RAD} = power radiated at Radiator 1 or 2

$q_B = \sigma T_B^4$

R_e = Reynolds number

(SF) = safety factor

S_u = ultimate tensile strength
 T_o = gas temperature when entering the tubes
 T_B = black body temperature
 T_G = gas temperature when leaving the tube
 T_W = transparent tube wall temperature
 V = velocity of CO gas in the tubes
 W = number of tubes per layer
 δ = thickness of the tube walls
 η = overall efficiency of the system
 η' = partial efficiency of the system
 η_{DIFF} = fraction of energy incident on the black body which is absorbed
 η_c = collection efficiency of solar radiation
 η_{EXC} = fraction of incident power going into gas excitation
 η_{EC} = efficiency of conversion of solar power to electrical power
 η_L = laser efficiency
 η_R = reflectance of the solar mirror
 μ = viscosity
 ν = Poisson ratio
 ρ = density of the laser gas
 ρ' = density of the optical material comprising the tubes
 $\sigma = 5.6697 \times 10^{-8} \text{ watt/m}^2 \text{ } ^\circ\text{K}^4$
 τ = time for a CO gas molecule to traverse a transparent tube

Using

$$V = \frac{\dot{m}}{\rho A} = \frac{\dot{m}}{\pi \rho W N R^2} \quad \text{and} \quad V = \frac{\ell}{\tau}$$

provides the following expression for $\ell W N$:

$$W N = \frac{m \tau}{\pi R^2 \rho} \quad (51)$$

The total mass of the tubes, M_T is given by $W N \rho' \text{ (volume/tube)}$ or

$$M_T = 2 \pi R \delta \rho' (\ell W N) \quad (52)$$

Heat transfer in the tubes will depend on whether the flow is laminar or turbulent. To determine this the Reynolds number must be evaluated using the equation

$$R_e = \frac{2 \rho V R}{\mu} \quad (53)$$

which becomes

$$R_e = \frac{2 \dot{m}}{W N \mu \pi R} \quad (54)$$

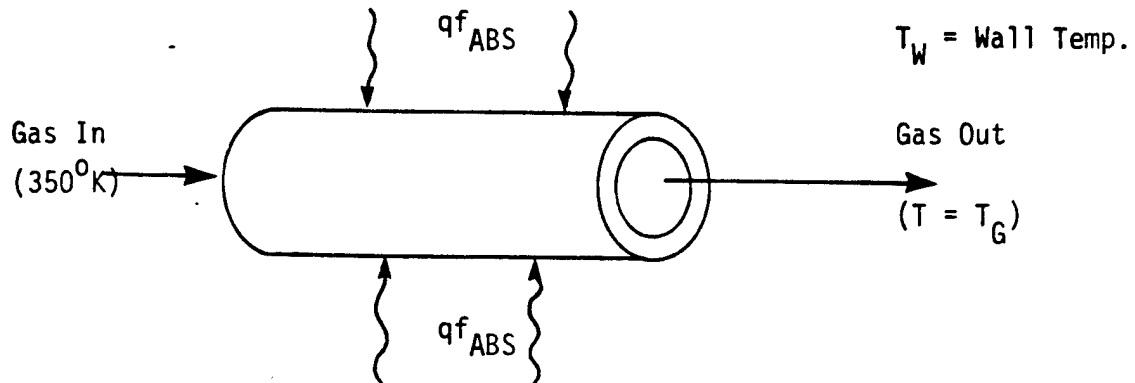
If $R_e \geq 10^4$ the flow is turbulent, and $R_e \leq 2000$ implies laminar flow. In order that the tubes not become excessively hot, turbulent flow is required, thus placing a restriction on $W N$ and \dot{m} (R is determined by the absorption length of IR radiation in the CO gas).

Assuming turbulent flow, \bar{h}_c is given by (Ref. 68, p. 379 ff)

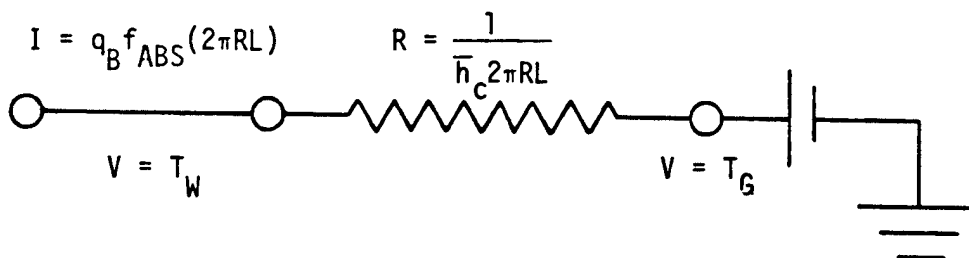
$$h_c = 0.023 C_p V \left(\frac{\mu_f}{2 R \rho V} \right)^{0.2} \left(P_{r_f} \right)^{2/3} \quad (55)$$

where the subscript "f" implies evaluation of the "mean film temperature" $T_f = \frac{1}{2}(T_w + T_g)$. Knowing \bar{h}_c , the temperature of the tube walls can be computed. Uniform irradiation of the tubes with a flux q_B will be assumed and an electrical analog to the actual system will be constructed according to the procedure of Ref. 68, p. 232 ff (Figure 47a).

(a) Heat Transfer in Cylinder



(b) Electrical Analog to Heat Transfer



78 01911

Figure 47. Heat Transfer in Laser Tubes

From Figure 47b, it is clear that "I" must be constant throughout the circuit. Using $\Delta V = IR$ then gives

$$(T_w - T_f) = [T_w - \frac{1}{2} (T_w + T_G)] = (q_B f_{abs} 2\pi R \ell) \left(\frac{1}{h_c 2\pi R \ell} \right) \quad (56)$$

or

$$T_w = \frac{2}{h_c} (q_B f_{abs}) + T_G \quad (57)$$

In order to evaluate T_G it will be assumed that all of the energy deposited in the tube walls is carried away by the gas. If the gas enters the tubes at T_o , then

$$T_G = T_o + \Delta T_G \quad (58)$$

where

$$\Delta T_G = (q_B f_{ABS}) \frac{2\pi R \ell}{C_p M_{gas}} \quad (59)$$

or

$$\Delta T_G = (q_B f_{ABS}) \frac{2\tau}{C_p \rho R} \quad (60)$$

T_G must remain less than 370°K for optimum pumping, and T_w obviously must remain far below the melting point of the optical material comprising the tubes. Also, T_o should remain above ~300°K so that a heat exchanger may be used to reduce the cooling requirements.

The thickness δ , of the cylindrical transparent tubes is given by (cf Ref.70, p. 298)

$$\delta = \frac{2(SF)Rp}{2S_u - p(SF)} \quad (61)$$

Knowing δ , the mass of the tube assembly can be calculated from Equations 51 and 52.

Absorptive losses in the tube walls are given by

$$P_{abs} = q_B W N \ell (2\pi R) f_{abs} \quad (62)$$

and the power going into CO excitation is given by

$$P_{exc} = \frac{1}{\eta} P_L \quad (63)$$

$$P_{exc} = \eta_{exc} (1 - f_{abs}) q_B 2\pi R \ell N W \quad (64)$$

η_{exc} is in turn given by

$$\eta_{exc}(T_B) = \frac{B(T_B)}{B_D(2000^\circ K)} \left(\frac{2000^\circ K}{T_B} \right)^4 \eta_{exc}(2000^\circ K), \quad (65)$$

where $\eta_{exc}(2000^\circ K)$ has been computed to be ≈ 0.04 .

In order to determine the mass of the heat exchanger, P_{HX} must be computed via

$$P_{HX} = (225^\circ K) [c_p(H_2O) \dot{m}(H_2O) + c_p(CO) \dot{m}(CO)] \\ + h_L(CO_2) \dot{m}(CO_2) + h_L(H_2O) \dot{m}(H_2O) \quad (66)$$

The H_2O is present in ~ 0.31 percent by weight, the CO_2 is ~ 6.17 percent by weight, and CO is ~ 93.52 percent by weight. Given these figures, \dot{m} for each gas can be computed as

$$\dot{m}(CO) = \dot{m} \\ \dot{m}(CO_2) = 6.598 \times 10^{-2} \dot{m} \\ \dot{m}(H_2O) = 3.315 \times 10^{-3} \dot{m} \quad (67)$$

and P_{HX} may be easily computed.

The partial efficiency of the laser system (neglecting pumping requirements in the gas cycle) is given by (Ref. 13)

$$\eta' = \frac{\eta_c \eta_L}{1 + \frac{P_{abs}^w}{P_L}} \quad (68)$$

If no active refrigeration unit is introduced for gas cooling, the only other power losses in the system derive from the power requirements of the gas compressors and the laser efficiency losses. The compressor power, P_c is approximately given by

$$P_c \cong 10^{-2} \text{ m Mwatt} \quad (69)$$

and the laser losses are given by

$$P_{\text{laser loss}} = \frac{1 - \eta_L}{\eta_L} P_L \quad (70)$$

This results in heating of the gas after the lasing stage. The total power which must be intercepted by the solar reflector is therefore

$$P_{IN} = [P_{ABS}^w + \frac{P_L}{\eta_L} + \frac{P_c}{\eta_{EC}}] \frac{1}{\eta_c \eta_R} \quad (71)$$

Assuming that the mirror can radiate away the power it absorbs from the solar flux, the total waste heat to be rejected by the radiators is given by

$$P_{\text{rad}} = P_{\text{abs}}^w + \frac{P_L}{\eta_L} + \frac{P_C}{\eta_{EC}} - P_L \quad (72)$$

The overall efficiency of the system is $\eta = P_L/P_{\text{in}}$

Using the powers calculated above, the mass of the satellite can be computed using the following coefficients

Mass of Ducts, Nozzles

Optical Cavities and Diffusers $\approx (144 \text{ sec}) \dot{m}$

Mass of Turbine, Compressors, and Associated Power Cycle = $300 P_C^{0.475}$

where P_C is given in KW and the resulting mass is in Kg.

Mass of Collector = $320 \frac{\text{kg}}{\text{mwatt}} P$

Mass of Radiator = $230 \left(\frac{\text{kg}}{\text{mwatt}} \right) P_{\text{rad}}$

Mass of Heat Exchange = 560 kg/MW

In addition, the black body will require about 250 kg of carbon, 1000 kg of carbon felt insulation, 150 kg for a structural shell and 100 kg for mirrors and other optical instruments. This adds an additional 1500 kg to the mass. Results of the calculations are shown in Tables 16 and 17 for material properties given in Table A1 of Appendix A and for

$$V = 40 \text{ m/sec} \ll \text{Mach } 1$$

$$P_{\text{EXC}} = 3.33 \text{ MW}$$

$$R_e = 4.3 \times 10^4 \text{ (Turbulent)}$$

$$\bar{h}_c = 100 \text{ W/m}^2 \text{ } ^\circ\text{K}$$

The results of mass and efficiency calculations are presented for two different methods of scaling radiator masses in Figures 49 and 50.

The only design which was thought to be a feasible alternative to the tubular layer arrangement depicted in Figure 45b was a similar structure with each layer of the tubes replaced by two parallel windows

Table 16. Absorption and Temperatures (Mixing Gas Laser)

f_{ABS}^* , ΔT_G^{**} , T_O , T_W ($T_G=360\text{K}$)

Optical Material	$T_B=3000\text{K}$				$T_B=2500\text{K}$				$T_B=2000\text{K}$				$T_B=1500\text{K}$			
	f_{ABS}	ΔT_G	T_O	T_W	f_{ABS}	ΔT_G	T_O	T_W	f_{ABS}	ΔT_G	T_O	T_W	f_{ABS}	ΔT_G	T_O	T_W
ZnSe	.0260	1050	-	-	.0096	186	174	785	.0057	45	315	463	.0012	28	332	424
KCl	7.27×10^{-4}	29	331	427	1.28×10^{-3}	25	335	417	2.45×10^{-3}	19	341	404	5.64×10^{-3}	14	346	392
CsI	6.61×10^{-4}	27	333	421	1.6×10^{-4}	3.1	357	367	1.78×10^{-4}	1.4	359	363	4.23×10^{-4}	11	359	362
MgO	.0359	1450	-	-	.0269	522	-	-	.0390	310	50	1070	.0081	222	138	866
Sapphire	.0266	1070	-	-	.0461	1550	-	-	.0904	719	-	-	.2116	533	-	-

* From Ref. 13

**All temperatures are in °K

Table 17. Mixing Gas Laser

System Parameters

	$T_B=3000K$			$T_B=2500K$			$T_B=2000K$			$T_B=1500K$		
	ZnSe	KCl	CsI	ZnSe	KCl	CsI	ZnSe	KCl	CsI	ZnSe	KCl	CsI
η_c (%)	-	35.2	35.2	-	58.6	58.6	77.9	77.9	77.9	90.9	90.9	90.9
δ^* (mm)	-	1.30	0.52	-	1.30	0.52	0.10	1.30	0.52	0.10	1.30	0.52
L_{WN} (m)	-	498	498	-	658	657	980	977	975	1740	1730	1730
M_T (Kg)	-	121	110	-	160	145	52.2	238	216	92.7	421	382
\dot{m} ($\frac{Kg}{sec}$)	-	5.15	5.15	-	6.80	6.79	10.1	10.1	10.1	18.0	17.9	17.8
P_{ABS}^W (MW)	-	.157	.142	-	.176	.0244	.478	.205	.0148	.529	.265	.0197
P_O (MW)	-	.0515	.0515	-	.0680	.0679	.101	.101	.101	.180	.179	.178
P_{HX} (MW)	-	1.65	1.65	-	2.18	2.15	3.23	3.22	3.21	5.74	5.70	6.66
P_{IN} (MW)	-	12.6	12.6	-	7.94	7.65	6.88	6.49	6.22	6.92	6.59	6.27
M_{RAD}	-	2380	2380	-	1410	1350	1190	1110	1060	1210	1130	1070
η' (%)	-	28.7	28.8	-	28.5	29.8	26.2	28.3	29.9	25.9	27.8	29.8
η (%)	-	7.91	7.94	-	12.6	13.1	14.5	15.4	16.1	14.4	15.2	15.9
M_{TOTAL}	-	1.16×10^4	1.16×10^4	-	1.00×10^4	9.85×10^3	1.09×10^3	1.09×10^4	1.07×10^4	1.44×10^4	1.45×10^4	1.42×10^4

*In view of the practical difficulties involved in constructing tubes less than .1 mm thick, $\delta < .1$ mm will not be allowed.

of supported IR transparent material. Since it is not possible for any thin substance appropriate for this use to support 3/4 atm of pressure over an area in excess of 1 m² without supports, it was necessary to consider a "mosaic" consisting of $(\frac{\ell}{\ell'})^2$ pieces of window material $\ell' \times \ell'$ meters square, supported by metal frames. The frames would be rectangular in cross section, d x b meters, and ℓ meters long.

Having settled on the alternative design, three problems must be considered: (1) Providing adequate structural strength to support 3/4 atm without appreciable deviations from a planar geometry; (2) Minimizing the mass of the window assembly; (3) Minimizing the power absorbed in the window assembly. The first and second considerations lead to square window plates. This geometry (see Ref. 70) provides the greatest strength with the least thickness. The second and third considerations require that vertical struts be placed between the top and bottom window support beams at each beam intersection. If this is not done, the support beams must be made very large ($bd \approx 10^{-2}$ to 10^{-3} m²), resulting in prohibitively large power losses and masses. Algebraic expressions for the window assembly mass, M_T , and power absorption, P_{abs}^W , were developed involving d and ℓ' as independent variables (ℓ was fixed by constraints on τ , R_e and N, and b and d are related through stress considerations). Minimizing the power absorption with respect to d provided a relationship between d and ℓ' ($d \propto \ell'$). Placing this expression into the equations for M_T and P_{abs}^W resulted in expressions depending only on ℓ' , which could then be varied in the search for reasonable values of M_T and P_{abs}^W . The structure of $P_{abs}^W(\ell')$ was such that no minimum existed until $\ell' = \ell$ was reached, which reflected the fact that the metal supports, even when 99.4 percent reflective, were absorbing immense amounts of power compared to the window material. This was partially due to the fact that the total surface area of the metal was very large and partially due to the broad band nature of the absorption. M_T , on the other hand, had

a minimum at very small values of λ' (1 to 4 cm). The smallest value for $\frac{P_{abs}^{PW}}{P_{exc}}$ which resulted in a real, positive λ' was 2.4,

corresponding to an η' of 5.6 percent. This is far less efficient than the tube-layer approach and would therefore require larger radiators and collectors. Furthermore, window masses in excess of 1500 kg resulted in all cases, so that the tube-layer approach is preferable from a net mass point of view as well.

The laser tubes will experience an apparent gravitational field at lift-off. The longitudinal force each tube experiences (if vertically oriented) will be between 1.2 mg^{71} and 3 mg^{72} when m = the mass of one tube and $g = 9.8 \text{ m/sec}$. The necessary wall thickness for a circular tube experiencing longitudinal compression is given by (Ref. 70, p. 352, Force = 3 mg)

$$\delta_g = \frac{15\sqrt{3}}{2} \frac{(1-\nu^2)^{1/2}}{E} R \text{ mg} \quad (73)$$

Using $m = \frac{M}{1200}$ gives $\delta_g = 2.4 \times 10^{-11} \text{ m}$ for KCl, which means that there should be no problem with regard to tube buckling for δ as given by Equation 62.

The excitation of CO gas by black body radiation has been examined in two geometries. The first of these, an arrangement of WN tubes of radius 1.5 cm into N layers of W tubes each, results in masses on the order of 10^4 Kg , and overall efficiencies of 10 percent. The other approach, involving the construction of N sets of two parallel windows through which the CO gas would flow, resulted in much greater masses (10^4 to 10^5 kg) and significantly lower efficiencies. The tube-layer approach would appear to be far easier to construct, involving no frames or struts for support, and would not require any cooling other than that

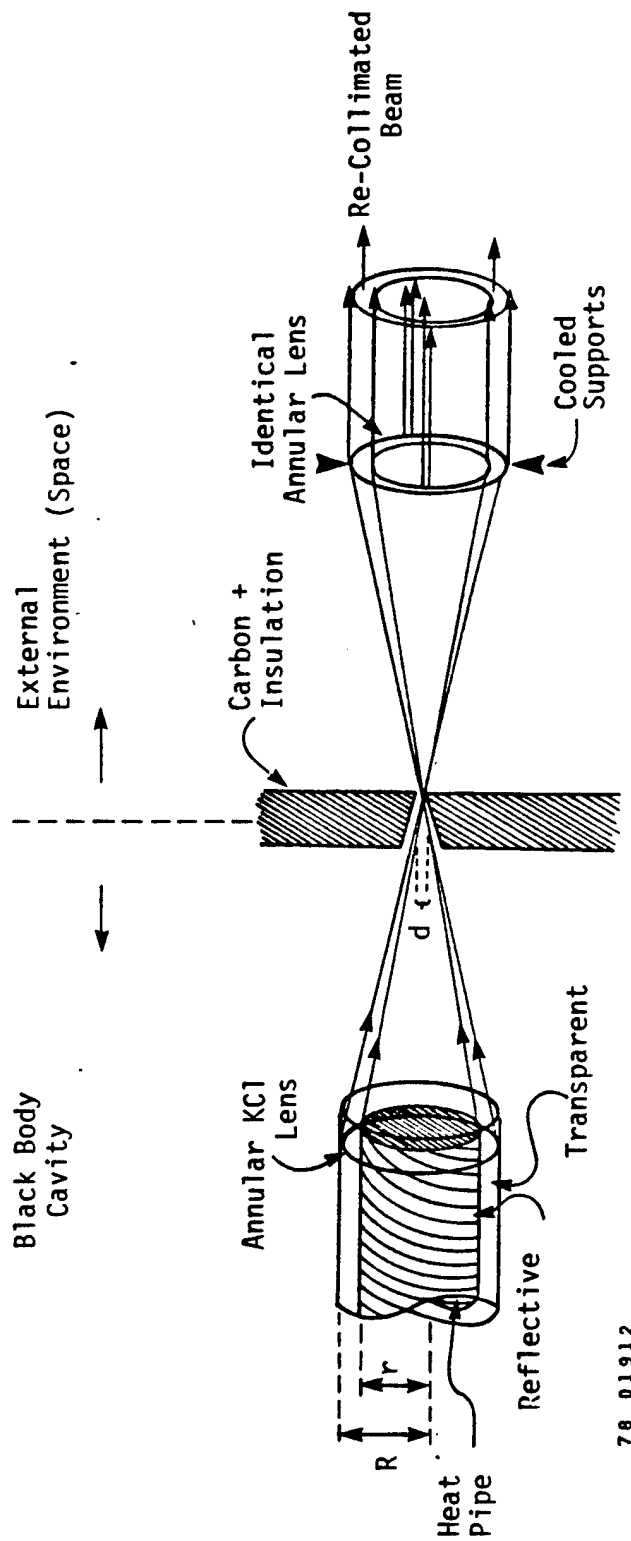
provided by the flowing CO gas itself. The window arrangement, aside from the complicated array of structural supports required, also requires cooling channels to be bored through the metal frames. Furthermore, the transportation of the tubes by low-G space shuttle could be easily and safely accomplished by simply stacking the tubes vertically, conceivably assembled into the gas excitation module. The window assembly, however, would probably prove more susceptible to damage when accelerated, and would probably need to be constructed in space.

4.2 Static CO Laser System

The static CO₂ system, while simpler than the mixing gas system, is more difficult to operate without large radiative losses from the tube ends. Since the laser cavities themselves are inside the black body, reflective baffles to prevent black body losses would also prevent any laser radiation from leaving the tubes. In order to circumvent this problem, the laser light may be focused to a small spot which can then be passed through the black body cavity walls and passed through a lens identical to the first, thus reforming the cylindrical beam (Fig. 48). The radiative power loss through NW holes of diameter d and in the wall is (see section 4.1 for nomenclature)

$$P'_{\text{RAD}} = \frac{\pi}{4} \sigma T_B^4 \text{ NW } d^2. \quad (74)$$

In addition to P'_{RAD} , there will be a power loss due to the presence of the lenses (assumed to be KCl). This loss arises both from the reflectance and absorptance of the KCl. While the reflected laser light is not rejected as heat, it does diminish the intensity of the laser beam, thus requiring that P_L be increased to compensate for this effect. Given a transmittance, T_r , and two lenses,



78 01912

Figure 48. Details of Bean Penetration of Black Body Cavity Wall (Static CO Laser)

$$P_L = \frac{P_{out}}{(1-T_r)^2} \quad (75)$$

where P_{out} is the desired laser power output of the satellite. The amount of power absorbed by the lenses is given by

$$P'_{ABS} = [2f_{ABS}(\lambda_L) - f_{ABS}^2(\lambda_L)]P_L \quad (76)$$

where λ_L = the wavelength of the laser radiation. This loss does make a demand upon the heat rejection system.

While the lens at the end of the laser cavity is cooled by the heat pipe and laser gas, the lens outside the cavity must be edge cooled to avoid heating. Quantitatively, about $\frac{1}{2}P'_{ABS}$ must be removed from the lens in order that it not be excessively heated. With a transmittance, T_r , and reflectance, R_f , the equilibrium temperature of an uncooled lens, T_{lens} , would be

$$T_{lens} = \left[\frac{P_L}{\sigma(T_r - R_f)} \right]^{0.25} \quad (77)$$

which would typically be 10^4 °K, too high for any lens material. The lens must therefore be cooled by the heat rejection system.

The total amount of heat to be rejected to the coolant in the static CO₂ system is given by the power absorbed in the laser tube walls and lenses, plus the power absorbed in the "silvered" coolant tube walls, plus the volume laser losses, P_v . If each laser tube contains a cooling tube of outer radius r with absorptance a , the power to be carried away by the coolant is given by

$$P_{cool} = 2\pi\sigma T_B^4 NWL [Rf_{ABS} + ra] + P_v + P'_{ABS} \quad (78)$$

The absorptance, a , of the silvered tube will be relatively independent of T_B ($a \sim .006$ in all cases of interest) however f_{ABS} varies greatly with the choice of optical materials and T_B .¹³ P_V is given by

$$P_V = \left(\frac{1 - \eta_L}{\eta_L} \right) P_L, \text{ so}$$

$$P_{cool} = 2\pi\sigma T_B^4 NW\ell [Rf_{ABS} + ra] + \left[\frac{1 - \eta_L}{\eta_L} + 2f_{ABS} - f_{ABS}^2 \right] P_L \quad (79)$$

P_L itself is defined by

$$P_L = 2\pi\sigma T_B^4 \eta_{EXC} \eta_L NW\ell R \left[\frac{1 - f_{ABS}}{T_r^2} \right] \quad (80)$$

where η_{EXC} = fraction of σT_B^4 used in pumping the laser gas and T_r is $\sim .92$ (Ref. 73) when the lenses are made of KCl; η_{EXC} for this CO_2 system is scaled from Table 6 of Section 2.35 so that

$$\eta_{EXC}(2000^\circ K) \cong .0046 \quad (81)$$

From (78) and (80) it is obvious that $NW\ell$ should be kept as small as possible and $NW\ell R$ as large as possible; R however is limited by the absorption length of the pumping radiation in the laser medium. For 18 isotopes of CO_2 lasant at 18 torr partial pressure diluted with an equal volume of helium a total path length of about 1 cm in the lasant has been computed to be optimum (see Section 2). This requires that $R - r = \lambda \cong 0.5$ cm (see Figure 48) in order that the total average path length in the lasant be 1 cm. The value of r will depend on the temperature at which the coolant pipe must be maintained in order to prevent excessive heating of the laser medium and the capacity of the coolant pipe for removing heat at that temperature. The details of the heat pipe and coolant require calculations that are rather complicated and not entirely germane to the present discussion; however, preliminary calculations indicate that for either a heat pipe or fluid flow, $r \sim 1.5$ cm is a reasonable dimension. If this value of r is assumed and P_{OUT} is taken to

be 10^6 Watt, then a value for $NW\lambda$ can be obtained from Equations 80 and 81 and P_{cool} can be determined from Equation 79. For the latter calculation, $\eta_L \approx 30\%$ can be assumed (see Section 2.3.5). Values for η_{exc} , $NW\lambda$, and P_{cool} are presented in Table 18. The values of N , W and λ are not computed separately since they will depend upon the details of the cooling apparatus. A knowledge of $NW\lambda$ will be sufficient for determining the mass and approximate efficiency of this system.

Having determined P_{cool} and $NW\lambda$ the only additional parameter which must be specified before making mass and efficiency estimates is the temperature of the coolant, T_C . This temperature will be given by $T_C = T_{max} - \Delta T \approx 370^\circ K - \Delta T$. ΔT , which is the difference in the temperature of the gas at r and that at R , is in turn given by the combined action of two effects: the power lost in the optical material of the laser tube and the volume absorption of radiation in the gas which does not go into optical pumping. The heat generated by absorption by the surface of the cooling tube does not contribute to ΔT , since this heat is presumably removed almost immediately by the coolant

Table 18. Static CO_2 Laser Properties

($r = 1.5$ cm, $\lambda = 0.5$ cm)

Optical Material	η_{exc}	$T_B=3000K$			$T_B=2500K$			$T_B=2000K$			$T_B=1500K$	
		$NW\lambda$ (m)	$P_{cool}^{(MW)}$	η_{exc}	$NW\lambda$ (m)	$P_{cool}^{(MW)}$	η_{exc}	$NW\lambda$ (m)	$P_{cool}^{(MW)}$	η_{exc}	$NW\lambda$ (m)	$P_{cool}^{(MW)}$
ZnSe	.0019	2620	48.9	.0029	3540	16.7	.0046	5410	9.06	.0076	1.05×10^4	8.71
KCl	"	2550	10.5	"	3510	8.41	"	5390	7.04	"	1.04×10^4	6.58
CsI	"	2550	10.4	"	3510	7.31	"	5380	5.63	"	1.04×10^4	4.60
MgO	"	2650	64.6	"	3610	34.3	"	5600	30.6	"	1.13×10^4	40.9
Sapphire	"	2620	49.9	"	3680	54.7	"	5920	67.0	"	1.31×10^4	105

If P = the heat generated per unit volume,

$$P = k \frac{d^2}{dr^2} T \quad (82)$$

or

$$\frac{P(R^2 - r^2)}{2k} = \Delta T_{vol} \quad (83)$$

Then P is in turn given by

$$P = \frac{1 - \eta_c}{\eta_c} \frac{P_L}{NW \ell \pi (R^2 - r^2)} \quad (84)$$

so that

$$\Delta T_{vol} = \frac{1 - \eta_c}{\eta_c} \frac{P_L}{2\pi NW \ell k} \approx 440^\circ K \quad (\text{for } T_B = 1500^\circ K) \quad (85)$$

Obviously, $T_B > 1500^\circ K$ will not be desirable, since $NW \ell$ decreases with T_B . The temperature difference due to heat absorption in the tube walls is given by $\Delta T_w = \frac{P}{kA} \Delta X$, or ($T_B = 1500^\circ K$)

$$\Delta T_w = f_{ABS} \sigma T_B^4 \frac{R(R-r)}{rk} \approx 110^\circ K \quad (86)$$

These results indicate a total temperature difference of about $550^\circ K$. Since the coolant must be kept above $\sim 200^\circ K$ in order for the CO_2 to remain gaseous, the temperature of the hottest layer of gas would be $750^\circ K$ according to this calculation. This is far too hot to lose well, so the gas will either have to be circulated to facilitate the removal of heat, or an artificial gravity will have to be introduced by rotating the satellite. This reduces the simplicity of the system, although it still has the advantage of radiating waste heat at $200^\circ K$ rather than $125^\circ K$. Preliminary calculations indicate that the convection introduced by spinning the satellite cools the gas more effectively than slowly flowing the gas through the tube. Angular velocities on the order of .14 rad/sec appear to be adequate for a tube 1/2 m from the axis of rotation (i.e., $8^\circ/\text{sec}$). This is a very modest rate of rotation which could easily be built into the system.

Knowing the temperature of the coolant and the amount of power to be rejected for each combination of T_B and optical materials, an estimate for the mass and area of the required radiator can be made. The radiator mass will be assumed to be 230 kg/MW and to have an absorptance of unity. It will be positioned so that both sides of the radiator may radiate. The masses and areas associated with the radiators (M_R , A_R) for rejecting P_{cool} (MW) at $T_C = 200^\circ\text{K}$ are given in Table 19. In view of their very large absorptances, sapphire and MgO are not included in the table. The addition of a refrigeration stage is also possible. This would greatly reduce the radiator area required, and may be desirable if ZnSe is used or if $T_B = 3000^\circ\text{K}$ is desired. In view of the additional complications introduced by the use of a refrigerator, no active refrigeration unit will be included in the mass and efficiency calculations to follow.

The mass of the cooling pipes is given by

$$M_C = 2\pi r \delta' (NW\ell) \rho_{AL} \quad (87)$$

where δ' = the thickness of the pipe walls, which are assumed to be made of aluminum. The thickness, δ' , will either be given by⁷⁰

$$\delta' = \frac{2r(SF)P'_{max}}{2S'u - (SF)P_{max}} \quad (88)$$

or

$$S'u \geq \frac{2Mg'\ell^2}{\pi[r^4 - (r - \delta')^4]} = \frac{2\rho[r^2 - (r - \delta')^2]g'\ell^3}{r^4 - (r - \delta')^4} \quad (89)$$

where (88) determines the thickness necessary to prevent bursting due to the internal gas pressure and (89) determines the thickness necessary for the pipe to withstand the artificial gravity, g' , when supported at only one end. For the aluminium cooling pipe, Equation 88 is the determining equation, and leads to $\delta' \approx .2\text{mm}$ when $SF = 2.5$ and $P'_{max} = 12 \text{ atm}$. For the optical pumping tube Equation 88 is again the appropriate equation to use. Indeed, the structure of (89) is such that it favors the smallest possible values of δ , so that the only function it serves is to check

Table 19. Radiator Area and Mass (Static CO₂ Laser)

Optical Material	T _B =3000K		T _B =2500K		T _B =2000K		T _B =1500K	
	A _{rad} (m ²)	M _{rad} (Kg)	A _{rad}	M _{rad}	A _{rad}	M _{rad}	A _{rad}	M _{rad}
ZnSe	2.70 x 10 ⁵	11200	9.20 x 10 ⁴	3840	4.99 x 10 ⁴	2080	4.80 x 10 ⁴	2000
KCl	5.79 x 10 ⁴	2420	4.64 x 10 ⁴	1930	3.88 x 10 ⁴	1620	3.63 x 10 ⁴	1510
CsI	5.73 x 10 ⁴	2390	4.03 x 10 ⁴	1680	3.10 x 10 ⁴	1290	2.54 x 10 ⁴	1060

that the value of δ determined by Equation 88 is adequately small. Values of δ calculated in this fashion are presented in Table 20. For g' , .03 m/sec² was used in Equation 88, and $\ell = 2.3\text{m}$ guarantees that values of δ satisfying (89) are possible.

Once δ and δ' are determined, the mass of the optical pumping and cooling tubes, M_T , is given by

$$M_T = \pi[R^2 - (R - \delta)^2]NW\ell\rho + \pi[r^2 - (r - \delta')^2]NW\ell\rho' \quad (90)$$

The results of Equation 90 are also presented in Table 20.

The mass of the solar collector depends upon the amount of power which must be collected, which in turn depends upon P_{cool} , η_c (the collection efficiency) and η_R (the reflectance of the mirror). Assuming that the collection losses, P_{cool} , and P_L are the only significant sinks of power implies that

$$P_{\text{IN}} = (P_{\text{cool}} + P_L) \frac{1}{\eta_c} \frac{1}{\eta_R} \quad (91)$$

η_c is as given in Section 3.2. and that $\eta_R \sim 0.9$, and using for the mirror mass⁸

$$M_m = (320 \frac{\text{kg}}{\text{MW}}) P_{\text{IN}} \quad (92)$$

provides the values for P_{IN} and M_m presented in Table 21.

Aside from those components previously weighed, there are a number of additional components which will be insensitive to the particular choice of T_B and optical material. Allowing 400 kg for carbon to form the black body, 1000 kg for carbon felt insulation, 400 kg for an outer structural shell, 1000 kg for liquid duct work and pumps for cooling and 200 kg for mirrors and other optical instruments implies that the total mass of the laser system, M_{total} is given by

$$M_{\text{total}} = M_m + M_{\text{RAD}} + M_T + 3000 \text{ kg.} \quad (93)$$

Table 20. Tube Mass (Static CO₂ Laser)

($\delta' = .2$ mm, $\ell = 2.3$ m, M_T in Kg)

Optical Material	δ^*	M_T (3000K)	M_T (2500K)	M_T (2000K)	M_T (1500K)
ZnSe	.1 mm	318	430	657	1270
KCl	.1 mm	193	265	407	785
CsI	.1 mm	273	376	576	1110

*In view of the practical difficulties involved in making tubes of less than .1 mm thickness, $\delta < .1$ mm will not be allowed.

Table 21. Total Input Power and Mirror Mass (Static CO₂ Laser)
(P_m in MW, M_m in Kg)

Optical Material	T _B =3000K		T _B =2500K		T _B =2000K		T _B =1500K	
	P _{IN}	M _m	P _{IN}	M _m	P _{IN}	M _m	P _{IN}	M _m
ZnSe	158	5.06 x 10 ⁴	33.9	1.08 x 10 ⁴	14.6	4670	12.1	3870
KCl	36.9	1.18 x 10 ⁴	18.2	5820	11.7	3750	9.49	3040
CsI	36.6	1.17 x 10 ⁴	16.1	5150	9.72	3110	7.07	2260

The results of equation (93) are presented in Table 22, and in Figs. 49 and 50 along with values for the overall laser efficiency which is given by

$$\eta = \frac{P_L}{\eta_R P_{IN}} = \frac{\eta_c P_L}{P_{cool} + P_L} \quad (94)$$

4.3 Non-Mixing Flowing CO Laser

The symbols used in this section are again identical to those of Section 4.1 (Mixing Gas) except where explicitly defined. Due to similarities between these systems the following equations can be taken over directly from the mixing laser case:

$$V = \frac{\dot{m}}{\pi \rho W N R^2} = \frac{\ell}{\tau} \quad (95)$$

$$\ell W N = \frac{\dot{m} \tau}{\pi R^2 \rho} \quad (96)$$

$$R_e = \frac{2 \rho V R}{\mu} \quad (97)$$

$$\bar{h}_c = 0.023 C_{p \rho V} \left(\frac{\mu_f}{2 R \rho V} \right)^{0.2} P_{r_v}^{-2/3} \quad (98)$$

where the "f" subscript implies evaluation at the "mean" film temperature, $T_f = 1/2(T_W + T_G)$.

$$T_W = \frac{2}{\bar{h}_c} (q_B f_{ABS}) + T_G \quad (99)$$

$$T_G = 125^\circ K + \Delta T_G \quad (100)$$

$$\Delta T_G = q_B f_{ABS} \frac{2\tau}{C_{p \rho R}} \quad (101)$$

The solutions of these equations are presented in Table 23.

The tube wall thicknesses for each choice of T_B and of optical materials will be the same as for the mixing laser system and, as in the mixing laser system,

Table 22. Total Mass and Efficiency (Static CO₂ Laser)

Optical Material	T _B =3000K		T _B =2500K		T _B =2000K		T _B =1500K	
	M _{TOTAL}	η (%)	M _{TOTAL}	η (%)	M _{TOTAL}	η (%)	M _{TOTAL}	η (%)
ZnSe	6.52 x 10 ⁴	0.83	1.81 x 10 ⁴	3.87	1.04 x 10 ⁴	8.99	1.01 x 10 ⁴	10.9
KCl	1.74 x 10 ⁴	3.56	1.10 x 10 ⁴	7.22	8.78 x 10 ³	11.2	8.34 x 10 ³	13.8
CsI	1.74 x 10 ⁴	3.59	1.02 x 10 ⁴	8.15	7.98 x 10 ³	13.5	7.43 x 10 ³	18.6

Table 23. Temperatures (Flowing CO Laser)
(All Temperatures in Kelvin)

Optical Material	T _B =3000K		T _B =2500K		T _B =2000K		T _B =1500K	
	ΔT_G	T _W	ΔT_G	T _W	ΔT_G	T _W	ΔT_G	T _W
ZnSe	348	1550	62.0	379	15.1	187	9.4	163
KCl	9.7	165	8.3	159	6.5	152	4.7	144
CsI	8.9	161	1.0	129	0.5	127	0.4	126
MgO	481	2100	174	838	103	548	73.7	428
Sapphire	356	1590	298	1350	239	1110	177	852

$$M_T = (\epsilon WN) 2\pi R \rho \delta \quad (102)$$

and

$$\delta = \frac{2R(SF)P}{2Su-(SF)P} \quad (103)$$

where (SF) = the safety factor.

$$P_{ABS}^W = \sigma T_B^4 WN \epsilon 2\pi R f_{ABS} \quad (104)$$

$$P_{EXC} = 2\pi \eta_{EXC} (1 - f_{ABS}) \sigma T_B^4 \epsilon WNR \quad (105)$$

where η_{EXC} is that fraction of the radiation passing into the gas which is used for optical pumping. $\eta_{EXC}(2000^\circ K)$, as in the mixing gas case, is $\sim .04$, η_c = the collection efficiency of the solar radiation (see Section 3.2) and η_L = the laser efficiency (≈ 0.50 , assuming an efficiency comparable to that obtained in EDLs with similar lasants).

Since

$$P_L = \eta_L P_{EXC} = 10^6 \text{ Watt} \quad (106)$$

P_{EXC} is known, which implies that ϵWN is known through Equation 105 for each material and value of T_B . Knowing ϵWN , P_{ABS}^W can be found via Equation 104, and M_T from Equation 102. The total solar power which must be intercepted by the reflector is then given by

$$P_{IN} = \left[P_{ABS}^W + \frac{P_L}{\eta_L} + \frac{P_c}{\eta_{EC}} \right] \frac{1}{\eta_c} \frac{1}{\eta_R} \quad (107)$$

where P_c = the power which must be supplied to the compression, and η_{EC} is the efficiency of conversion of the solar energy to electrical energy.

P_c is approximately given by

$$P_c \sim 10^4 \text{ m Watt}, \quad (108)$$

$\eta_{EC} \sim 10\%$ will be assumed and \dot{m} is given by Equation (96).

These results are presented in Table 24.

M_{RAD} can also be computed once P_{IN} is known. Since P_L is the laser output power, the waste energy must be radiated away at the rate $P_{IN} - P_L$. If no refrigerator is used, this must be done at $125^\circ K$. Using

$M_{RAD} \sim (230 \frac{\text{kg}}{\text{MW}}) (\eta_R \eta_C P_{IN} - P_L)$ yields the values tabulated in Table 24.

The efficiency η is given by

$$\eta = \eta_C \frac{P_L}{\eta_R P_{IN}} \quad (109)$$

and η' is as previously defined. Finally, the total masses for each T_B optical material combination may be computed using the following coefficients:

Mass of ducts, nozzles, optical cavity, and diffusers = $(144 \text{ sec})\dot{m}$

Mass of turbines, compressors and associated equipment = $[300 P_C^{0.475} (\text{kW})] \text{kg}$

Mass of collector = $(320 \text{ kg/MW}) P_{IN}$

There is then an additional 1500 kg associated with the black body itself, as in Section 4.1. These results are also presented in Table 24. Basic data and assumptions include:

$$\begin{aligned} \mu(125\text{K}) &= 8.34 \times 10^{-6} \text{ kg/m-sec} \\ \mu(150\text{K}) &= 9.91 \times 10^{-6} \text{ kg/m-sec} \\ \mu(200\text{K}) &= 1.30 \times 10^{-5} \text{ kg/m-sec} \\ C_p(125\text{K}) &= 1040 \text{ Joule/kg-K} = C_p(150\text{K}) = C_p(200\text{K}) \\ \rho &= 2.198 \text{ kg/m}^3 \text{ at } 125 \text{ K and } 3/4 \text{ atm} \\ R &= 0.015 \text{ m (due to absorption length of IR in CO)} \\ p &\sim 7.58 \times 10^4 \frac{\text{Nt}}{\text{m}^2} \end{aligned}$$

Stipulating that $\lambda = 2.0 \text{ m}$, $\tau = .05 \text{ sec}$ implies that

$$\begin{aligned} V &= 40.0 \text{ m/sec} \\ R_e(125\text{K}) &\sim 3.16 \times 10^5 \text{ (Turbulent flow)} \\ R_e(150\text{K}) &\sim 2.66 \times 10^5 \text{ (Turbulent flow)} \\ \bar{h}_c &\sim 221 \frac{\text{Watt}}{\text{m}^2\text{-K}} \end{aligned}$$

Only those systems boxed in Table 23 are involved in Table 24. Mass and efficiency scaling with temperature are shown in Figures 49 and 50.

Table 24. System Parameters (Flowing CO Laser)

	$T_B=3000K$			$T_B=2500K$			$T_B=2000K$			$T_B=1500K$		
	ZnSe	KCl	CsI	ZnSe	KCl	CsI	ZnSe	KCl	CsI	ZnSe	KCl	CsI
η_c	-	.352	.352	-	.586	.586	.779	.779	.779	.909	.909	.909
δ (mm)	-	1.30	0.52	-	1.30	0.52	0.10	1.30	0.52	0.10	1.30	0.52
λ_{WN} (m)	-	299	299	-	395	394	588	586	585	1050	1040	1040
M_T (Kg)	-	72.8	66.0	-	96.1	87.2	31.3	143	129	55.8	253	229
\dot{m} (Kg/sec)	-	9.29	9.29	-	12.3	12.2	18.3	18.2	18.2	32.6	32.3	32.3
P_{ABS}^W (MW)	-	.0940	.0855	-	.105	.0132	.287	.123	.0089	.317	.159	.0118
P_C (MW)	-	.0929	.0929	-	.123	.122	.183	.182	.182	.326	.323	.323
P_{IN} (MW)	-	9.54	9.52	-	6.32	6.14	5.87	5.63	5.46	6.82	6.59	6.41
M_m (Kg)	-	3050	3050	-	2020	1960	1880	1800	1750	2180	2110	2050
M_{RAD} (Kg)	-	465	463	-	536	515	716	677	650	1050	1010	976
η' (%)	-	16.8	16.9	-	27.8	29.1	34.1	36.7	38.8	39.2	42.1	45.2
η (%)	-	11.6	11.7	-	17.6	18.1	18.9	19.8	20.4	16.3	16.9	17.3
M_{TOTAL}	-	6450	6450	-	5940	5840	6870	6730	6650	9600	9450	9350

4.4 Comparative Analysis of Indirect Solar Pumped Lasers

The results of Hughes' mass coefficients applied to the systems of this work are presented in Figure 49 on the next page. The results of total system mass estimates based on T^4 scaling of the radiator mass are presented in Figure 50 and summarized in Table 25. Before making comparisons of these systems using either set of coefficients, however, the scaling law for the satellite mass with laser power should be determined. In this way, each system can be evaluated with regard to the possibilities for similar but larger systems. An examination of pertinent equations for all three systems reveals that P_L , M_{TOTAL} , and P_{IN} all vary as $(NW\lambda)$ when no active refrigeration unit is included. The gas temperature, overall efficiency, η , and gas velocity all remain constant. This being the case, comparisons of these LMW systems can be taken to be indicative of the power-to-mass ratios and efficiencies of larger systems as well.

According to estimates in Figure 49, the lightest flowing CO system is lighter than the lightest mixing gas system by ~40%, and lighter than the lightest static system by ~20%. The estimates shown in Figure 50, however, place the weight of the lightest static system nearly on order of magnitude under the mixing or flowing systems. Furthermore, the static system can be made lighter relatively easily by either slowly flowing the gas or rotating the satellite to provide an artificial gravity. Both of these actions increase the heat flow from the gas into the coolant, thus allowing the coolant to be maintained at a higher temperature and thereby reducing the required radiator area. No techniques of comparable simplicity exist for reducing the mass of the other systems. The simplicity of the static system also makes it very attractive in comparison to the mixing and flowing gas systems, which would probably require greater amounts of maintenance than would the static CO₂ system.

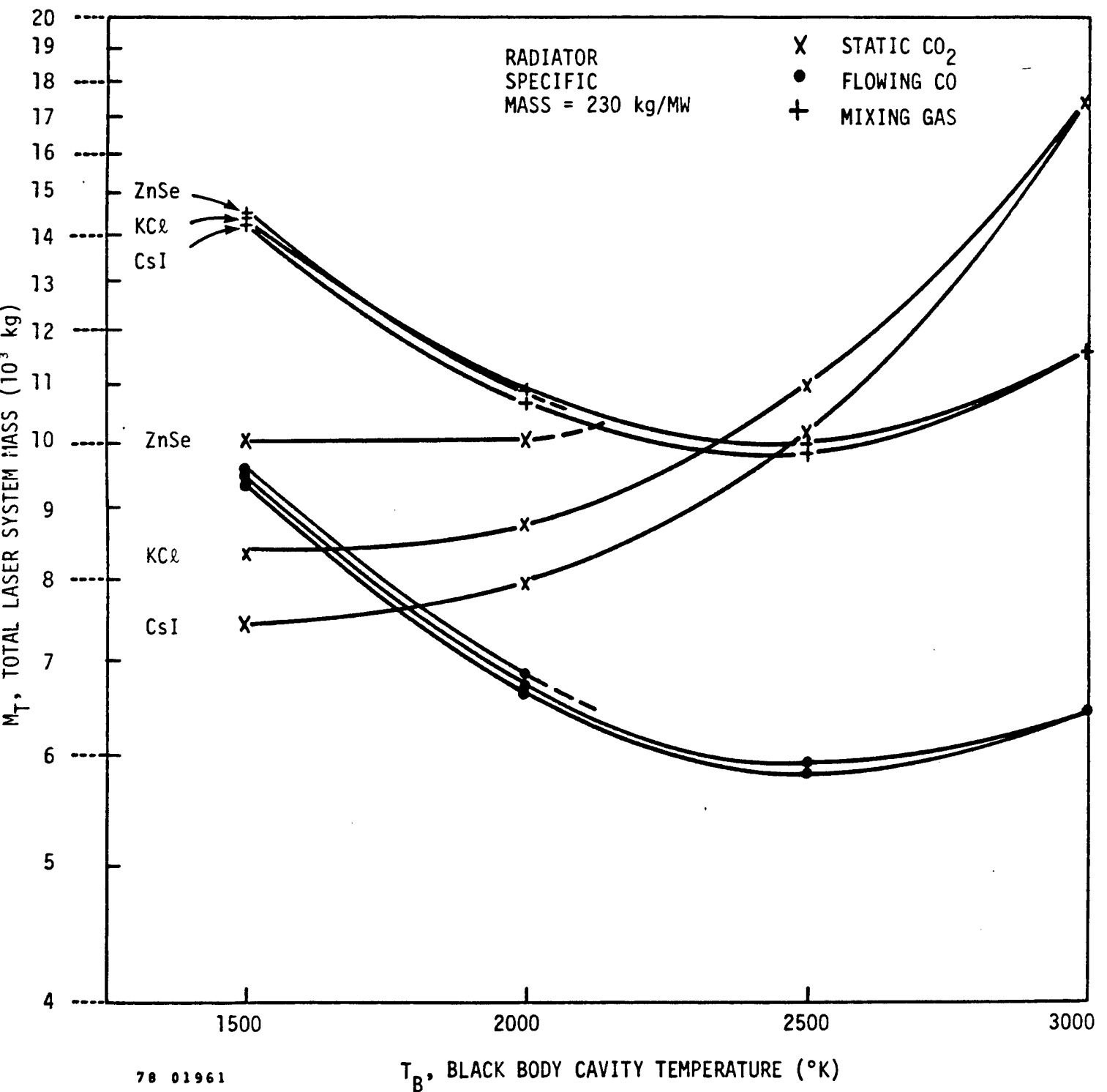


Figure 49. Indirect Optically Pumped Solar Laser System Mass vs. Pumping (Black Body) Temperature with Constant Specific Radiator Mass

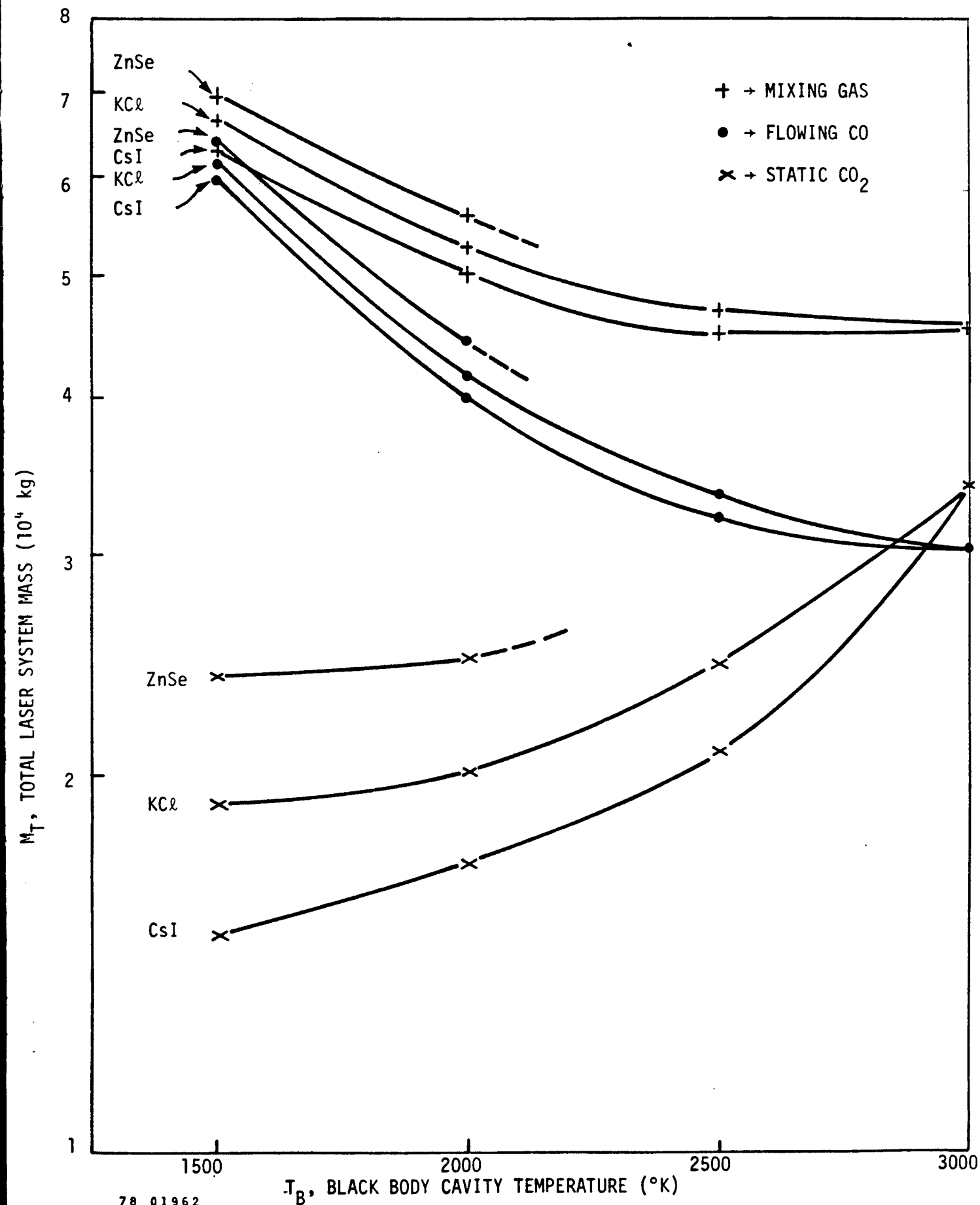


Figure 50. Indirect Optically Pumped Laser System Mass vs. Pumping (Black Body) Temperature with T^4 Scaling of Radiator Mass for $T_R > 475$ °K

Table 25. Summary of Radiator and Total System Masses
(T^b Scaling of Specific Radiator Mass)

System	$T_B = 3000K$			$T_B = 2500K$			$T_B = 2000K$			$T_B = 1500K$		
	KCl	CsI		KCl	CsI	ZnSe	KCl	CsI	ZnSe	KCl	CsI	
<u>Fixing</u>												
M_{RAD}	3.60×10^4	3.60×10^4		3.84×10^4	3.65×10^4	4.60×10^4	4.27×10^4	4.05×10^4	5.61×10^4	5.29×10^4	4.97×10^4	
M_{TOTAL}	4.52×10^4	4.52×10^4		4.70×10^4	4.50×10^4	5.57×10^4	5.25×10^4	5.01×10^4	6.93×10^4	6.63×10^4	6.28×10^4	
<u>Flowing</u>												
M_{RAD}	2.43×10^4	2.43×10^4		2.81×10^4	2.69×10^4	3.75×10^4	3.55×10^4	3.41×10^4	5.51×10^4	5.29×10^4	5.11×10^4	
M_{TOTAL}	3.03×10^4	3.03×10^4		3.35×10^4	3.22×10^4	4.44×10^4	4.16×10^4	4.01×10^4	6.37×10^4	6.13×10^4	5.95×10^4	
<u>Static</u>												
M_{RAD}	1.93×10^4	1.91×10^4		1.55×10^4	1.34×10^4	1.66×10^4	1.29×10^4	1.03×10^4	1.60×10^4	1.21×10^4	8450	
M_{TOTAL}	3.43×10^4	3.41×10^4		2.46×10^4	2.19×10^4	2.49×10^4	2.01×10^4	1.70×10^4	2.41×10^4	1.89×10^4	1.48×10^4	

The mixing gas laser would be the most difficult to construct and maintain. The requirement that CO_2 and H_2O be separated and re-joined with a CO stream results in demands for future technological capabilities which may be difficult to meet. Since neither estimate of system masses places the mixing gas laser in a competitive position when passive cooling is used for separating the gases, substantial advances in refrigeration, molecular sieve or electrochemical cell techniques would be necessary to make this system attractive. In view of its inherent complexity in comparison to the flowing CO or static CO_2 systems, it is not considered worthwhile to expend the effort to develop the necessary technologies for this system.

The Flowing CO System does not suffer from the gas separation difficulties facing the mixing gas system; however, it does require heat to be extracted from the CO stream at 125°K. This requires either very large radiators or very large refrigerators. If large refrigerators are ruled out as impractical (they would have to provide about 10 MW of cooling for this system) then large radiators, with their associated meteorite puncture problems and large masses are required. Furthermore, the flowing CO system appears to be much heavier than the static system (see Figure 50) and is undesirable for that reason as well.

Due to its relative simplicity, reduced radiator size, good power to mass ratio and to the fact that this system requires few technological advances to make it practical, the static CO_2 laser system is considered to be the best choice for a solar powered laser satellite system.

4.5 Optimum Design Parameters for the Solar Pumped Laser

The conceptual design of the static system has already been carried out in section 4.2, however a number of choices remain to be made with regard to specific parameter choices. In particular, the best optical material and black body temperature must be chosen, a choice must be made between flowing fluid cooling tubes and heat

pipes, and some discussion of the relationship between N , W , and ℓ should be engendered.

In choosing the best optical material for the static laser system, the structural attributes of the materials should be considered as well as the net mass resulting from their usage. CsI, for example, provides the best power-to-mass ratio, but it is very water soluble, making it quite difficult to manufacture the laser tubes with this material and the use of water for a coolant, inadvisable. In addition, neither KCl nor CsI have ever been formed into tubes of the sort contemplated, so that first it would be necessary to develop some means for doing so. Since mono-crystalline structures are not required for this application, forging of the alkali metal salts may be the simplest way of forming long, thin tubes. If it is not possible to form tubes in this way, ZnSe can already be made in very thin tubes via chemical vapor deposition.

The best values of T_B for each material are; CsI at $T_B = 2000^\circ\text{K}$ providing 91.7 Watt/Kg, KCl at $T_B = 1500^\circ\text{K}$ with 80.0 Watt/Kg, and ZnSe at $T_B = 1500^\circ\text{K}$ with 24.4 Watt/Kg. In view of the very small difference in mass between the CsI and KCl systems (~15%), and noting that the KCl system operates at 1500°K , which should be an easier temperature to obtain and which should cause less severe melting and vaporization problems than would $T_B = 2000^\circ\text{K}$, and recalling the unfortunate water solubility of CsI, the KCl system must be considered preferable to the CsI system. Only if neither KCl nor CsI is capable of being formed into long, thin tubes would ZnSe be an attractive alternative, so that KCl at $T_B = 1500^\circ\text{K}$ is the optimum system.

In choosing N , W , and ℓ , compactness and cooling are the determining factors. If "heat pipes" are chosen to remove the heat generated in the laser tubes, the restrictions on ℓ are more severe than for simple fluid flow cooling pipes.^{47,48} The equations for the heat pipe dimensions relate ℓ (the evaporator" section length) to the

length of the condensing section ℓ_c . These lengths also depend upon the temperature to be maintained at various sections of the pipe and the amount of heat to be transferred by the pipe. Preliminary calculations indicate that heat pipes operating over a temperature difference of 100°K to 200°K (as for KCl or ZnSe at $T_B = 1500^\circ\text{K}$) would have to be at least 2 ℓ in length. Also, there is a geometric problem of arranging the ends of a bundle of heat pipes so that the waste heat can be radiated properly. These features of heat pipes may make the choice of a flowing fluid coolant desirable despite the necessity to pump the coolant.

According to the computations in Section 4.2, $NW\ell = 1.10 \times 10^4 \text{ m}$ for both cases of interest. If the black body is to be approximately cubical, then $\ell \equiv (.03W)\text{m} \equiv (.04N)\text{m}$, since each tube in a layer occupies 3 cm, and each layer will be assumed to occupy 4 cm. This gives $\ell \approx 2.30 \text{ m}$, $W = 80$, and $N = 60$, which results in an approximately cubical structure, 2.3m x 2.40m x 2.40m. These dimensions are similar to those which apply to fluid flowing cooling.

SECTION 5

DEVELOPMENT PROGRAM

Two different approaches to the development of a prototype indirect solar pumped laser for space applications have been examined. The first is a minimum risk approach in which the technology with the least risk is used, possibly with a sacrifice in the rate at which the system will be ready for orbit. The second is a crash development program where funding is essentially unlimited but, for example, a less efficient laser system may be used in order to meet a foreshortened development schedule. The differences between these two approaches can be characterized by the technologies used and by the resulting laser system configurations and performance. Each approach is presented below and compared in the final section.

5.1 Minimum Risk Development Program

The function of a "minimum" risk program is to assure orderly development of solar laser systems. A minimum risk program will necessarily emphasize adequate time periods between items which absolutely require sequential development in order to make sure that other parts of the program relying on the outcome of that development are not compromised by slippage in the completion time. Similarly, the designs may be adjusted for a minimum risk program by relying on proven technology as a development base rather than looking for material or engineering design breakthroughs to accelerate the program.

The term "minimum risk" will be interpreted to mean the use of technology which allows the greatest chance of success of the mission; namely to provide a reliable solar-pumped laser of a given size and power in orbit by a generally prescribed date, where the date is flexible to a certain extent to allow the mission to succeed. At present, we set the date at approximately 1995 for completion of the development program. In those areas of greatest technological uncertainty the minimum risk program should include a back-up or "fail safe" development program in addition to the mainline program to secure the greatest likelihood of success.

The mainline development is devoted to the CO₂ static laser system, because it has the best performance; the failsafe development alternative focusses on the CO flow laser system because the technology is somewhat more conventional and requires less development than the mainline system even though the laser performance is less desirable than the static laser. These two alternatives are carried forth to a certain extent as parallel efforts of a combined development program.

The indirectly pumped static laser consists of the following basic components:

- solar collector/concentrator
- black body pumping cavity
- laser tubes
- heat pipe/radiator
- pointing and control system
- laser transmitting optics

An artist's rendering of this system is shown in Figure 51. The last two component subsystems listed above will not be considered in this study; it is assumed that the transmission optics will be adaptive and approximately the same weight and configuration for each case considered. Also pointing and control systems for astronomical satellites have already been developed to the accuracy required, for example, for the SLPS application of solar lasers [see Table 26].

The basic tasks in the initial laser development program are:

1. Prove out the basic laser cavity (if required)
2. Make engineering tests of the critical component technologies to test concept feasibility
3. Carry out component development programs if indicated by the results of task 2
4. Develop a detailed conceptual systems design

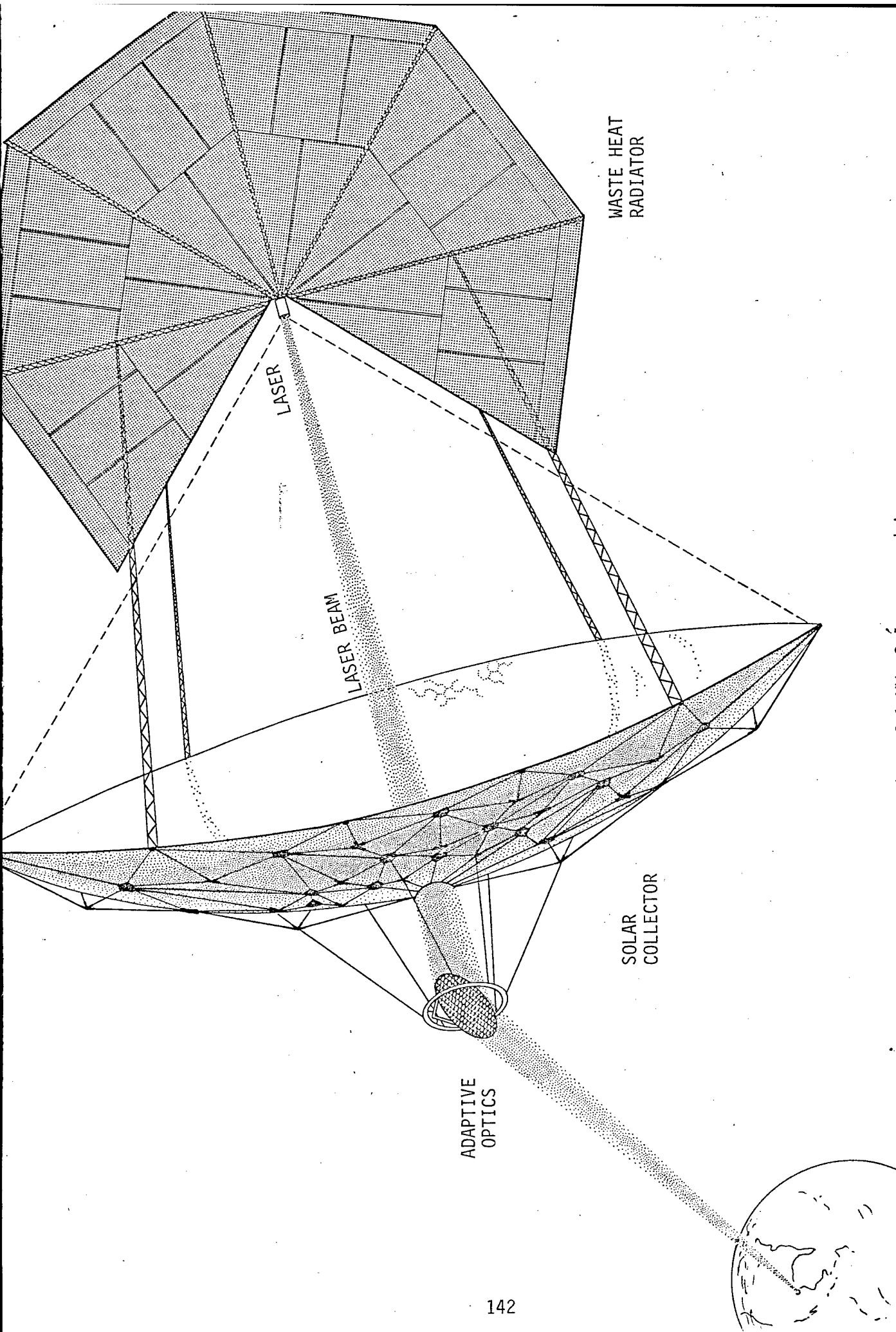


Figure 51. Artist's Conception of 1 MW Solar-pumped Laser
Mathematical Sciences Northwest, Inc.

78 02176

Table 26. Pointing Accuracy Requirements
[Taken from Ref. 2]

VEHICLE	POINTING ACCURACY (radians)
Strap (Balloon) ¹	2×10^{-5}
Stratoscope (Balloon) ^{1,2}	4×10^{-8}
Orbiting Solar Observatory ¹	1×10^{-5}
Orbiting Astronomical Observatory ¹	2×10^{-6} 2×10^{-7} (find hole)
3-Meter Space Telescope	4×10^{-7} (off axis) 2×10^{-8} (on axis) 2×10^{-8} (stability) 8×10^{-6} (roll)
Manned Orbiting Telescope	2×10^{-8} (pitch & yaw) 4×10^{-7} (roll)
Apollo Telescope Mount	5×10^{-6} (pitch & yaw) 2×10^{-5} (roll)
Laser Satellite Power Station	1×10^{-7}

1 - Vehicle has been flown

2 - Projected from existing systems

5. Design a small scale laser system prototype [e.g., 25 kW]
6. Build 25 kW prototype laser.
7. Ground test laser prototype (e.g., in space simulation chamber] and prepare final schedule and costs for lift-off, orbit insertion and operation/maintenance in orbit.

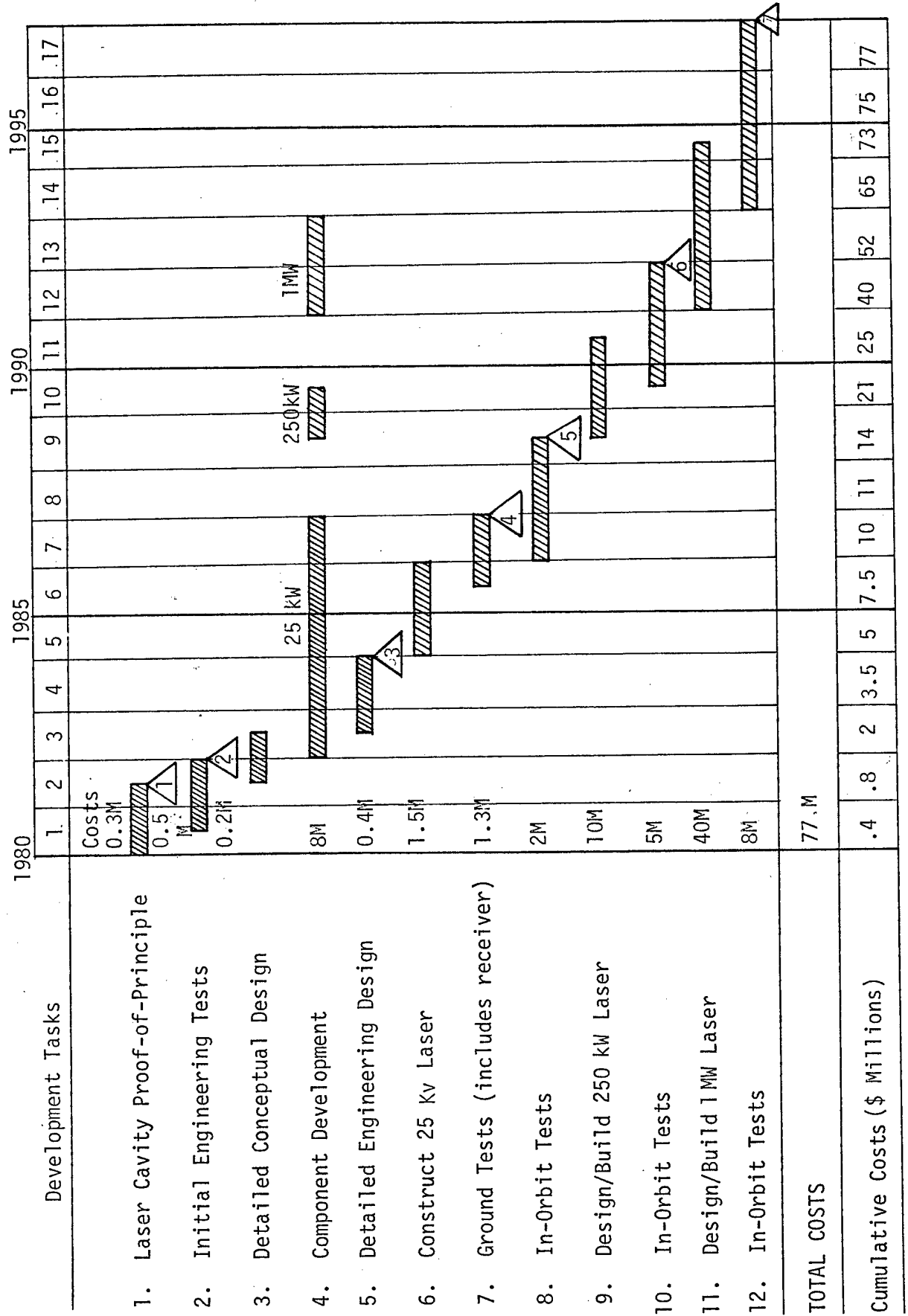
At the end of task #5 the initial development program is complete and a go/no go decision can be made for constructing the in-flight 25 kW laser system. Additional R and D steps needed to place the full scale 1 MW solar-pumped laser in orbit are shown in Table 27, which summarizes the minimum risk program.

Specific decision points punctuate the program to allow a re-assessment of the path with the least risk at the completion of each major stage in the development. By carrying parallel efforts in some areas the back-up technology is sufficiently advanced at each decision point that it can serve as a fall-back position guaranteeing success of the mission.

The first decision point occurs after 18 months when the results of the laser cavity experiments are complete. The purpose of this experiment is to extend existing gain measurements with a proof-of-principle experiment demonstrating lasing under circumstances close to the projected static system operating conditions [see section 4.2]. The successful completion of this experiment is essential for a high confidence decision to proceed with the mainline development program.

The laser cavity proof-of-principle experiment can be conducted without delay; that is, no optical tube development is required to precede this step. All of the required equipment is off-the-shelf and can be constructed in a matter of several months. Auxiliary cooling techniques can be used to keep the lasant at the appropriate temperature. A black body cavity with adjustable temperature must be constructed. The experiment must show cw lasing at appropriate output power for the proper mix of gases. The performance of the laser cavity

Table 27: Minimum Risk Development Program for the Static CO₂ Solar-Pumped Laser



should be tested under different pressure, temperature, gas mixture and optical cavity conditions.

If the cavity experiments are negative then the flowing CO system should undergo similar tests. Perfunctory tests are in order to demonstrate the laser pumping cavity behavior and the same black body cavity used for the static CO₂ laser could be used for the flowing CO laser. Under this case the minimum risk program would proceed entirely with the fail-safe CO flow laser technology development.

Assuming successful completion of the mainline cavity tests, the initial engineering tests of component technology would be carried through to completion by the end of the second year (task 2). The first 6 months of Task 2 concentrate on technologies which are required by both mainline and alternative laser development programs; namely, the solar collector concentrator, the black body cavity, laser transmission optics, and possible common features of the waste heat radiators. The goal of these tests is to qualify materials and design choices identified by the preliminary conceptual designs given in section 4 of this report (e.g., the availability, manufacturability and properties of critical materials for the metallized plastic used in mirrored solar collectors, coolants, radiator tubes, carbon felt insulation, black body structure, etc.). After a positive decision at the end of Task 1, Task 2 will emphasize the critical questions concerning the development of thin transparent optical materials for the laser tubes. The results of these tests will be used to isolate the best designs and identify the hardest component development problems.

Also with a positive decision at point 1 a detailed conceptual design (task 3) needs to be carried out. This design would have the benefit of the laser cavity tests (task 1) and some significant materials and design choice evaluation (task 2). The objective of the design would be to elaborate on the component requirements and system performance. Design data on the components would be used to guide the

major component development effort in task 4 and the system's performance evaluation would frame the component requirements from a self-consistent, operational point of view.

The second decision point comes at the end of Task 2 when the results of the initial engineering tests allow a re-assessment of the chances for technical success. If the decision is positive then the full scale component development program may proceed. While it is premature to lay this part of the program out in detail [that will be possible only after the completion of task 3], it is worthwhile discussing some of the obvious development areas for the static laser case. Considering the rather thin laser tubes called for in the main-line conceptual design, (i.e. 0.1mm wall thickness for the static solar pumped laser) this technology appears to have the greatest risk associated with it. The development of this component should include the following features:

- Explore additional materials besides KCl, CsI and ZnSe to determine their optical, thermal and strength characteristics for the current application.
- Investigate various fabrication techniques such as polycrystalline forging, vacuum deposition, chemical vapor deposition, etc.
- Prepare sample tubes and test for strength under the appropriate thermal and optical loads.
- Test sample tubes with lasant in place to determine lasant pumping characteristics.
- Develop techniques for connecting lasant tubes to concentric inner heat pipes or coolant tubes.
- Test reflective coatings on heat pipe/laser tube combination.
- Test the rotating tube, induced convection cooling concept.
- Test the gas flow cooling concept.

- Select the best cooling concept and tube material/construction techniques and build a tube for testing as a complete laser cavity.

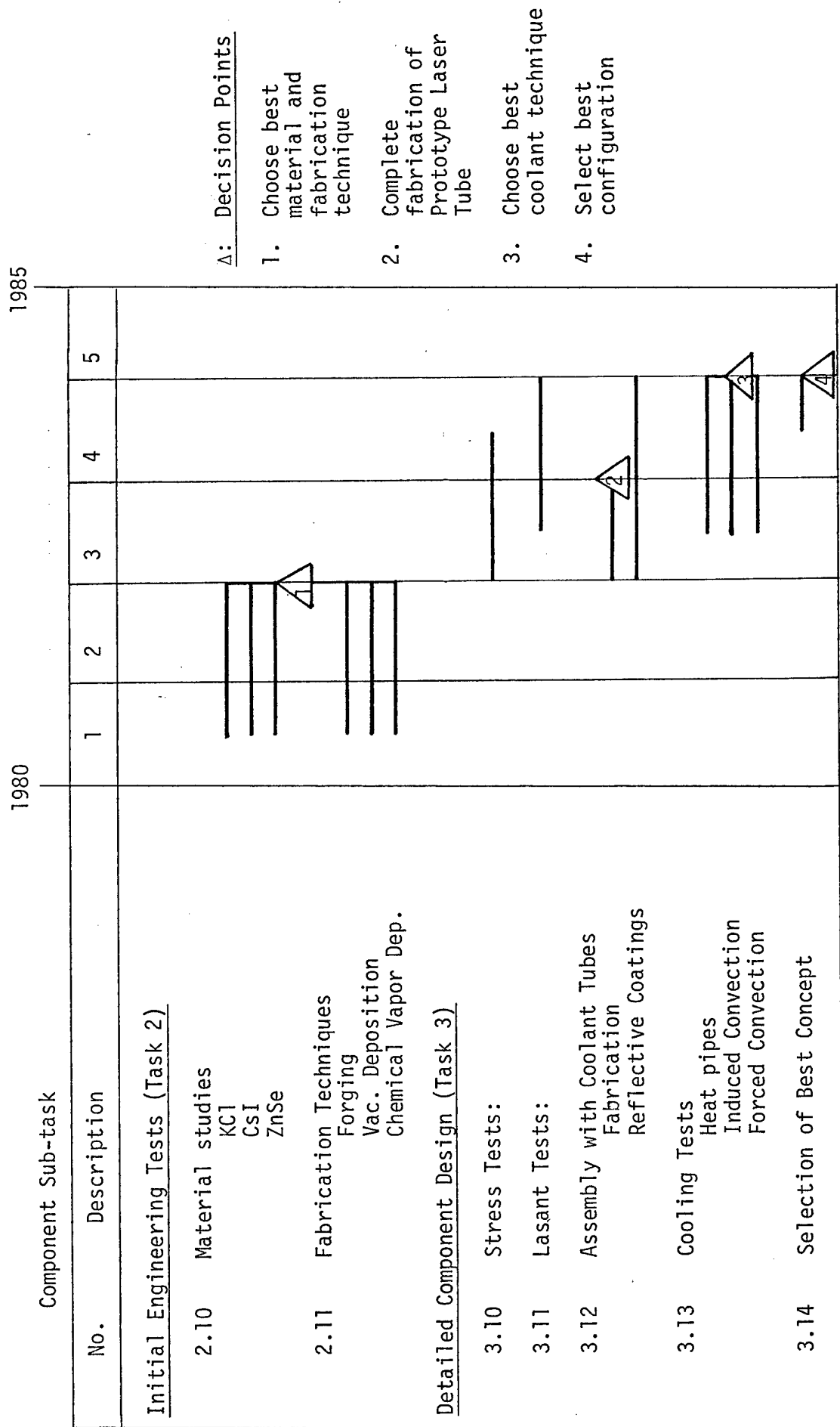
An approximate laser tube component development schedule illustrating parallel development to reduce technological risk is shown in Table 28 along with decision points to select the best path to take at each stage. The timing for each sub-task of this schedule has been estimated on the basis of related technologies, for example in the development of new infrared transparent materials, in thin tube manufacture, in joining materials with differing coefficients of thermal expansion and in the evolution of heat pipe technology for space radiators.

The laser tube component/development program assumes that only one solar pumped laser would be developed; namely the static system. However, at the earliest stage it would be wise to explore the flowing gas laser, too; if the static laser tube problem proves intractable for some unforeseen reason then the flowing system's tubes, while heavier, would be brought into the development stream as the successful laser.

In contrast to laser tube development, the solar collector/concentrator already has undergone substantial development both for small and large space solar power systems. While the collector will require further development to achieve the lightest weights and the high concentration ratios desired, there is a general agreement that a hundred meter diameter collector could be built using current materials technology. Assembly in space is still an open question. At present both Johnson and Goddard Space Flight centers are sponsoring hardware research on automated space structure fabricating machines. These devices will manufacture rigid beams in a zero-g space environment using packaged or rolled thin metal stock. Laying the metallized plastic skins on each mirror facet can also be accomplished as a subsidiary task by the same or similar machine.

Table 28: Laser Tube Development Schedule

[Component Sub-tasks of Tasks 2 and 3 of Program No. 1]



As an alternative, the collector facets could be manufactured on the ground in relatively small sizes (e.g. each facet 1 meter² in area, 10⁴ of them for a 1 MWatt laser) and attached on the framework built in orbit. Packing ten thousand facets for a shuttle load presents its own special problem; for example, the rims supporting the plastic reflectors would have to stack yet leave space or holes for out-gassing during ascension to orbit. These details require additional design and testing. However, because they already are part of the NASA R and D program scheduled during the next ten years, we do not include them as distinct laser development program elements.

Component development is shown to continue throughout the development program up to the 13th year when construction of the 1 MW laser is nearly complete. Additional aspects of this task are discussed below.

The third decision point (Table 27) marks the end of the fourth year when the detailed engineering design is complete. This design will also include costs and construction schedules for the 25 kW prototype laser and ground testing facilities in order to provide sufficient material for an interim review of the development program. The next task is to construct the closed cycle 25 kW laser; then in task 7, the ground test site must be prepared and tests carried out. The purpose of these tests is to evaluate closed cycle performance of the laser under carefully controlled conditions and to make necessary design adjustments in the system before modifying it for space flight.

The fourth decision point is the go/no-go decision for committing the program to laser space flight tests. At this point the full orbitable design and ground test results are reviewed; this is the last point in time that a change to the fail-safe flowing CO laser system could be contemplated and still meet the 1995 deadline.

The 25 kW laser is sufficiently small that it can be stowed in its entirety on-board the space shuttle, with folded radiator and collector elements to be deployed in low earth orbit (LEO). As the

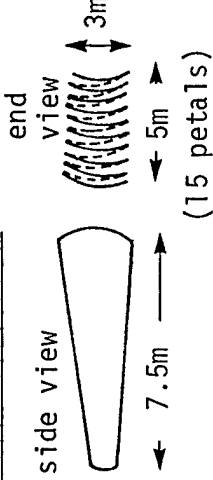
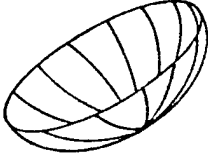
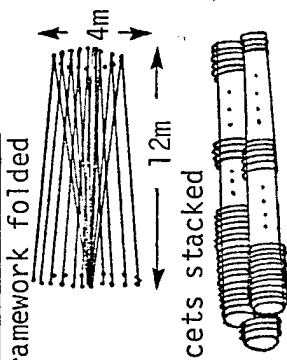
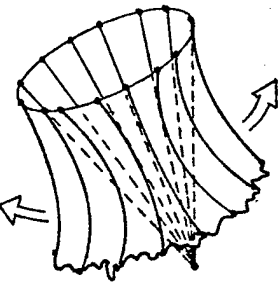
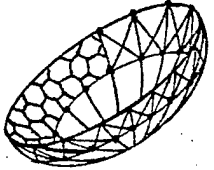
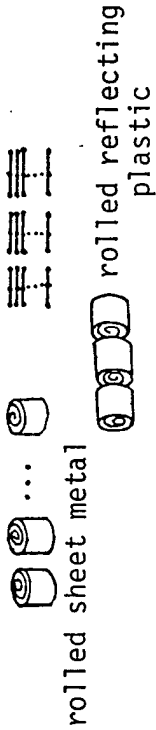

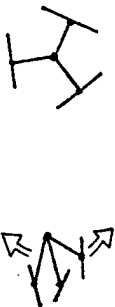
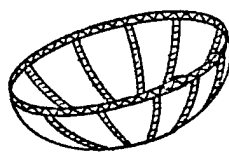
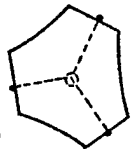
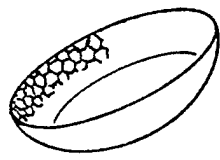
development progresses to larger laser systems, then the problems of fabrication and/or space manufacture of these elements must be considered. A possible sequence of collector technologies is sketched out in Figure 52 for each of the three stages in increasing sizes of laser development up to the 1 MW level. The final collector technology (1 MW size) was chosen here to be a simple extension of the next smaller size; it might be more useful to consider developing a more synthetic approach at this last stage if even larger laser systems are contemplated. The costs shown in Table 27 reflect these differences in collector (and radiator) technology very approximately; that is, by area and by the construction technique.

5.2 Crash Development Program

The objectives of the crash development are deployment of a 1 MW solar-pumped laser in orbit in the shortest practicable time. Funding is essentially unlimited. The constraints are to construct a system that works in a short period of time. This may necessarily involve a compromise in the level of performance in exchange for better guarantees for the success of the mission in a limited time scale. These guidelines lead us to suggest the flowing CO solar-pumped laser as the mainline approach for the crash development program. The flowing laser is heavier than the static CO₂ laser for the same power output. It may also be less reliable because of the need for a brayton power cycle (or photovoltaic power system) to run flow loop compressors. However, it employs more conventional materials and design than the static laser and therefore can be developed faster. A close-up artist's view of the laser loop is shown in Figure 53. The basic components are:

- Solar collector/concentrator
- Black body pumping cavity
- Laser tubes and laser cavity
- Compressor and power system
- Radiator
- Pointing and control system
- Laser transmitting optics

Figure 52. Examples of Collector Technology for Solar Laser Program

25 kW Laser (Collector diam. = 15m)	250 kW Laser (Collec. diam. = 48m)	1 MW Laser (Collec. diam. = 95m)
<p>Prefabricated Petal Collector</p>	<p>Folded Frame Work (Umbrella) Prefabricated Facets</p>	<p>Sheet Metal Rolls for Beam-Frame Fabrication Folded Facet Frames Metalized Plastic Rolls for Facet Surfaces</p>
<p><u>Packed for Shuttle:</u></p>  <p>side view end view 7.5m 3m 5m (15 petals)</p> <p><u>Deployed in Space:</u></p> 	<p><u>Packed for Shuttle:</u></p>  <p>framework folded 12m 4m facets stacked</p> <p><u>Partly Unfolded Frame:</u></p>  <p><u>Fully Deployed Frame, some Facets Attached:</u></p> 	<p><u>Packed for Shuttle:</u></p>  <p>rolled sheet metal facet frames rolled reflecting plastic</p> <p><u>Initial Construction:</u></p> <p>Fabricate Beams (helical network)</p>  <p><u>Unfold Facet Frames</u></p>  <p><u>Intermediate Assembly:</u></p> <p>Connect Circumferential Beams and Collector Ribs</p>  <p><u>Apply Reflecting Plastic to Facet Frames</u></p>  <p><u>Final Assembly:</u></p> <p>Attach Facets to Frame</p> 

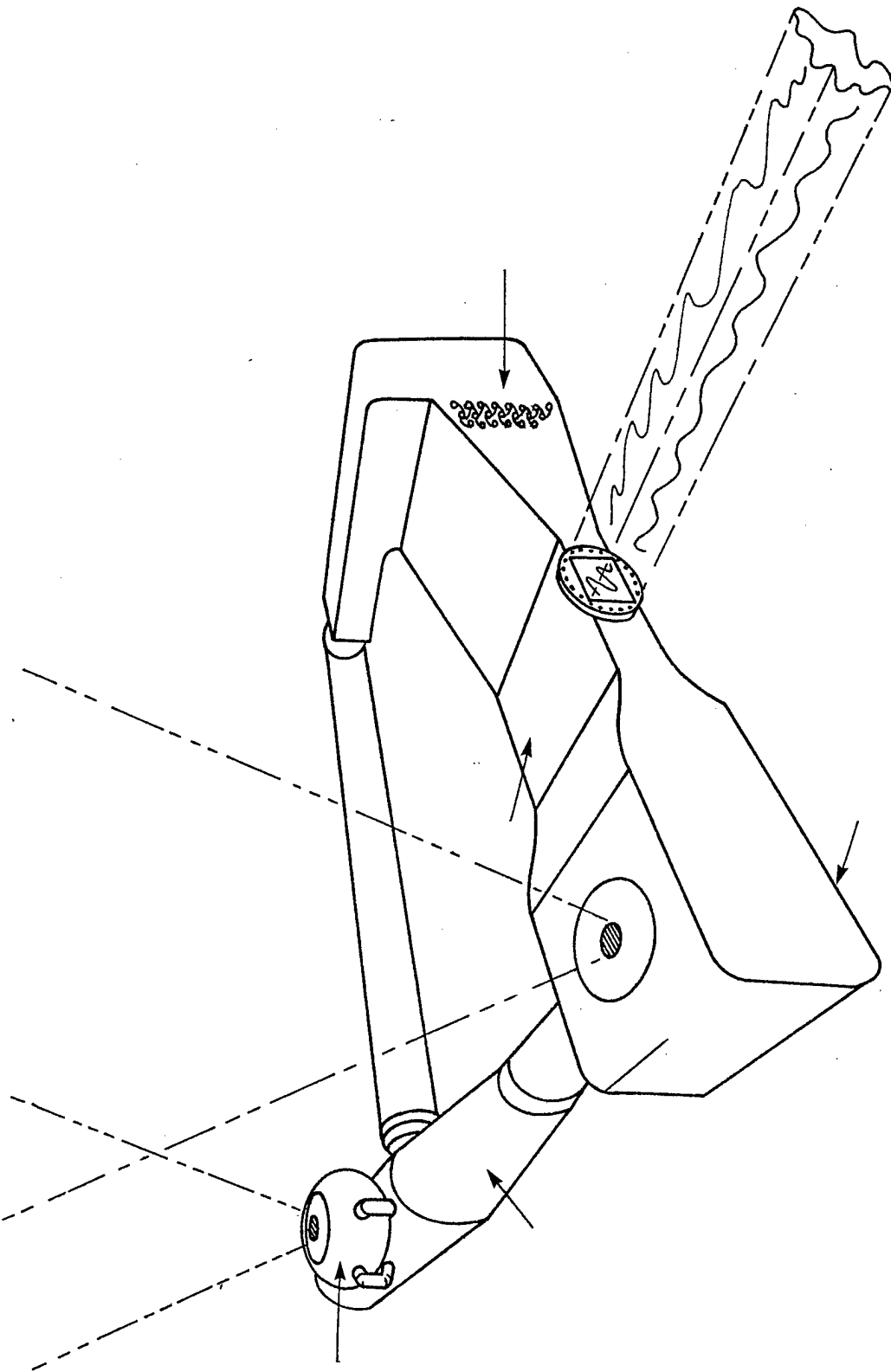


Figure 53. Close-up Artist's View of Flowing CO Solar-Pumped Laser

A brief examination of this list shows that the third, fourth and fifth items differ from the static case. The laser tube development is simplified by using thicker tubes. A separate laser cavity, external to the black body pumping cavity, is probably desirable, but not essential; the laser cavity and laser tubes could be combined. Since tube cooling is accomplished by flowing the lasant around a closed loop, a compressor and power system must also be developed. This is a low temperature, low mass flow compressor which will require minimal amounts of development. If a Brayton cycle is chosen as the power system then some development in addition to that which has already been performed by NASA-Lewis may be necessary. If photovoltaic power is used then the system is available now. A larger collector would be required for the photovoltaic system to achieve power output equivalent to the Brayton cycle system. However, the total flow loop compressor power needed is sufficiently small (i.e., 0.1 MW) to make these components a small part of the total program. In some respects the radiator development is simplified, compared to the heat pipe system required for the static laser. However, cooling takes place at relatively low temperatures in the flowing CO laser, so the large radiator areas are necessary from the outset. Development on this component will concentrate on light-weight, deployable radiators for the smaller lasers (e.g., 25 kW) and a simple radiator construction technique for the larger lasers [e.g., pre-fabricated panels and threaded pipe connections].

Using the minimum risk program as a guide, a compression of approximately 5 years was achieved for the crash program, assuming approximately identical program development tasks. These are shown in Table 29 along with approximate costs for the program. The costs have been escalated relative to the minimum risk program by assuming they are inversely proportional to the task duration. In addition certain costs remain fixed, such as the transportation cost to orbit, and costs for assembly in orbit. A more thorough discussion of costs is given in the next section.

Table 29: Crash Development Program for the Static CO₂ Solar-Pumped Laser

1980

Laser Component Tasks	1	2	3	4	5	6	7	8	9	10	11	12
Laser Cavity Proof-of-Principle	Costs 0.3M											
Initial Engineering Tests												
Detailed Conceptual Design												
Component Development												
Detailed Engineering Design												
Construct 25 kW Laser												
Ground Tests												
In-Orbit Tests												
Design/Build 250 kW Laser												
In-Orbit Tests												
Design/Build 1 MW Laser												
In-Orbit Tests												
Total Costs	\$121.M											
Cumulative Costs (\$ Millions)	2.5	7.0	12.5	16.5	28.5	37	72.5	103.5	111.5	121		

The crash program can be accelerated further, with attendant increase in the risk of success, by eliminating the 250 kW laser tasks. This would shorten the program by another two years, giving a completion time of 1988 instead of 1990. This decision could be made midway through the orbit tests for the 25 kW laser, in 1985.

5.3 Program Costs

The costs of the solar pumped laser include those due to design development, test and evaluation (DDT&E), production, transportation (i.e., to orbit), assembly in orbit (if required), and operating and maintenance costs (O&M). Each cost category is estimated below on the basis of an eventual operating system consisting of many lasers in the multi-megawatt class. These costs are highly approximate, since they depend on extrapolations of present technologies and on a variety of assumptions about the scaling of these technologies to space. A more detailed study is required to determine these figures precisely and to search for the minimum cost options in laser design and deployment. A cost summary is provided in the last table of this section.

Design, Development, Test and Evaluation Costs:

Probably the best DDT&E cost estimates related to the laser power transmission system are derived from the SSPS program. The SSPS DDT&E costs estimated by Glaser are approximately \$50 Billion.⁷⁴ Approximately half of this cost is associated with development of the technology for constructing large space structures and for the transportation system, and half is for the collector, microwave transmitter and receiver components.

In contrast, the laser systems being considered here (i.e., 1 Megawatt) employ collector and radiator sizes which are just on the border of requiring space manufacture; that is, at this power, it may be feasible to assemble prefabricated collector and radiator elements in space and avoid the complications of making structural

beams in space. Also such systems do not require any transportation system development beyond the shuttle. Hence the small power versions of the solar pumped laser might allow a significant reduction in the DDT&E costs, at least by a factor of 2 compared to the full-scale SSPS system and perhaps even by several orders of magnitude. Very simple cost estimates have been included in Tables 27 and 29; these estimates should be viewed with a great deal of caution since no detailed program plan exists yet to substantiate them.

Production Costs: •

Production costs are sensitive to the quantity and sizes of the laser units produced. Considering the laser loop alone, Coneybear⁶ estimates that very large laser assemblies (i.e., totaling a Gigawatt in power) will cost in the neighborhood of 20¢ per watt, whereas a 1 Megawatt laser will cost approximately \$10 per watt. Hence we can estimate on the basis of these crude approximations that the solar pumped laser will cost \$10 per watt for the first 1 megawatt production unit and about 50¢ per watt after the first 100 production units (i.e., 100 MW net production). These costs may be somewhat high in the sense that they are derived for closed cycle gas flow lasers; the static solar-pumped laser is a technically simpler device and may cost less to build.

Transportation Costs:

Transportation costs will depend on the numbers (and total weights) of the lasers to be lifted into orbit, and also on the rate and year at which they are to be in orbit. In particular, Coneybear⁶ has developed four levels of transportation required for missions in space, as shown in Table 30. Clearly level I, which only requires the space shuttle, will suffice for placing 1 Megawatt laser systems in low earth orbit by 1990. However, if larger lasers are desired, or if a full-scale solar laser power satellite system is required then the transportation needs swiftly escalate through levels II and III to level IV. For large volumes, the transportation unit cost in \$/kg

Table 30: Space Transportation Costs Through 1990, Three Options
 [Taken from Ref. 6]

Present			1980		1985		1990	
Destination from Earth	Payload, lb	\$/lb	Payload, lb	\$/lb	Payload, lb	\$/lb	Payload, lb	\$/lb
Option 1 Existing Shuttle and Boeing Study Vehicles	LEO	20,000 (Titan III-D)	1,000	250	65,000 (Shuttle)	250	500,000 (Boeing Study)	20
	GEO	8,000 (Titan/Centaur)	4,000	3,000	18,000 (Shuttle & Space Tug, Expanded)	1,000	100,000 (Boeing Vehicle & Super Space Tug, Expanded)	100
	Moon	500 (Titan/Centaur with Added Upper Stages)	40,000	40,000	500	40,000	500	40,000
Option 2 HI Energy Upper Stages	LEO	NA	65,000 (Shuttle)	250	65,000 (Shuttle)	250	500,000 (Boeing Study)	20
	GEO		7,000 (Shuttle & 3-stage IUS)	3,000	18,000 (Shuttle & Space Tug, Expanded)	1,000	100,000 (Boeing Vehicle & Super Space Tug, Expanded)	100
	Moon		NA	NA	6,000 (Shuttle & High Energy Upper Stages)	8,000	30,000 (Boeing Vehicle & Larger & Higher Performance Upper Stages)	1,000
Option 3 Ram Rocket First Stage, HI Energy Upper Stages	LEO	NA	NA	NA	500,000 (Ram Rocket Single-stage-to-orbit Vehicle)	20	500,000	15
	GEO				100,000 (Ram Rocket & Larger & Higher Performance Upper Stages)	100	100,000	80
	Moon				30,000 (Ram Rocket & Larger & Higher Performance Upper Stages)	600	30,000	500

Vehicle & Fuel Combinations Which Could be Available
 If Decisions are Made & Development Implemented

is reduced compared to the early space shuttle costs. However, the costs of developing the transportation system itself must be borne in mind. These are considerable and should rightly be assigned to the development costs of the first systems requiring their use, in this case the laser power systems. Figure 54 shows an amalgated projection of transportation costs which assumes that the larger space tugs will be developed by 1990. Hence we can assign an early transportation cost of \$250/lb. (i.e., 1980-83) and a future cost of \$20/lb (i.e., by 1990). Placing a 1 Megawatt system (i.e., 10^4 kg) in LEO in 1990 will therefore cost \$440K.

Assembly and O&M Costs:

Once the parts of the laser system have been lifted to LEO the components must be assembled. In its simplest, 1 megawatt configuration, the laser collector and radiator are small enough to be assembled from prefabricated pieces, requiring perhaps no more than 100 person work hours utilizing semi-automated EVA technologies currently under development by NASA. That is, the parts must be removed from the space shuttle, unpacked, bolted and welded together, connected to the laser and power units, filled to working pressure with the lasants and coolants and tested for basic operating characteristics prior to routine use. These activities are nearly identical to those which will be performed for early scientific experiments in the space shuttle and which have their immediate precursors in the recent Space Lab flights. The cost is estimated at \$3000/working hour for assembly⁷⁴.

Cost estimates for annual O&M costs are 3 mills/kW.hr⁷⁵, assuming a three man crew.

Larger laser units will require the use of beam machines in order to fabricate the structures in space. A beam machine has already been built by Grumman, which manufactures triangular cross-section beams from rolled sheets of aluminum foil⁷⁶. The Grumman device is to be redesigned for a take-off weight of 7000 kg by the early 1980's and hence

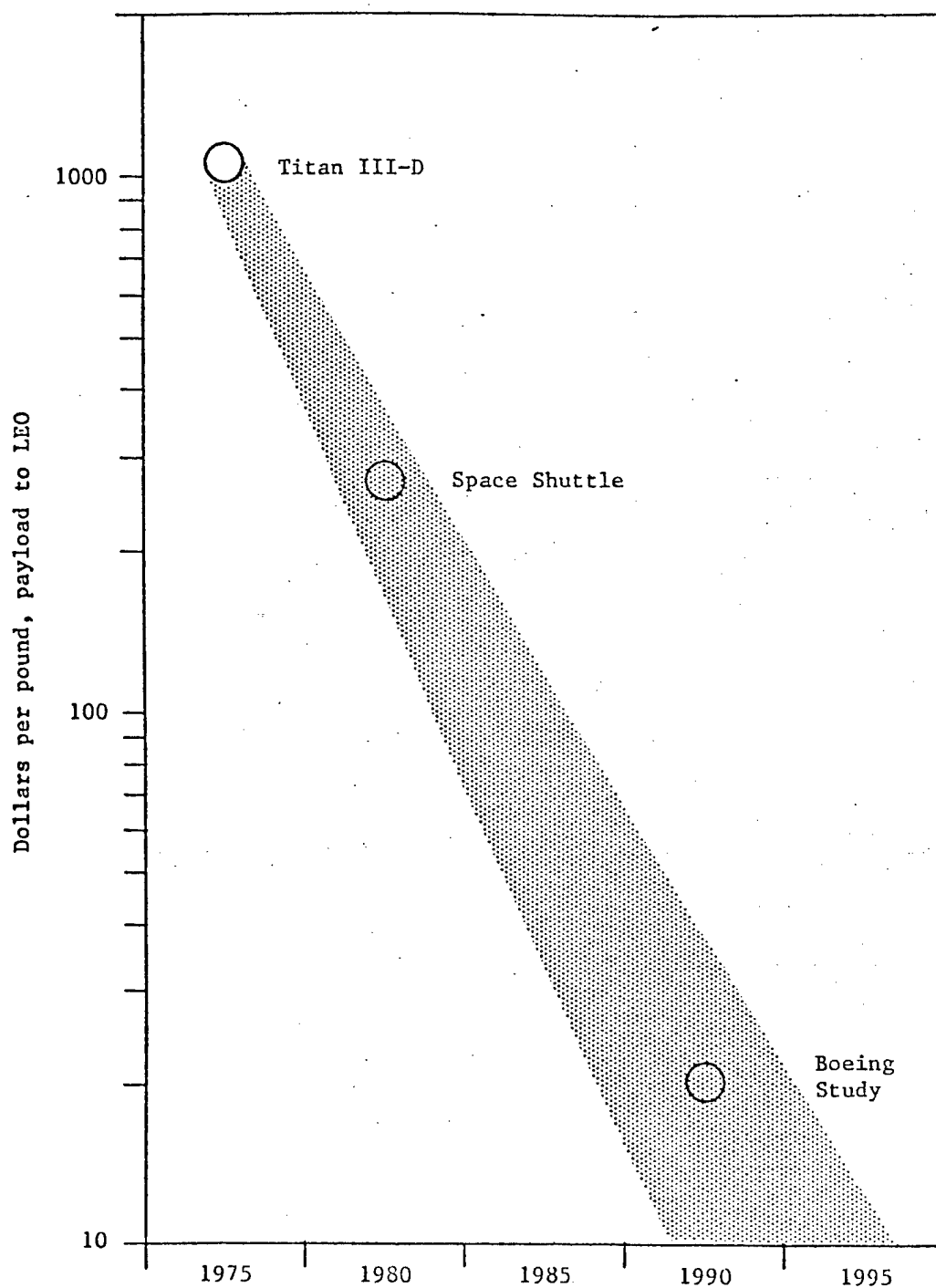


Figure 54. Costs for shipping to Low Earth Orbit [taken from Ref. 6].

should be available in time for larger laser power satellite systems. The rate of beam construction is such that most of the structural members for the 1 Megawatt unit could be fabricated in a few hours; additional assembly time would be needed to form them into the collector and radiator components. Project costs are summarized in Table 31.

Table 31: Program Cost Summary: 1 MW Solar-Pumped Laser

	<u>Minimum Risk</u>	<u>Crash</u>
DDT&E ^(a)	77.2	120.8M
Production Unit Cost ^(b) 1st (100th)	\$10M (\$.5M)	
Transportation Costs to LEO ^(c) 1982 (1990)	\$5.5M (\$.44M)	
Assembly Costs	\$0.3M	
O&M Costs/year ^(d)	\$0.026M/year	

(a) Totals taken from Tables 27 and 29.

(b) Laboratory Prototype costs are assumed to be four times the first unit production costs in Tables 27 and 29.

(c) Tables 27 and 29 used only the 1982 figures

(d) Assumes a large number of laser power satellite with a continuous maintenance schedule; cost excludes ground based activity in support of satellite operation.

SECTION 6

SUMMARY AND CONCLUSIONS

A comparative evaluation of gas dynamic, electric discharge and optically pumped solar laser systems has been carried out on the basis of weight, cost, efficiency and technical merits in order to determine their feasibility and relative advantages for space applications. The indirect optically pumped lasers (IOPL's) were judged to be the lightest, most efficient and reliable solar lasers. Both conventional and advanced power unit, collector and radiator technologies have been examined to test the sensitivity of these results to technological development. Such improvements will undoubtedly lead to higher performance IOPL's in the 1990 time frame but will not significantly alter the relative advantages which lead to the choice of the IOPL for conceptual design and program development.

Specifically, the static CO₂ solar IOPL was chosen for a \$77M minimum risk development program completing in 1995 with orbit tests for a 1 MW laser system. The static IOPL has complete system redundancy by its use of many individual laser tube plus heat pipe radiator combinations and it is, therefore, the most reliable solar IOPL system considered. Optical tube material development may be required for this laser system, but its essential design simplicity will keep overall development costs to a minimum. For instance, there are no gas pumps required; only minimal station keeping power for pointing and tracking is necessary and this can be supplied by a small bank of photocells. The overall efficiency of the 1 MW static CO₂ system is estimated to be 14% and the weight is 8,300 kg. The entire laser system can be packed in modular and/or constructable form in a single shuttle payload envelope.

A \$120M crash development program was also formulated for the flow CO solar IOPL which would be completed in 1988 with orbit tests for 1 MW laser. This laser system would require the use of monolithic

radiators and solar brayton power cycles in addition to development of laser tube materials. The 1 MW unit would weigh approximately 9,500 kg and have an efficiency of 17%.

It is clear from recent system studies that both of the solar IOPL's chosen for detailed study have sufficiently high performance to permit a solar laser power satellite system to be competitive with a solar microwave power satellite. These lasers may also be used to power other satellites or provide energy for propulsion.

Considering the relatively modest costs and short times (eg about 5 years) to prove out the technical feasibility of laser power transmission technology based on a solar pumped laser, we recommend that a trial development program be initiated immediately in order to obtain the empirical data needed to verify the competitiveness of the laser solar power satellite concept, as well as its utility for other space power and propulsion missions.

References

1. D. L. Nored, "Applications of High Power Lasers to Space Power and Propulsion" pp. 95-108 in the Second NASA Conference on Laser Energy Conversion ed. by K. W. Billman, NASA SP-395 27-28 Jan. 1975.
2. C. F. Hansen & G. Lee, "Laser Power Stations in Orbit", Astronautics & Aeronautics, pp. 42-55 July 1972.
3. R. T. Taussig, P. E. Cassady and J. F. Zumdieck, "Study, Optimization, and Design of a Laser Heat Engine" pp. 498-523 in Radiation Energy Conversion in Space, Progress in Astronautics and Aeronautics, Vol. 61 ed. by K. W. Billman (AIAA, N.Y.C., N.Y.) 1978.
4. W. S. Jones, "Laser-Powered Aircraft and Rocket Systems with Laser Energy Relay Units", pp. 264-270 in Ref. 3 (op. cit.) Space Laser Power System, Draft Report, Lockheed, Palo Alto Research Laboratory, June 1978.
5. H. H. Legner and D. H. Douglas-Hamilton, "CW Laser Propulsion", J. Energy 2, pp. 85-94, 1978.
6. J. Frank Coneybear, "The Use of Lasers for the Transmission of Power", pp. 279-310, Ref. 3 (op. cit.)
7. W. E. Young and G. W. Kelch, Closed-Cycle Gas Dynamic Laser Design Investigation, NASA Report CR-135130, prepared by the Pratt and Whitney Aircraft Group, United Technologies Corporation, Jan. 1977.
8. P. K. Baily and R. C. Smith, Closed-Cycle Electric Discharge Laser Design Investigation, Final Report Hughes Aircraft Co., prepared for the NASA-Lewis Research Center, March 1978.
9. J. D. G. Rather, E. T. Gerry and G. W. Zeiders, Investigation of Possibilities for Solar Powered High Energy Lasers in Space, Final Report, W. J. Schafer Associates, prepared by NASA, May 1977.
10. J. M. J. Madey, "Stimulated Emission of Bremstrahlung in a Periodic Magnetic Field", J. Appl. Phys. 42, 1906 (1971).
T. Kwan, J. M. Dawson and A. T. Lin, The Free Electron Laser, Report No. PPG-267, Plasma Physics Group, University of California, Los Angeles, July 1976.
11. D. J. Monson, "Systems Efficiency and Specific Mass Estimates for Direct and Indirect Solar-Pumped Closed-Cycle High Energy Lasers in Space:", pp. 333-345 in Ref. 3 (op. cit.)

12. C. N. Bain, Potential of Laser for SPS Power Transmission, PRC Energy Analysis Co., Report No. R-1861, prepared for US-DOE, Sept. 1978.
13. W. H. Christiansen, "A New Concept for Solar Pumped Lasers", pp. 346-356 in Ref. 3 (op. cit.)
14. Mitchell & Zemansky, Resonance Radiation & Excited Atoms, Cambridge at the Univ. Press, p. 95, 1961.
15. R. L. Byer, R. L. Herbst, H. Kildal and M. D. Levenson, Appl. Phys. Lett. 20, 463, 1972.
16. B. Wellegehausen, K. H. Stephan, D. Friede and H. Welling, Optics Commun. 23, 157, 1977; J. B. Koffend and R. W. Field, J. Appl. Phys., 1977.
17. M. A. Henesian, R. L. Herbst and R. L. Byer, J. Appl. Phys. 47, 151, 1976.
18. H. Itoh, H. Uchiki and M. Matsuoko, Optics Commun. 18, 271, 1976.
19. H. Welling and B. Wellegehausen, Springer Series in Optical Sciences, Vol. 7: Laser Spectroscopy III, eds. J. L. Hall and J. L. Carlsten.
20. F. J. Wodarczyk and H. R. Schlossberg, J. Chem. Phys., 1977.
21. S. R. Leone and K. G. Kosnik, Appl. Phys. Lett. 30, 346, 1977.
22. D. R. Guyer and S. R. Leone, 5th Conf. on Chemical and Molecular Lasers, St. Louis, Mo., 1977.
23. E. J. Schmitschek and J. E. Celto, Optics Letters 2, 64, 1978.
24. Topics in Applied Physics, Vol. 1, "Dye Lasers", ed. F. P. Schafer, Springer Verlag, e.g. p. 97, 1973.
25. C. R. Giuliano and L. D. Hess, J. Appl. Physics, 38, 4451, 1961.
26. J. Rather, E. Gerry, and G. Zeiders, "Investigation of Possibilities for Solar Powered High Energy Lasers in Space", W. J. Schafer Assoc., Inc., Rept. 77SR-VA-U3, May 25, 1977.
27. A. Hariri and C. Wittig, J. Chem. Phys. 67, 4454, 1977.
28. A. B. Petersen and C. Wittig, J. Appl. Phys. 48, 3665, 1977.
29. A. B. Petersen, L. W. Braverman and C. Wittig, J. Appl. Phys. 48, 230, 1977.

30. M. I. Buchwald and G. J. Wolga, J. Chem. Phys. 62, 2828, 1975.
31. C. B. Moore, et al., J. Chem. Phys. 46, 4222, 1967.
32. W. A. Rosser, E. Hoag and E. T. Gerry, J. Chem. Phys. 57, 4153, 1972.
33. A. S. Biriukov, et al., J. Exp. Theor. Phys. 67, 2064, 1974.
34. D. F. Starr and J. K. Hancock, J. Chem. Phys. 62, 3747, 1975.
35. J. C. Stephenson and C. B. Moore, J. Chem. Phys. 56, 1295, 1972.
36. D. R. Siebert and G. W. Flynn, J. Chem. Phys. 64, 4973, 1976.
37. J. K. Hancock, D. F. Starr and W. H. Green, J. Chem. Phys. 61, 3017, 1974.
38. L. A. Gribov and Smirnov, Sov. Phys. Uspekhi, 4, 919, 1962.
39. J. W. Rich, R. C. Bergman, and J. W. Raymond, Appl. Phys. Lttrs. 27, 656, 1975.
40. N. Skribanowitz, et al., Appl. Phys. Lttrs. 20, 428, 1972.
41. H. Kidal and T. F. Deutsch, Appl. Phys. Lttrs 27, 500, 1975.
42. C. W. Allen, Astrophysical Quantities, Univ. of London, The athlone Press, 1955.
43. G. Merrill, Ed. Handbook of Satellites & Space Vehicles, pp. 376-393, Van Nostrand, 1965.
44. J. W. L. Kohler and C. O. Jonkers, Philips Tech. Rev. 16, 69, 1954.
J. W. L. Kohler and C. O. Jonkers, Philips Tech. Rev. 16, 105, 1954.
J. W. Kohler, Progress in Cryogenics 2, 41, 196 .
Philips Tech. Rev. 25, 340, 1963/1964.
45. Private communication, Lou Morgan, Lockheed Aerospace Co.
46. ASHRAE Applications, Section II, 1974.
47. F. C. Yip, J. Spacecraft 13, 237, 1976.
48. K. H. Sun and C. L. Tien, AIAA Journal 10, 1051, 1972.
49. T. J. McCusker, "Solar Concentrator Design and Construction", pp. 687-700 in Space Power Systems Engineering, ed. G. C. Szego and J. E. Taylor, Academic Press, New York, 1966.

50. A. Pietsch, Coal Fired Prototype High Temperature Continuous Flow Heat Exchanger, EPRI Report No. AF-684, prepared by the AiResearch Manufacturing Company of Arizona, Feb. 1978.
51. E.V. Tishchenko, Investigation of High-Temperature Regenerator for Power Plan using Inert-Gas Closed Cycle, Soviet Energy Machinery 1, 44-49, 1978. (Energomashinostroenie, No.1 22-26, 1977)
52. C. F. McDonald, "The Role of the Recuperator in High Performance Gas Turbine Applications", ASME paper No. 78-GT-46, presented at the Gas Turbine Conference and Products Show, London, England, 9-13 April 1978.
53. A. Hertzberg, R. Decher, A. T. Matlick and C. V. La , "High Temperature Solar Photon Engines", AIAA paper No. 78-1177, presented at the 11th Fluid and Plasma Dynamics Conference, Seattle, Washington, 10-12 July 1978.
54. A. D. Tonelli and T. C. Secord, "Auxiliary Power Generating System for a Large Space Laboratory", pp. 299-322, Ref. 49 (op. cit.)
55. D. L. Southam, "Power Systems Comparison for Manned Space Station Applications", pp. 335-360, Ref. 49 (op. cit.)
56. M. G. Coombs and L. W. Norman, "Application of the Brayton Cycle to Nuclear Electric Space Power Systems:", pp. 419-482, Ref. 49 (op. cit.)
57. G. R. Seikel and L. D. Nichols, "Potential of Nuclear MHD Electric Power Systems", J. Spacecrafts and Rockets 9, pp. 322-326, 1972.
58. G. R. Woodcock, "Solar Satellites - Space Key to our Power Future", Astronautics and Aeronautics, pp. 30-43, July/August 1977.
59. Satellite Power System Engineering and Economic Analysis Summary, Marshall Space Flight Center, Huntsville, Alabama, NASA-TM-X-73344, November 1976.
60. D. L. Gregory, "Alternative Approaches to Space Based Power Generation", J. of Energy 1, 85-92, 1977.
61. Ref. 56
62. Ref. 3
63. C. Seippel, "Pressure Exchanger", US Patent No. 2,399,394, 1946.
64. W. E. Smith and R. C. Weatherston, "Studies of a Prototype Wave Superheater Facility for Hypersonic Research", Cornell Aeronautical Laboratory Report HF-1056-A-1-AFOSR-TR-58-158, AD207244, December 1958.
65. K. Kunberger, "Progress in Compres Supercharger Development", Diesel and Gas Turbine Progress, Worldwide Editions, 1973.

66. R. Taussig, High Thermal Efficiency, Radiation Based, Advanced Fusion Reactor, Mathematical Sciences Northwest, Inc. Report No. MSNW-77-1067-1, April 1977.
67. The Liquid Metals Handbook.
68. F. Kreith, Principles of Heat Transfer, Second Edition, International Textbook Co., p. 382ff, Penn., 1965.
69. B. Z. Henry and J. P. Decker, "Future Earth Orbit Transportation Systems/Technology Implications", Astronautics and Aeronautics, pp. 18-28, Figure 19, p. 27, Sept. 1976.
70. Raymond J. Roark, Formulas for Stress and Strain, McGraw-Hill Book Company, New York, 1971.
71. G. R. Woodcock, "Large-Scale Space Operations for Solar Power Satellites", presented at AIAA/EEI/IEE Conference on New Options in Energy Technology, San Francisco, California, 2 August 1977.
72. Ref. 69, p. 22, Fig. 8.
73. Harshaw Optical Crystals data sheet, published by the Harshaw Chemical Company, Solon, Ohio.
74. P. E. Glaser, "Perspectives on Satellite Solar Power", J. of Energy 1, 75-84, 1977.
75. K. W. Billman, W. B. Gilbreath and S. W. Bowen, "Introductory Assessment of Orbiting Reflectors for Terrestrial Power Generation", NASA Technical Memorandum, NASA TMX-73, 230, April 1977.
76. "Space Machine Demonstrated", in Briefing the Record, Mechanical Engineering Journal (ASME), p. 54, August 1975.
77. Physical Sciences Research Papers, No. 635, "Infrared Laser Window Materials Property Data for ZnSe, KCl, NaCl, CaF₂, SrF₂, CaF₂", compiled by Stanley K. Dickinson, 1975.
78. Tyco Sapphire data sheet, published by Tyco laboratories, Inc. 16 Hickory Drive, Waltham, MA 02154.
79. Kodak IRTAN IR Materials Data Book, published by the Eastman Kodak Company, Rochester, New York, 14650
80. L. Friedman et al., "Solar Sailing-The Concept Made Realistic", AIAA 16th Aerospace Sciences Meeting, Huntsville, Ala., paper no. 78-82, 16-18 Jan 78.
81. Central Receiver Solar Thermal Power System: Phase 1, 10-MW Electric Pilot Plant Appendix B to ERM RFP EG-R-03-1468, Sandia Laboratories, Jan. 1977.
82. Closed Cycle High-Temperature Central Receiver Concept for Solar Electric Power EPRI Report SY 32, prepared by the Boeing Engineering and Const., Feb. 1976.

Table A1
Optical Crystal Properties (MKS Units)

Optical Material	M.P.	$\rho(293K)$	$E(293K)$	$F_A^*(293K)$	C_p	k	α	γ
^{77,79} ZnSe	1793K	5651	7×10^{10}	5×10^7	-	(367K) 950 (441K) 390	(280K) 7.0×10^{-6} (300K) 7.2×10^{-6}	0.30
^{73,77} KCl	1049K	1987	3.5×10^{10}	2.28×10^6	(350K) 702 (400K) 713	(373K) 6.3	(298K) 36.84×10^{-6} (373K) 38.79×10^{-6}	0.11
⁷³ CsI	894K	4510	5.3×10^9	5.58×10^6	(298K) 201	(298K) 1.13	(298K) 5×10^{-5} (323K) 5×10^{-5}	-
⁷⁹ MgO	3073K	3580	3.24×10^{11}	1.32×10^8	(273K) 875	(273K) 370	(293K) 1.06×10^{-5}	-
⁷⁸ Sapphire	2326K	3965	4.66×10^{11}	2.85×10^7	(298K) 754	(1200K) 46 (1500K) 46	(1200K) 9.2×10^{-6} (1500K) 9.3×10^{-6}	-

*Values for S_u were not available for these materials, so F_A will be used in all calculations requiring S_u . $F_A < S_u$ is typically true. Measurements of S_u would be prudent before constructing any system.

NOMENCLATURE LIST

SPS	Solar Power Satellite
SLPS	Solar Laser Power Satellite
EDL	Electric Discharge Laser
GDL	Gas Dynamic Laser
OPL	Optically Pumped Laser
DOPL	Direct Optically Pumped Laser
IOPL	Indirect Optically Pumped Laser
CW	Continuous Wave
IR	Infrared
UV	Ultraviolet
τ	Radiative lifetime; also flow transit time for gas in laser tube
g_i	Statistical weight of electron bound state
λ	Wavelength
A_{ij}	Einstein Coefficient
P	Pressure
T	Temperature
N	Number of absorbing molecules
$g(\nu)$	Line shape
ν	Frequency; also, Poisson ratio
α	Absorption coefficient; also, half angle subtended by the solar disc; also, mirror quality (radianse)
Ω	Solid angle
P	Power (also Power per unit volume)
I_ν	Radiation intensity per unit frequency interval
h	Planck's constant; also waste heat radiator thickness
T_B	Black body temperature
T_S	Suns radiation temperature
η	Total system efficiency (laser and power units)
η_R	Cavity efficiency
η_{DIFF}	Aperture efficiency
η_B	Spectrum utilization efficiency
η_L	Laser efficiency

η_{EC}	Efficiency of solar energy conversion into electricity
η_M, η_r	Collector mirror reflectivity
η_c	Collector efficiency; also, adiabatic compressor efficiency
η'	Overall laser efficiency for indirect optical pumping
η''	Overall laser efficiency for direct optional pumping
f	Aperture number
S, E_s	Solar flux at earth orbit
s	Specific entropy
F_s	Solar flux at sun's surface
\bar{F}_{FS}	Average radiation flux at focal spot
θ_m	Rim angle of paraboloidal collector
A	Focal spot area
A_a	Aperture area
A_h	Heat exchanger tube surface area
P_{in}, P_s	Input Power
$P_{Re-emit}$	Re-emitted Power
σ	Stefan-Boltzmann constant
k	Boltzmann constant
λ_C^I	Infrared absorption cutoff wavelength
λ_C^V	Ultraviolet absorption cutoff wavelength
B_v	Planck radiation distribution function
P_M, P_{EXC}	Power absorbed in laser medium
P_{cond}	Power lost by heat conduction
P	Laser power output
P_T, P_{ABS}	Total power absorbed by laser tube materials
P_{TR}	Power transmitted through tubes and lasent
ϵ	Fraction of incident sunlight used in optical pumping; also, regenerator effectiveness; also, surface emissivity
Q_{rad}	Radiated waste heat
P_c	Compressor input power
\dot{m}_{in}	Mass flow rate
D	Collector diameter
R_s	Radius of sun
R_e	Earth-sun distance

L	Focal length
b, d_o	Diameter of aberatted image
d_i	Diameter of first order image
r	Radius in focal plane
E	Radiation intensity in focal plane; also, Young's modulus
a	Gaussian distribution e-folding half width
π_t	Turbine pressure ratio
π_c	Compressor pressure ratio
T_c	Peak compressor temperature
\bar{M}	Average molecular weight
η_t	Adiabatic turbine efficiency
ΔP	Pressure change
ϕ_{in}	Total radiation entering the black body cavity
h_f, h_c	Heat transfer coefficient
T_f	Liquid metal temperature
C_p	Specific heat at constant pressure
ρ	Mass density; density of laser gas
ρ'	Density of laser pumping tube materials
v	Fluid velocity
Re	Reynolds number
Pr	Prandtl number
T_H	Heat exchanger temperature
T_{rad}	Radiator temperature
R	Gas constant; also, maximum radius of laser tube
W_{total}	Total Weight
M_{total}	
W	Laser loop weight
W_{sc}, W_{coll}	Solar Collector Weight
W_{H1}	Absorber cavity weight
W_{RE}	Laser recuperater weight
W_{H2}	Heat sink heat exchanger weight
W_{RA}, M_{rad}	Laser loop waste heat radiator weight

W_p	Solar Brayton power unit weight
W_c	Laser loop compressor weight
T_{exit}	Compressor exit temperature
P_{out}	Net output power (eg of laser, of compressor or turbine)
P_{recup}	Power transferred as heat across the recuperator
$P_{collect}$	Solar power collected
P_{rad}, P_{cool}	Waste heat power radiated
P_{HX}	Heat flow in heat exchanger
F_A	Flexural apparent limit
f_{ABS}	Fraction of incident black body radiation absorbed in the Laser tubes
h_l	Latent heat
l	Length of laser pumping tubes
M_T	Mass of laser tubes
N	Number of layers of tubes
W	Number of tubes per layer
q_B	Black body radiation heat loss
(SF)	Safety factor
S_n	Ultimate tensile strength
T_o	Gas temperature entering laser tubes
T_g	Gas temperature leaving laser tubes
δ	Thickness of tube walls
μ	Viscosity
M_m	Collector mirror mass
T_r	Transmittance
R_f	Reflectance

DISTRIBUTION LIST FOR LASER FINAL REPORTS

1. National Aeronautics & Space Administration
Lewis Research Center
21000 Brookpark Road
Cleveland, OH 44135

Attn: Contracting Officer, MS 500-213 1
Technical Utilization Office, MS 7-3 1
Technical Report Control Office, MS 5-5 1
AFSC Liaison Office, MS 501-3 2
Library, MS 60-3 2
Office of R&QA, MS 500-211 1
N. T. Musial, Patent Counsel, MS 500-311 1
Richard B. Lancashire, Project Manager MS 500-202 10
Wolfgang E. Moeckel, MS 3-12 1
2. National Aeronautics & Space Administration
Headquarters
Washington, D.C. 20546

Attn: Office of Aeronautics & Space Technology 1
Director, Space Power and Propulsion/RTS-3

Attn: F.C. Schwenk/RT-3 1

Attn: Office of Space Transportation Systems 1
Director, Advanced Program/MT-3

Attn: Jerome P. Mullin/RP-6 1
Lynn Randolph/RP-6 1

Attn: Stanley R. Sadin/RX-4 1
3. National Aeronautics & Space Administration
Ames Research Center
Moffett Field, CA 94035

Attn: Library 1
Dr. Kenneth W. Billman 1
4. National Aeronautics & Space Administration
Flight Research Center
P. O. Box 273
Edwards, CA 93523

Attn: Library 1
5. National Aeronautics & Space Administration
George C. Marshall Space Flight Center
Huntsville, AL 35812

Attn: Library 1
Lott W. Brantley 1

6. National Aeronautics & Space Administration
Goddard Space Flight Center
Greenbelt, MD 20771

Attn: Library 1
7. National Aeronautics & Space Administration
John F. Kennedy Space Center
Cocoa Beach, FL 32931

Attn: Library 1
8. National Aeronautics & Space Administration
Lyndon B. Johnson Space Center
Houston, TX 77058

Attn: Library 1
Tony E. Redding 1
9. National Aeronautics & Space Administration
Langley Research Center
Langley Station
Hampton, VA 23365

Attn: Library 1
R. Hess 1
10. NASA Scientific & Technical
Information Facility
P.O. Box 8757
Balt/Wash International Airport
Maryland 21240

Attn: Accessioning Department 10
11. Jet Propulsion Laboratory
4800 Oak Grove Drive
Pasadena, CA 91103

Attn: Library 1
G.R. Russell 1
12. Defense Documentation Center
Gameron Station
Building 5
5010 Duke Street
Alexandria, VA 22314

Attn: TISIA 1
13. Defense Advanced Research Projects Agency
1400 Wilson Blvd.
Arlington, VA 22209

Attn: Director, Laser Division 1

14. ODDR&E
Pentagon
Washington, D.C. 20301
Attn: Asst. Dir. (Space and Advanced Systems) 1
15. Commander
U.S. Army Intelligence Agency
Ft. George G.
Meade, MD 20755
Attn: MIIA-OSS, Mr. Sherman Delmage 1
16. Ballistic Missile Defense Program Office
5001 Eisenhower Avenue
Alexandria, VA 22333
Attn: Albert J. Bast, Jr. 1
17. U.S. Army Missile Research and Dev. Command
Redstone Arsenal, AL 35809
Attn: DRCPM-HEL (V.P. De Fatta) 1
18. Commander
U.S. Army Missile Research and Dev. Command
Redstone Arsenal, AL 35809
Attn: DRDMI-NS 1
19. Director
Ballistic Missile Defense Advanced Technology Center
P.O. Box 1500
Huntsville, AL 35807
Attn: ATC-O, Mr. W. O. Davies 1
20. Director
U.S. Army Ballistic Research Laboratory
Aberdeen Proving Ground, MD 21005
Attn: Dr. Robert Eichelberger 1
21. Department of the Navy
Office of the Chief of Naval Operations
Washington, D.C. 20350
Attn: Cdr. L.E. Pellock (OP-982F3) 1
22. Office of Naval Research
495 Summer Street
Boston, MA 02110
Attn: Dr. Fred Quelle 1

23. Office of Naval Research
800 N. Quincy Street
Arlington, VA 22217
Attn: Dr. W.J. Conde11 (421) 1
24. Naval Research Laboratory
Washington, D.C. 20375
Attn: Dr. J. M. MacCallum (Code 4109) EOTPO 1
25. Commander
Naval Surface Weapons Center
White Oak
Silver Springs, MD 20910
Attn: Dr. Leroy Harris 1
26. Air Force Weapons Lab
Kirtland, AFB, NM 87117
Attn: Col. J.C. Rich (AR)
Dr. Peter Avizonis, Tech. Div. 2
27. Hq, SAMSO
P.O. Box 92960, Worldway Postal Center
Los Angeles, CA 90009
Attn: Lt. Col. J.R. Doughty (DYV) 1
28. AF Aero Propulsion Lab
Wright Patterson AFB, OH 45356
Attn: Lt. Col. Bobbie L. Jones 1
29. AF Rocket Propulsion Lab.
Edwards AFB, CA 93523
Attn: B.R. Bornhorst (LKCB) 1
30. Defense Intelligence Agency
Washington, D.C. 20301
Attn: Mr. Seymour Berler (DTIA) 1
31. Central Intelligence Agency
Washington, D.C. 20505
Attn: Dr. Bernard Lubarsky 1
32. Aerospace Corp.
P.O. Box 92957
Los Angeles, CA 90009
Attn: Dr. G.P. Millburn 1

33. Mr. A. Colin Stancliffe
AiResearch Manufacturing Company
2525 West 190th Street
Torrance, Ca 90503
Attn: Dept. 93-6 1
34. AVCO - Everett Res. Lab.
2385 Revere Beach Parkway
Everett, MA 02149
Attn: Dr. Jack Dougherty 1
35. Battelle Columbus Labs
505 King Avenue
Columbus, OH 43201
Attn: Mr. Fred Tietzel 1
36. Eastman Kodak Company
901 Elmgrave Road
Rochester, NY 14650
Attn: R.E. Keim Dept. 394 1
37. General Electric Company
P.O. Box 8555
Philadelphia, PA 19101
Attn: Dr. Thomas W. Karras 1
38. Hughes Aircraft Company
Centinela and Teale Streets
Culver City, CA 90230
Attn: Dr. Eugene Peressini (Bldg. 6, MS/E-125) 1
39. Itek Corp.
Optical Systems Division
10 Maguire Road
Lexington, MA 02173
Attn: R. J. Wollensak 1
40. Institute for Defense Analyses
400 Army Navy Drive
Arlington, VA 22202
Attn: Dr. Alvin Schnitzler 1
41. Lawrence Livermore Lab.
P.O. Box 808
Livermore, CA 94550
Attn: Dr. R.E. Kidder
Dr. E. Teller 1

42. Los Alamos Scientific Lab
P.O. Box 1663
Los Alamos, NM 87544
Attn: Dr. Keith Boyer (MS 350) 1
43. Lockheed Palo Alto Research Lab
3251 Hanover Street
Palo Alto, CA 94304
Attn: L.R. Lunsford 1
Org. 52-03,201, 2 1
W. Jones 1
44. Massachusetts Institute of Technology
Lincoln Lab
P.O. Box 73
Lexington, MA 02173
Attn: Dr. L.C. Marquet 1
45. MITRE Corporation
P.O. Box 207
Bedford, MA 01730
Attn: Norman F. Harmon 1
46. Northrop Corporation
Research & Technology Center
3401 West Broadway
Hawthorne, CA 90250
Attn: Dr. M.L. Bhaumik 1
47. Razor Associates
420 Persian Drive
Sunnyvale, CA 94086
Attn: Dr. Ned S. Razor 1
48. Physical Sciences, Inc.
30 Commerce Way
Woburn, MA 01801
Attn: Dr. Anthony N. Pirri 1
49. Perkin-Elmer Corporation
Central Library
Main Avenue
Norwalk, CT 06856
Attn: M. D. Wood 1

50. Rockwell International Corporation
Rocketdyne Division
6633 Canoga Avenue
Canoga Park, CA 94304

Attn: Dr. Stan V. Gunn 1
51. Riverside Research Institute 1
1701 N. Fort Myer Drive, Suite 711
Arlington, VA 22209
52. Rockwell International Corporation
3370 Miraloma Avenue
Anaheim, CA 92803

Attn: Dr. Cecil Hayes 1
53. SANDIA Labs
P.O. Box 5800
Albuquerque, NM 87115

Attn: Dr. A. Narath, ORG 5000 1
54. Dr. Frank A. Horrigan 1
Science Applications, Inc.
3 Preston Court
Bedford, MA 01730
55. Stanford Research Institute
Menlo Park, CA 94025

Attn: Dr. Don M. LeVine (JASON) 1
56. Systems, Science and Software
P.O. Box 1620
La Jolla, CA 92037

Attn: Mr. Alan F. Klein 1
57. TRW Systems Group
One Space Park
Redondo Beach, CA 90278

Attn: Mr. Norman F. Campbell (Bldg. 01, Room 1050) 1
58. United Technologies Research Center
400 Main Street
East Hartford, CT 06108

Attn: Mr. A.W. Angelbeck 1
Mr. Jack Davis

59. United Technologies Corporation
Pratt & Whitney Aircraft Group
P. O. Box 2691
West Palm Beach, FL 33402

Attn: Mr. E. A. Pinsley

1

60. Princeton University
Box 708
Princeton, NJ 08540

Attn: Gerard K. O'Neill

1

61. Grumman Aerospace
NASA Space Programs MS A09-25
Bethpage, NY 11714

Attn: Sima Winkler

1

62. U.S. Department of Energy
Room 509
400 First Street N.W.
Washington, D.C. 20545

Attn: Dr. Fred A. Koomanoff

1